YAMID ALBERTO CARRANZA SÁNCHEZ

Exergy and environmental assessment of FPSO offshore platforms with CO_2 capture and storage

São Paulo - Brazil

2017

YAMID ALBERTO CARRANZA SÁNCHEZ

Exergy and environmental assessment of FPSO offshore platforms with CO_2 capture and storage

Thesis submitted to the Polytechnic School of the University of São Paulo in the fulfillment of the requirements for the degree of Doctor in Sciences

São Paulo - Brazil
2017

YAMID ALBERTO CARRANZA SÁNCHEZ

Exergy and environmental assessment of FPSO offshore platforms with CO_2 capture and storage

Thesis submitted to the Polytechnic School of the University of São Paulo in the fulfillment of the requirements for the degree of Doctor in Sciences

Concentration area:
Mechanical Engineering - Energy and Fluids

Advisor:
Prof. Dr. Silvio de Oliveira Junior

São Paulo - Brazil
2017

Este exemplar foi revisado e corrigido em relação à versão original, sob responsabilidade única do autor e com a anuência de seu orientador.

São Paulo, _____ de _____ de _____

Assinatura do autor: 

Assinatura do orientador: _____

Catalogação-na-publicação

Carranza-Sánchez, Yamid Alberto
Exergy and environmental assessment of FPSO offshore platforms with CO2 capture and storage / Y. A. Carranza-Sánchez -- versão corr. -- São Paulo, 2017.
134 p.

Tese (Doutorado) - Escola Politécnica da Universidade de São Paulo. Departamento de Engenharia Mecânica.

1.Exergia (avaliação) 2.Poluição ambiental (redução) 3.Impactos ambientais (redução) 4.Plataforma continental 5.Plataforma offshore I.Universidade de São Paulo. Escola Politécnica. Departamento de Engenharia Mecânica II.t.

This thesis is dedicated to my Lu-wife and my Lu-daughter

ACKNOWLEDGEMENTS

I would like to express my deepest and sincere gratitude to my advisor, Prof. Silvio de Oliveira Jr., for his guidance, continued support and for providing valuable feedback during my doctoral study.

My special thanks go to my friends Cristiaann, Carlos, Ricardo, Jhonny, Juan Esteban, Alvaro, Yesid, Rey, Lina, Oneida, Paola, Miguel, Alexander, Sra. Mara, Ana, and Regina, for their unconditional and friendly support.

It is my pleasure to thank the colleagues and friends of the Laboratory of Environmental and Thermal Engineering LETE: Izabela, Pablo, Daniel, José Luis, Tuong-Van, Felipe, Cadu, Julio, and Rafael.

A special thanks to my family. Especially, I wish to thank my mother and my brother for their encouragement and for always being there for me. I also want to thank Rubiela, Juan, Steven and Camilo, they were very important in decisive moments of our stay in Brazil.

I wish to acknowledge the support from Technological University of Pereira, Colciencias, and BG Brazil.

ABSTRACT

Offshore oil platforms are used for the exploitation and production of hydrocarbons and consist of a processing plant and a utility plant. The oil and gas industry operations are energy-intensive and, in the case of offshore platforms, the need to decrease energy consumption and reduce CO_2 emissions has increased. In the oil and gas industry, the ISO 50001 standard promotes the implementation of energy management systems and proposes indicators based on energy. Interestingly, after several decades of knowledge of the concept of exergy, this has not been formally implemented in the programs and strategies of the oil and gas industry organizations. In this research, the implementation of the exergy method and the carbon capture and storage strategy for the assessment of the performance of a floating, production and storage offloading units FPSO is proposed. FPSO platforms and their processing and utility plants may have different configurations depending on, among others, the reservoir characteristics and production requirements. The possible configurations can therefore be numerous. In this sense, some operation scenarios based on different well-fluid compositions and operation modes are studied. The platform models are developed and simulated using the software Aspen HYSYS®. Results show that, on average, the reduction of 88.8% in CO_2 emissions is penalized with a reduction in exergy efficiency of 1.7 points. Further, results allow a better understanding of exergy and environmental performance of the FPSO.

Keywords: Exergy assessment. Environmental assessment. FPSO platform. Offshore platform. CO_2 capture and storage.

RESUMO

Plataformas de petróleo offshore são utilizadas para a exploração e produção de hidrocarbonetos e consistem em uma planta de processamento e uma planta de utilidade. As operações da indústria de petróleo e gás são de energia intensiva e, no caso de plataformas offshore, é necessário cada vez mais diminuir o consumo de energia e reduzir as emissões de CO_2. Na indústria de petróleo e gás, a norma ISO 50001 promove a implementação de sistemas de gestão de energia e propõe indicadores baseados em energia. Entretanto, após várias décadas de conhecimento do conceito de exergia, este não foi formalmente implementado nos programas e estratégias das organizações da indústria de petróleo e gás. Neste trabalho, propõe-se a implementação da análise exergética e a estratégia de captura e armazenamento de carbono para a avaliação do desempenho de unidades flutuantes, de produção, de armazenamento e transferência FPSO. As plataformas FPSO e suas plantas de processamento e utilidade podem ter diferentes configurações dependendo, entre outras, das características do reservatório e dos requisitos de produção. As configurações possíveis podem, portanto, ser numerosas. Neste sentido, são estudados alguns cenários de operação baseados em diferentes composições dos fluidos do poço e em três modos de operação. Os modelos de plataforma são desenvolvidos e simulados usando o software Aspen HYSYS®. Os resultados mostram que, em média, a redução de 88,8% nas emissões de CO_2 é penalizada com uma redução da eficiência exergética de 1,7 pontos. Além disso, os resultados permitem uma melhor compreensão da exergia e desempenho ambiental do FPSO.

Palavras-chave: Avaliação exergética. Avaliação ambiental. Plataforma FPSO. Plataforma offshore. Captura e armazenamento de CO_2.

List of Figures

List of Tables

List of Symbols

Abbreviations

avg	Average
BAT	Best available technology
bkW	Brake kilowatts
boe	Barrels of oil equivalent
bpd	Barrels per day
BS&W	Basic sediment and water
CCS	Carbon capture and storage system
CS	Compression system
CT	Compression train
CWS	Cooling water system
EES	Engineering equation solver
EG	Exported gas
EOR	Enhance oil recovery
FPSO	Floating production, storage and offloading unit
FWKO	Free-water knockout
GDS	Gas dehydration system
GOR	Gas-to-oil ratio
GT	Gas turbine
HR	Heat recovery
HRU	Heat recovery unit
HWS	Hot water system
HVAC	Heating, ventilation and air conditioning
IOR	Improved Oil Recovery
IPIECA	International petroleum industry environmental conservation association
ISO	International organization for standardization
LHV	Lower heating value
MC-A	Main Compressors A
MC-B	Main Compressors B
MEA	Monoethanolamine
MW	Molecular weight
IOGP	International association of oil and gas producers

OECD Organization for economic co-operation and development
OPEC Organization of the petroleum exporting countries
ORC Organic Rankine cycles
ppm Part per million
RIT Rotor inlet temperature
Sbpd Standard barrels per day
SEC Specific exergy consumption
SED Specific exergy destruction
SEU Specific energy use
SG Specific gravity
ST Separation Train
TLP Tension leg platforms
toe Tonne of oil equivalent
VRU Vapor recovery unit
WIS Water injection system
WOR Water-oil ratio
WHRU Waste heat recovery unit

Greeks letters

β Chemical exergy correction factor
ϵ Exergy destruction
γ Activity coefficient
η Energy efficiency
η_b Exergy efficiency
λ Renewability exergy index

Roman letters

b Specific exergy
$\bar{b}$ Molar specific exergy
$\dot{B}$ Exergy flow rate
$\dot{B}^Q$ Thermal exergy flow
CV Control volume
h Specific enthalpy

i	Chemical compound
$\dot{m}$	Mass flow
$o.e.$	Oil equivalent
$\bar{R}$	Universal gas constant
s	Specific entropy
S	Standard
$S\%$	Weight % of sulfur in a petroleum fraction
SG	Specific gravity
t	Ton
T	Temperature
$\dot{W}$	Power
x	Molar fraction

Subscripts

0	Restricted dead state
Aux	Auxiliary
b	Boiling
b, B	Exergy
ch	Chemical
d	Destroyed
e, el	Electric
Exh	Exhaust
fg	Fuel gas
$FPSO$	Floating production, storage and offloading unit
$fuel$	Fuel
gen	Generator
h	Heating
in	Inlet
k	Kinetic
mix	Mixture
$norm$	Normalized
$o.e.$	Oil equivalent
out	Outlet

p	Potential
ph	Physical
$prod$	Products
$pump$	Pump
reb	Reboiler
rf	Reservoir fluid
sep	Separation
u	Useful
vol	Volume

Superscripts

i	i-th component
Q	Thermal exergy

TABLE OF CONTENTS

1 INTRODUCTION

1.1 Background and motivation

Environmental problems are directly related to the development of the industry as natural resources are exploited to satisfy our needs. Pollutants generated by industrial processes have negative effects on the environment and human health. Visibility reduction and temperature alteration in the atmosphere, chemical deterioration of materials and vegetation, and potential increase of sickness and mortality of the population, are some of the most relevant effects of pollutants (SEINFELD, 1986).

The oil and gas exploration and production industries recognize the importance of taking into account environmental aspects for training, management and best practice measures throughout the world. The International Association of Oil and Gas Producers (IOGP) aims to compare of the environmental performance of each member company. Environmental information has thus been compiled by the IOGP in order to contribute to the improvement of environmental performance of the IOGP members (INTERNATIONAL ASSOCIATION OF OIL&GAS PRODUCERS, 2015). Further, energy efficiency and energy savings have been essential to the oil and gas industry operations (INTERNATIONAL ASSOCIATION OF OIL AND GAS PRODUCERS; THE GLOBAL OIL AND GAS INDUSTRY ASSOCIATION FOR ENVIRONMENTAL AND SOCIAL ISSUES, 2013) and environmental and energy policies are useful to assess the sustainability of the exploration and production processes.

Six environmental indicator categories are included in the environmental data report of oil and gas industry (INTERNATIONAL ASSOCIATION OF OIL&GAS PRODUCERS, 2015): gaseous emissions, energy consumption, flaring, aqueous discharges, discharges of non-aqueous drilling fluids retained on cuttings, and spills of oil and chemicals. In the case of gaseous emissions, specifically carbon dioxide emissions, different taxes are being levied in some countries to promote the mitigation of contamination, and the common proposal is that the carbon dioxide taxes start low and increment in time. These taxes are directly impacting the oil and gas industry. CO_2 taxes in some countries are presented in Table 1. Emissions of carbon dioxide can be mitigated by e.g. on-site carbon capture and storage. This carbon capture strategy can capture up to 90% of the CO_2 emissions produced from the use of fossil fuels in electricity generation and industrial processes.

Table 1. CO_2 tax in some countries. Prices on April 1, 2015.

Country	CO_2 tax [US$/t$CO_2$]
Sweden	130
Finland (transport fuels)	62
Switzerland	62
Norway (upper)	53
Finland (other fossil fuels)	47
Denmark	24
Ireland	22
Slovenia	19
France	15
Iceland	8
Portugal	5
Mexico (upper)	3
Norway (lower)	3
Estonia	2
Japan	2
Mexico (lower)	1
Poland	1

Source: (WORLD BANK GROUP; ECOFYS, 2015)

In oil and gas activities, energy planning includes a review of the energy consumption inventory and the variables affecting energy consumption, and the selection of performance indicators. Although the oil and gas industry uses energy-based indicators, the global oil and gas industry association for environmental and social issues (IPIECA) and IOGP mention the use of exergy-based indicators to account for the quality levels of products and resources (INTERNATIONAL ASSOCIATION OF OIL AND GAS PRODUCERS; THE GLOBAL OIL AND GAS INDUSTRY ASSOCIATION FOR ENVIRONMENTAL AND SOCIAL ISSUES, 2013). In comparison with energy analysis, exergy analysis allows identifying opportunities to improve the operations performance. It provides rational information about how the systems use the consumed exergy and how far are the systems from their ideal operation conditions in the overall plant.

Offshore platforms have been used by the oil and gas industry in order to expand oil and gas exploration and production around the world. Oil and gas companies have been encouraging the implementation of sustainability guidelines as a requisite for their operations. Floating, production, storage, and offloading units FPSOs are offshore installations used to perform operations of production of petroleum. An advantage of FPSOs is their storage capacity for

the treated crude oil produced as well as the possibility to operate in remote areas. A FPSO incorporates all equipment related to a fixed installation in its processing and utility plants (MATHER, 2000).

FPSOs have experienced positive trends in the primary petroleum industry. In Brazil, FPSOs have a high impact in oil production operations, particularly in the Campos Basin, where several facilities have been installed and will be implemented in the future. FPSO operations are energy-intensive processes; therefore, the oil and gas industry is interested in the research and development of projects that would decrease the energy use and environmental impact of these offshore operations, thus enhancing their sustainability.

The issues associated with the energy-exergy and environment performance of offshore platforms have motivated the development of this research. The aim is to integrate these concepts for the analysis of operations of primary petroleum processing, and to understand and evaluate the performance of these processing plants. Investigating offshore platforms, in particular FPSO, is the primary focus of this research. The analysis of the environmental performance is based on carbon dioxide emissions indicators.

1.2 Problem Statement

The use of energy on-site (power and heat) for e.g. petroleum heating and gas compression operations results in large emissions of pollutants in the offshore oil and gas industry, making energy efficiency improvement an attractive opportunity to reduce emissions and improve the performance indicators. A FPSO unit must be able to operate under a variety of process conditions, and the Brazilian platforms may process different well-fluid compositions and operate in different operation modes. On the one hand, the application of exergy method to the oil industry and gas is not widespread because of the complexity and particularity of each offshore platform. It is thus not easy to have generic guidelines for predicting the behavior of the FPSO, improving energy performance and reducing their environmental impact. On the other hand, the clear need to minimize emissions of pollutants in the oil and gas industry requires research into technologies such as CO_2 capture for limiting these emissions to the atmosphere.

1.3 Objective

The objective of this thesis is to use exergy analysis to assess the performance and the CO_2 emissions of a floating, production and storage offloading units FPSO considering changes in the composition of the well-fluids and the operating modes, and the implementation of a CO_2 capture and storage strategy.

1.4 Key contributions

One of the aspects that highlight the importance of this work is based on the oil and gas industry´s initiative for encouraging research into more sustainable offshore production. Specifically, this research is part of the project *Sustainable Configurations of Petroleum Primary Processing Offshore Plants*, developed by the Laboratory of Environmental and Thermal Engineering of the University of São Paulo within the *Energy Efficiency Program* promoted by BG Brasil (BG BRASIL, 2014; BG GROUP, 2012). On the other hand, the novelty is associated with the implementation of exergy method and carbon sequestration for the conceptual analysis of FPSO operations, looking for a better energy and environmental performance. The contributions of this thesis can be summarized as follows:

- The integration of exergy analysis and carbon capture and storage strategy in analyzing the operation of FPSO offshore platforms.
- The application of the exergy assessment and the CO_2 mitigation technology to the Brazilian FPSO´s.
- Exergy Analysis of a FPSO project considering its peculiar characteristics: different well-fluids and operation mode variations.

1.5 Structure of the thesis

The thesis is divided into six chapters. Following the Introduction in the Chapter 1, Chapter 2 contains a brief overview of the offshore industry, focusing on Floating, Production, Storage and Offloading units FPSOs. Further, this chapter gives a brief revision of the application of exergy analysis and carbon capture ad storage in FPSOs. Chapter 3 describes the methodology, which includes the description of the FPSO plants, well-fluid compositions and operation modes studied. Additionally, the exergy concepts and exergy and environmental performance indicators applied in this research are included. In Chapter 4, the results and their analysis and discussion are presented. Conclusions and further work are presented in Chapter 5, and references are listed in Chapter 6.

2 OFFSHORE INDUSTRY, EXERGY ANALYSIS. AND CARBON CAPTURE AND STORAGE (CCS) IN FPSO UNITS

In this chapter, a brief description of the current oil and gas industry data including the offshore sector is first presented. Then, a brief description of the primary petroleum processing industry offshore is given, with a focus on the FPSO applications and its applications in the Brazilian industry. Then, a literature review on application of exergy method and carbon capture systems to offshore oil platform is detailed, with a summary of the main research results.

2.1 A brief overview of the oil, gas and offshore industry

The global oil and gas industry has significantly increased its reserves by intensive explorations and enhancing recoveries, especially by reserves addition from OPEC Members Countries in the last ten years. Figure 1 shows the evolution of the crude oil proved reserves in the world since 1990. A remarkable growth can be observed since 2003. According to OPEC, in 2014, 81% of the world's proven oil reserves are located in OPEC nations, and the remaining 21% is located in Non-OPEC countries (OPEC, 2015).

Figure 1. Crude Oil Proved Reserves in the world.

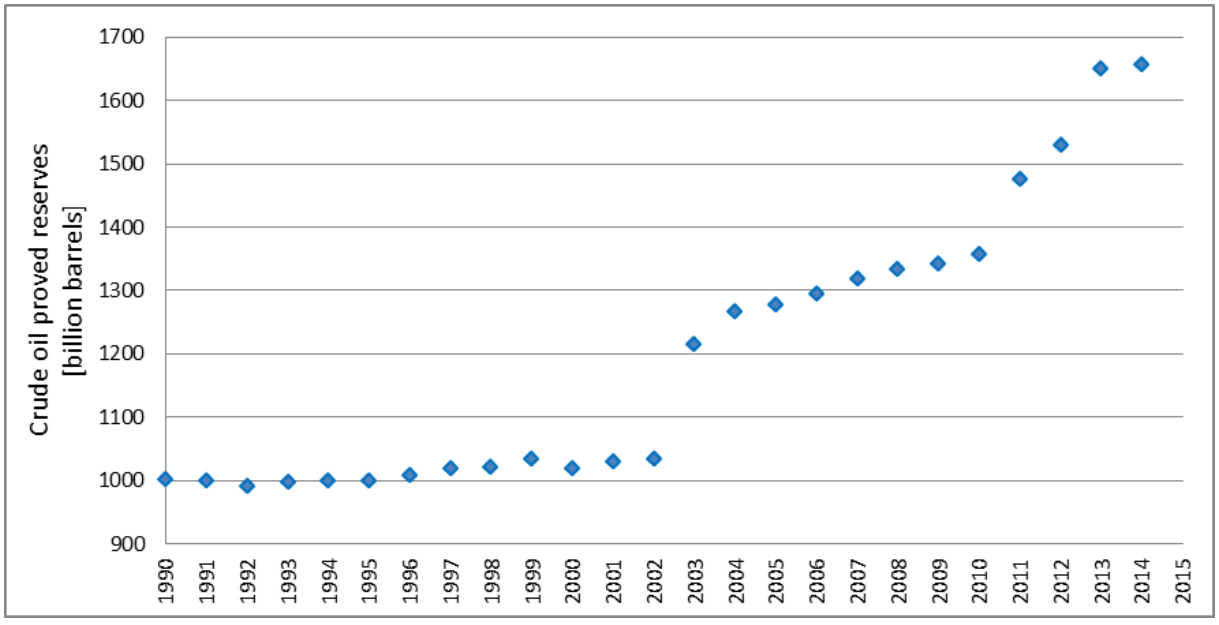

Source: Adapted from (U.S. ENERGY INFORMATION ADMINISTRATION, 2016)

Table 2 provides the ten countries with the biggest proved oil reserves in the world in 2015. As shown in this table, Venezuela has the greatest oil reserves in the world, closely followed by Saudi Arabia. These two countries have approximately 40% of total oil reserves. Brazil is in the fourteenth position with 15.3 billion barrels. Another aspect worth highlighting is that eight OPEC Members are in the top ten of proven oil reserves. Additionally, it can be seen from this table that Middle East countries provide most of the crude oil reserves. Also, the right side of Table 2 shows the ten countries with the highest oil production in the world in 2014. In this ranking, United States, Saudi Arabia and Russia are the main oil producers with about 65% of the oil production. Some OPEC countries are among the main oil producers.

Table 2. The top countries with the biggest crude oil proved reserves in 2015 and total oil supply in 2014.

COUNTRY		CRUDE OIL RESERVES IN 2015 [billion barrels]	COUNTRY	OIL SUPPLY IN 2014 [Millions barrels per day]
Venezuela	OPEC	298	United States	14021
Saudi Arabia	OPEC	268	Saudi Arabia	11624
Canada		173	Russia	10847
Iran	OPEC	158	China	4598
Iraq	OPEC	144	Canada	4383
Kuwait	OPEC	104	United Arab Emirates	3474
United Arab Emirates	OPEC	98	Iran	3377
Russia		80	Iraq	3364
Libya	OPEC	48	Brazil	2966
Nigeria	OPEC	37	Mexico	2812

Source: Adapted from (U.S. ENERGY INFORMATION ADMINISTRATION, 2016)

In the case of natural gas, Table 3 presents the top ten countries by the largest reserves in 2015 and those by the greatest production in 2014. Russia and Iran are the most significant contributors to the proved reserves of natural gas with about 55% of the total proven world reserves. Also, OPEC countries have an important participation in the ranking of countries with the largest reserves. It can be seen from the right side of the Table 3 that United States and Russia lead the global natural gas production with around 65% of the total supply. It is interesting to note that OPEC countries are not among the main five natural gas producers.

Table 3. The top countries with the biggest proved reserves of natural gas in 2015 and natural gas production in 2014.

COUNTRY		PROVED RESERVES OF NATURAL GAS In 2015 [trillion cubic feet]	COUNTRY	NATURAL GAS PRODUCTION In 2014 [billion cubic feet]
Russia	OPEC	1688	United States	25728
Iran	OPEC	1201	Russia	20437
Qatar		872	Canada	5338
Saudi Arabia	OPEC	294	China	4291
Turkmenistan	OPEC	265	Norway	3976
United Arab Emirates	OPEC	215	Saudi Arabia	3616
Venezuela	OPEC	197	Algeria	2942
Nigeria		180	Netherlands	2481
China	OPEC	164	Australia	2215
Algeria	OPEC	159	Mexico	1603

Source: Adapted from (U.S. ENERGY INFORMATION ADMINISTRATION, 2016)

The offshore production is very promising for the global oil and gas industry as it has expanded the source of hydrocarbon resources to meet increasing energy demand. The first offshore exploration and production initiative began as an extension of onshore fields at Summerland, California, in 1897 (RAYMOND; LEFFLER, 2006). Offshore production began in 1947 when the first productive well was drilled in the Louisiana coast in approximately 66 m of water. Technological improvement and adaptation began to create comfortable conditions in the oil industry that allowed the operation and expansion in offshore environments (NATIONAL COMMISSION ON THE BP DEEPWATER HORIZON OIL SPILL AND OFFSHORE DRILLING, 2010). Then, fixed platforms were built as the depths increased to 100 feet, but when in the Gulf of Mexico, the water depth was between 100 and 400 feet, the first jack-up rigs were implemented to guarantee the demand for drilling equipment. In 1961, the first-semi submersible platform was built and, since then, many platforms in floating mode were put into operation (OFFSHORE ENERGY TODAY, 2010). Offshore industry may use different structures depending on variables such as size, water depth and localization (SHELL, 2011). Fixed platforms were initially built for offshore exploration and production. Other types of offshore platforms such as Tension Leg Platforms (TLPs), Spars, and Semi-Submersible platforms, have been used to extract hydrocarbons in deeper waters, but Floating Production Storage and Offloading (FPSO) vessels are a flexible

solution in order to expand the production at water depths from 200 to 2000 meters (DEVOLD, 2006).

Figure 2 presents current information on the number of offshore platforms in different fields in the world. As can be seen from this figure, Gulf of México has the highest number of platforms, followed by the North Sea. Brazil is in the seventh position in number of offshore rigs.

Approximately 30% of global oil production and 27% of world gas production is supplied by the offshore industry. This industry accounts for 20% of global estimated oil reserves and 30% of the world estimated gas reserves (PLANETE ENERGIES, 2015). Table 4 presents the five largest offshore oilfields in the world according to estimated recovery reserves. The three largest offshore oil fields are located in the Persian Gulf. As can be seen from this table, Lula reservoir in the Santos Basin in Brazil is a large oilfield in the pre-salt area and it is the fifth largest oilfield in the world. The production phase of the Lula field started in 2011.

Figure 2. Number of offshore rigs worldwide as of 2015, by region.

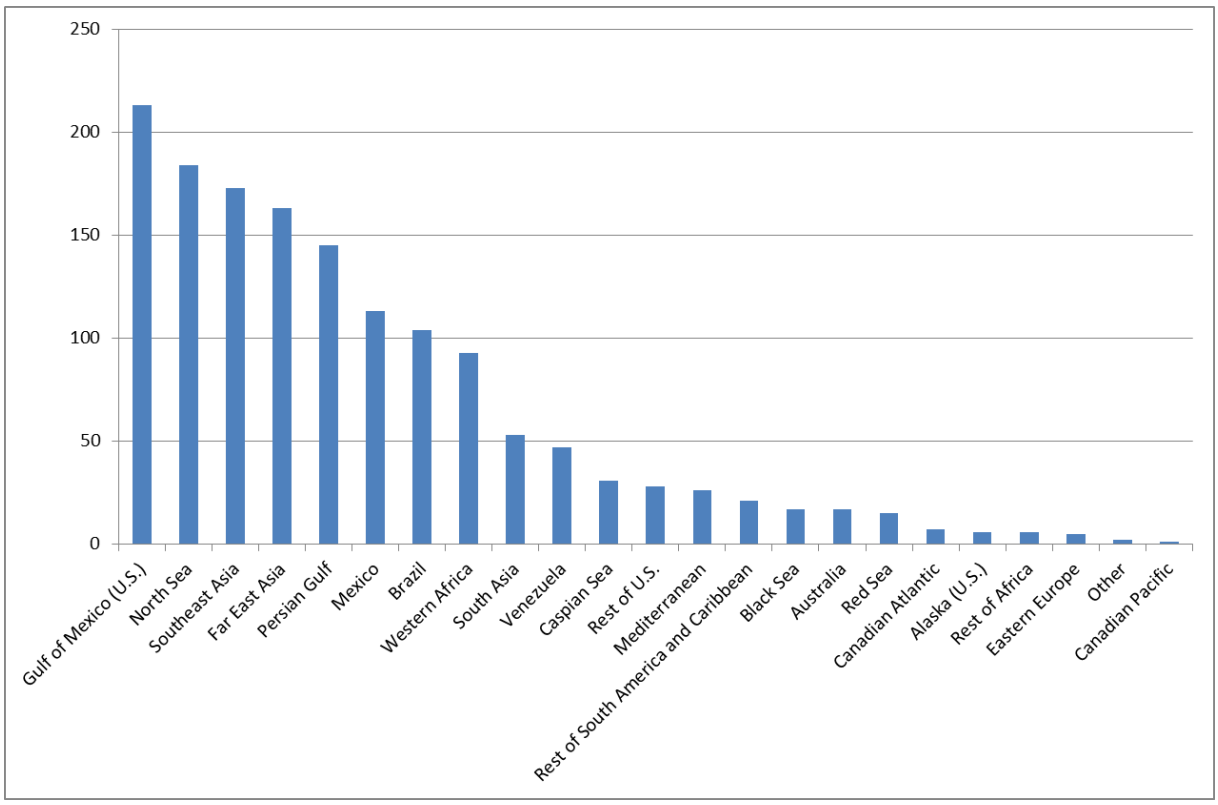

Source: www.rigzone.com

Table 4. Largest offshore oilfields in the world by the estimated recovery reserves in 2013.

OFFSHORE OIL FIELD	LOCALIZATION	RECOVERABLE OIL RESERVES [billion barrels]	DISCOVERY DATA
Safaniya	Persian Gulf Saudi Arabia	36	1951
Upper Zakum	Persian Gulf United Arab Emirates	21	1963
Manifa	Persian Gulf Saudi Arabia	13	1957
Kashagan	North Caspian Sea Kazakhstan	9	2000
Lula	Santos Basin Brazil.	6.5	2007

Source: www.offshore-technology.com

2.2 Floating Production Storage and Offloading (FPSO) unit

A primary petroleum processing plant consists of several operations used to separate crude oil into its gas, liquid and aqueous phases. A typical offshore platform has a processing plant where separation, treatment, compression and pumping processes are carried out, and a utility plant where power and heating required in the processing plant are produced. In the processing plant, the separation process is an important operation and its performance may be affected by several factors: well-fluid flow rates, operating pressures and temperatures, fluid properties, final product specifications, among others (ARNOLD; STEWART, 1998).

In the processing plant, separated gas, oil and water require specific treatment operations to guarantee the production specifications. Gas is scrubbed, dehydrated and compressed to be used for fuel, injection or exportation. Produced oil passes onto the separation processes where water is removed, and then the oil may be stored, transferred or exported. Separated water is treated for removing the emulsified oil before disposal at sea. All oil productions operations are coupled in a complex and well-structured processing plant to meet different demands of the production process. Figure 3 shows a scheme of the typical and optional operations in the processing plant of a standardized FPSO unit. In the processing plant crude from subsea wells enters in the separation train, which has two separation stages: high and low pressure. Separated gas goes to the several treatment processes such as compression and dehydration in order to be injected, exported or used as gas lift. Separated oil is subjected to a set of treatments to ensure the final specifications. Drain water from separation equipment is

treated to be discharged to the sea. Additionally, sea water may be treated to be injected in the wells.

Figure 3. Standardized FPSO processing scheme.

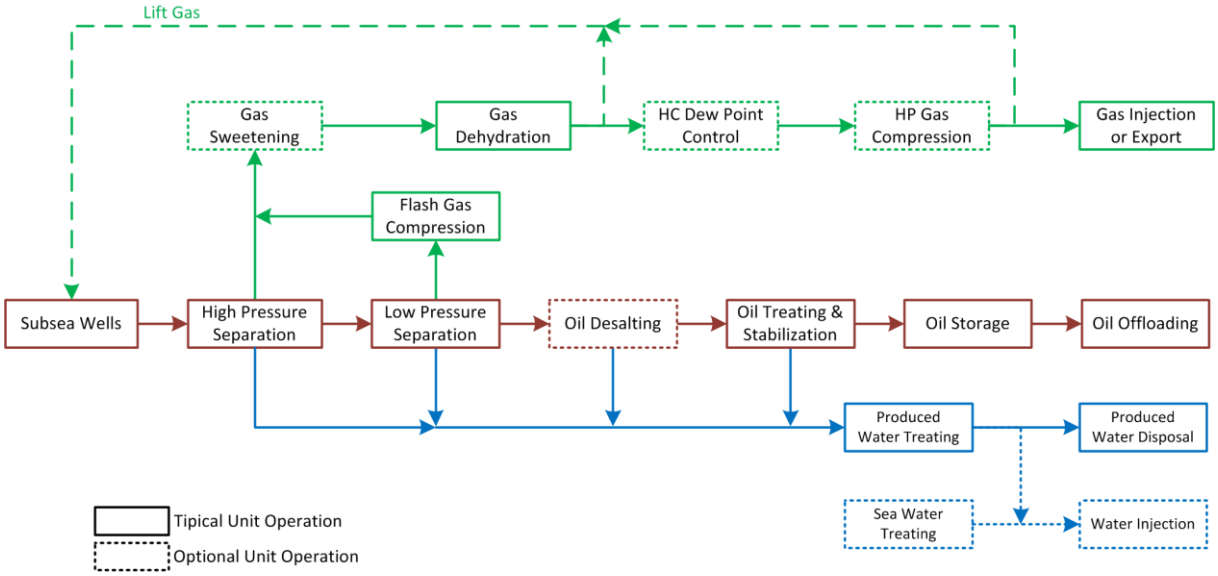

Source: Adapted from (MUELLER; ROOBAERT, 2008)

The utility plant consists of several systems: power generation system, sea water lift system, cooling water system, hot water system, water injection system and fuel gas system, among others. The number and complexity of these systems vary depending on the well-fluid and the product requirements. In offshore industry, electric demand is commonly supplied by gas turbine packages. Depending on the application, compressors and pumps may be driven by gas turbines. Another alternative for generation are diesel generation sets. The typical capacity range of offshore gas turbines is between 1-50 MW (WALL; LEE; FROST, 2006), but the increasing development of offshore production activities indicates that the power demands may exceed 100 MW. The hot water system is utilized to supply heat requirement of distinct consumers. Production heaters are the main heat consumers in a typical FPSO. Other hot water consumers are the gas dehydration system and CO_2 removal unit. The cooling water system supplies the cooling water to classified and non-classified areas. The heat exchangers and compressors are the main energy consumers in the classified area of an offshore platform. The water injection systems consist of a treatment process and pumps to inject water in the well and to enhance the oil recovery. The fuel gas system allows for treatment the gas fuel prior to the gas turbines. The fuel gas may be heated and permeated in the CO_2 removal unit

for its final use. Figure 4 shows the topside of the FPSO Cidade de Paraty operating in Santos Basin in Brazil.

Figure 4. FPSO Cidade de Paraty in Santos Basin-Brazil.

Source: Steferson Faria / Banco de Imagens Petrobras [online]. Available from: http://www.petrobras.com.br/infograficos/tipos-de-plataformas/desktop/index.html#

2.3 Offshore industry in Brazil

Exploration operations in Brazil have identified significant reserves potential for developing offshore petroleum resources, especially in the pre-salt area in the Santos Basin. At present, the offshore production constitutes more than 91% of the Brazil´s total oil production, and the post-salt production is the main contributor to domestic oil production. Pre-salt area, discovered in 2007, is characterized by a ultra-deep oil field with water depth around 2200 m and a layer of salt that reaches about 2000 m in thickness (FORMIGLI, 2007).

Most FPSOs have been installed and new facilities may be implemented in the pre-salt area, and this is projected to boost the Brazilian oil production. In the period from 2009 to 2013 US$ 174.4 billion were invested in the Brazilian oil and gas sector. This has allowed for the inclusion of 63 new vessels and platforms in the offshore structure. Although these technological developments suggested some years ago that the Brazilian offshore industry would grow significantly, recent economic difficulties and corruption scandals involving Petrobras have decreased these optimistic expectations (OFFSHORE CENTER DENMARK, 2009; U.S. ENERGY INFORMATION ADMINISTRATION (EIA), 2015). Even so, in the

last years, the production of liquid fuels in Brazil has increased due to the operation of four new FPSOs: P-62, P-58, Cidade de Ilhabela, and Cidade de Mangaritiba (U.S. ENERGY INFORMATION ADMINISTRATION (EIA), 2015).

Several operators handle the production activities in Brazil. Petrobras is the main company involved in the upstream activities. Some foreigner operators are also present in the production operations: Royal Dutch Shell, Chevron, Repsol, BP, Anadarko, El Paso, Galp Energia, Statoil, BG Group, Sinopec, ONGC, TNK-BP, among others. In 2007, Tupi field in Pre-salt oilfield was drilled by a consortium of Petrobras, BG Group, and Petrogal, and the production capacity is estimated to 5-8 billion barrels. After Tupi field, others field were found in Santos Basin (U.S. ENERGY INFORMATION ADMINISTRATION (EIA), 2015).

As shown in Figure 2, Brazil has 104 offshore oil rigs. Table 5 presents some offshore platforms operating in Brazil. Recent Brazilian FPSOs projected to operate in some pre-salt fields in the Santos Basin are designed for a production capacity of 150000 barrels/day (23848 m^3/day) of oil and 6 million of cubic meter per day of gas.

Table 5. Details of some Brazilian FPSOs.

Name	Oil Production [barrels/day]	Gas Production [million m^3/day]	Water depth [m]	Field Location
Cidade Angra dos Reis[a]	100000	5	2149	Tupi Field
Cidade de Caraguatatuba[a]	100000	5	2100	Carioca Field
Cidade de Campos dos Goytacazes[a]	150000	5	765	Tartaruga Verde and Tartaruga Mestiça
Cidade de Itaguaí[a]	150000	8	2240	Iracema
Cidade de Mangaratiba	150000	8	2200	Iracema
Cidade de Niteroi[a]	100000	3.5	1400	Jabuti
Cidade de Santos[a]	35000	10	1300	Urugua/Tambau
Cidade de São Paulo[a]	120000	5	2140	Guara
Cidade de Rio de Janeiro[a]	100000	2.5	1350	Espadarte Sul
Fluminense[a]	81000	2	740	Bijupira-Salema
Cidade de Maricá[b]	150000	6	2120	Lula
Cidade de Saquarema[b]	150000	6	2200	Lula
Cidade de Paraty[b]	120000	5	2120	Lula
Espirito Santo[b]	100000	1.4	1780	Parque das Conchas

Source: Adapted by author. Data for [a] from <http://www.modec.com/fps/fpso_fso/>, for [b] from <http://www.petrobras.com.br/fatos-e-dados/busca/?q=fpso>.

2.4 Exergy based analyses and its application to offshore platform

This section presents a review of the literature dealing with exergy analyses applied to offshore platforms. Although the exergy analysis has not been strongly used in the offshore industry, in recent years, there has been an increase in the amount of literature on exergy studies performed to assess the performance of offshore platforms. Not many studies have been developed and published from the first exergy application to an offshore platform published in 1997 in comparison with the growth that is observed in other productive sectors. However, it is still important to highlight the contribution of these studies in the development of research on the application of exergy to offshore industry. It should also be noted that the concept of exergy is barely mentioned in one of several documents produced by the oil and gas industry (INTERNATIONAL ASSOCIATION OF OIL AND GAS PRODUCERS; THE GLOBAL OIL AND GAS INDUSTRY ASSOCIATION FOR ENVIRONMENTAL AND SOCIAL ISSUES, 2013). This document mentions only that the exergy could be considered to take into account the quality of products and resources where energy performance is evaluated.

According to the literature, the first exergy study applied to an offshore installation was developed by Oliveira and Van Hombeeck (OLIVEIRA JR; VAN HOMBEECK, 1997) in the University of São Paulo with support from Petrobras. They performed an exergy analysis of petroleum separation processes of a typical Brazilian offshore platform. This study concluded that heating operations in petroleum separation processes are the main exergy consumers of the plant. This study was made by using the process simulator HYSIM.

In recent years, there has been an increasing amount of literature on the exergy analysis applied to offshore platforms. Nearly a decade later, the research on the subject was retaken by different works developed at the Norwegian University of Science and Technology with support from Statoil ASA. In 2010, Voldsund et al. (VOLDSUND et al., 2010) applied the exergy analysis method to a North Sea oil platform. The oil platform was divided in two systems: process plant and power plant, but only the processing plant was analyzed. The study found that the platform has an irreversibility of 12 MW and it is allocated as follows: 20% in the separation train, 11% in the gas re-compression train, 66% in the gas injection trains, and 3% in the oil export section. According to these results, the injection train was identified as the best place to reduce the destroyed exergy of the platform. The exergy efficiency of the

process plant was about 36%, but the efficiency of the whole plant was not calculated. Processes were simulated using Aspen HYSYS®.

In 2012, Voldsund et al. (VOLDSUND et al., 2012) pursued the previous work and performed a study to assess the oil and gas processing platform on a real production day by using exergy analysis, obtaining more realistic results. Three cases were defined: a first case including anti-surge system, a second case with increased compressor efficiencies, and a third case without anti-surge system. Additionally, the work included also the fuel gas treatment process and the anti-surge control of the compressors. The following exergy parameters were used to evaluate the process performance: power consumption, destroyed exergy, product exergy, specific power consumption and exergetic efficiency. Simulations were made using Aspen HYSYS®. Results show that the processes that destroy more exergy are compression and cooling gas for injection. This result is similar to the one found in previous work. Comparison between the three cases shows that Case 1 is the worst scenario for the exergy parameters used, whereas Case 3 has the best parameters. This result confirms the negative effect of the anti-surge system and low compressor efficiency on the plant performance.

The previous study was complemented by Voldsund et al. (VOLDSUND et al., 2013a) and the results were published in 2013. The research presents a detailed assessment of the exergy analysis of the processing plant in the North Sea oil platform. In comparison with the previous work, this work included the production manifold system. Physical exergy variations are described and analyzed, and the gas stream to injection is identified as the major physical exergy carrier in the plant. The highest exergy destruction rate occurs in the reinjection train, followed by the production manifolds and the recompression system. Simulations were built with Aspen HYSYS®.

In 2013, new works were published by the Technical University of Denmark, International Research Institute of Stavanger, Norwegian University of Science and Technology, and Statoil ASA.

Nguyen et al. (NGUYEN et al., 2013) described a generic model of the overall offshore and presented a comparative analysis of an offshore platform with six cases of study. These cases have similar processes and operating conditions but different reservoir fluid compositions and loads. The model included power generation, oil and gas processing, and seawater injection

sub-models. Processes were simulated using Aspen Plus®. This work showed higher exergy destruction on the utility system than on the processing plant. In the processing plant, the largest exergy destruction occurs in the production manifold and in the gas compression systems, meanwhile, in the utility system, the largest irreversibility occurs in the combustion chamber. The rejection of high-temperature gases from the utility is the major contributor to the exergy losses. They compared their results with results obtained by Oliveira and Van Hombeeck (OLIVEIRA JR; VAN HOMBEECK, 1997) and concluded that offshore platforms located in different regions may considerably differ due to their process and characteristics.

Voldsund et al. (VOLDSUND et al., 2013b, 2014) carried out a comparative study of the sources of exergy destruction on four North Sea oil and gas platforms. Operation conditions for the four platforms are different. These operation conditions are: reservoir temperature and pressures, feed GOR and WOR ratios, feed properties, product specifications and recovery strategies. Generalized overview of the studied platforms includes the following systems: production manifold, separation train, oil/condensate treatment, recompression train, gas treatment, condensate treatment, fuel gas system, produced water treatment, and seawater injection. Platform A has operated for 20 years. Oil is exported nearby platforms and gas is injected into the wells. Water from other platform is injected as a recovery strategy, but this system was not considered in the analysis. Platform B has been in operation for 10 years and has high reservoir temperature and pressure. Produced water is injected for disposal. Gas is exported, and there is low compression power demand. Platform C has also been in operation for 10 years. The separation process requires oil heating after the first separation stage. Gas lifting and gas injection are used to enhance the oil recovery, and a part of this gas is imported. Platform D has been operated for 20 years. Gas, oil, and condensate are exported. The separation process uses heating, and gas and condensate requires dehydration treatment. Gas lifting and gas injection are also utilized to improve the oil recovery. The process simulations were carried out with Aspen HYSYS® for platforms A-C and with Aspen Plus® for platform D. The study found that the sum of power and heat exergy consumption is less than 2% of the exergy content of the exported products. Power is mainly used for re-compression and compression processes, and specific power and heat exergy consumption (MJ/Sm^3o.e) is highest for Platform A, followed by Platform D, and finally by Platforms B and C. Regarding the destroyed exergy, production manifold represents 10%-24% of the total

exergy destruction in all platforms, while gas treatment system accounts 27%-57%, and 13%-29% of the exergy destroyed occurs in the recompression train.

Other interesting work was carried out in 2013 by Voldsund et al. (VOLDSUND et al., 2013c). This work introduced energy and exergy based performance indicators such as the *best available technologies BAT*, *specific energy use SEU*, *specific exergy consumption SEC*, *specific exergy destruction SED*, and *exergetic efficiency*, to assess the four oil and gas platforms studied in the work described above. Three exergetic efficiency equations were used to assess the overall platform performance. It is interesting to note that this work does not consider the exergy efficiency expression (rational efficiency) for a separation process defined by Kotas (KOTAS, 1995). Simulations were performed in Aspen HYSYS®. Results show that Platform A has the highest *specific energy use* (667 MJ/Sm^3o.e), followed by Platform D (371 MJ/Sm^3o.e), Platform C (136 MJ/Sm^3o.e) and Platform B (20 MJ/Sm^3o.e). Regarding the *specific exergy consumption*, the results are similar to *specific energy use*. Results of *specific exergy destruction* indicates that Platform A has the highest value (162 MJ/Sm^3o.e), followed by Platform D (84 MJ/Sm^3o.e), Platform B (17 MJ/Sm^3o.e), and Platform C (20 MJ/Sm^3o.e). Exergetic efficiencies give different results and conclusions depending on the equation used, which indicates that a comparison of exergy performance based on exergetic efficiency metric should be made with care. *Input-output* exergetic efficiency equation gives values of performance within 99.4%-99.9%, while the exergetic efficiency calculated with Rian and Ertesvåg model ranges from 50% to 84%. Low exergetic efficiency values are reported for the equation proposed by Tsatsaronis, and the platform performance is within 2% to 46%.

In 2013, at the Federal University of Santa Catarina-Brazil, an exergy analysis for the waste heat recovery in offshore platforms was performed by Barrera, Sahlit and Bazzo. (BARRERA; SAHLIT; BAZZO, 2013). Energy and exergy balances were carried out in order to identify possible uses for recovered energy. In addition to the base case, three scenarios were used to recovery the waste heat: first scenario is used to generate power, the second one is utilized to supply cold to the plant, and the third one is used for simultaneous generation of power and cold. The plant includes separation, gas compression, oil pumping, and gas turbine systems. Results showed that 80% of the exergy is destroyed in the gas turbine, where the combustion process accounts 31.9% of the exergy destruction. The calculation of the overall exergy efficiency for the base case and the three established scenarios was made by using the

degree of perfection equation proposed by Szargut (SZARGUT, 1988). High exergy efficiencies were obtained: 96.25% for base case, 96.75% for Case 1, 96.32% for Case 2, and 96.79% for Case 3. No more exergy details were analyzed in this work.

Nguyen et al. (NGUYEN et al., 2014b) investigated the applicability of *pinch*- and *exergy-based* methods for evaluating the life efficiency of oil and gas platforms. They analyzed a North Sea platform by comparing three lifetime stages: early-life, plateau, and end-life. The platform was simulated using Aspen Plus®. Results indicate that exergy destroyed in the platform is 65 MW for early-life, 64 MW for plateau, and 58 MW for end-life. The utility plant presents higher exergy destruction in comparison with the processing plant. In the utility plant, most exergy destruction takes place in the gas turbine, while in the processing plant the distribution of destroyed exergy per system varies considerably, and most destroyed exergy occurs in the production manifolds and gas treatment processes for the start-life of the field. Total exergy losses of the platform are higher in the end-life of the field due to the increment of the produced water and the diminishing of the heat requirements, which increments the gas exhaust temperature. The specific exergy destruction SED is about 70, 50 and 210 kWh/Sm^3o.e for early-life, plateau, and end-life stages, respectively.

A work published in 2014 by Nguyen et al. (NGUYEN et al., 2014a) reviewed and studied different definitions of exergy efficiency for petroleum systems and, specifically, its application to offshore platforms. This work studied in more detail the exergy efficiency calculations and analysis performed in (VOLDSUND et al., 2013c). High chemical efficiency of hydrocarbons has a noticeable influence in the exergy efficiency models. Exergy efficiency models were applied to four oil platforms operating at different conditions. The analyzed oil and gas offshore platforms are the same ones as studied in (VOLDSUND et al., 2013b). The model of exergy efficiency suggested by Kotas for separation process gives the following results: Platform A: 12.7%, Platform B: -215%, Platform C: 20.6%, and Platform D: 23.6%. Other model results were presented in (VOLDSUND et al., 2013c). They concluded that the conventional efficiency definitions present low sensitivity to efficiency improvements, calculation inconsistences or applicability limitations. Then, based on the fuel-product approach, they suggest a model of efficiency called *component-by-component* exergy efficiency. This model gave the following results: Platform A: 17.9%, Platform B: 1.7%, Platform C: 26.8%, and Platform D: 29.6%.

A study performed by Carranza and Oliveira (CARRANZA SÁNCHEZ; OLIVEIRA JR, 2014a, 2015a) compared the exergy performance of an offshore platform considering two configurations: Case 1 with CO_2 capture system, and Case 2 without CO_2 capture system. Simulated offshore platform was based on the plant studied by Oliveira and Van Hombeeck (OLIVEIRA JR; VAN HOMBEECK, 1997) and included processing plant and utility plant. Processing plant includes the separation train, oil pumping system, and gas compression train; and the utility plant consists of the gas turbine and CO_2 capture and storage systems. The CCS system was based on chemical absorption by monoethanolamine MEA solutions. This work assessed the destroyed exergy and exergy efficiency of the whole plant and its systems. Simulations were performed using Aspen HYSYS®. This study concluded that the implementation of the carbon capture system results in an increase of 37% in the plant exergy destruction and in a reduction of 77% in the CO_2 emissions. In the Case 1, separation train has the highest exergy destruction, followed by the destroyed exergy in the gas turbine and in the gas compression trains. In the Case 2, separation train is still the main system destroying exergy, followed by the carbon capture system and the gas turbine. Oil pumping systems has a low destroyed exergy and is negligible. The CO_2 reduction is penalized with a reduction in exergy efficiency of 2.8 points.

In 2014, Carranza and Oliveira (CARRANZA SÁNCHEZ; OLIVEIRA JR, 2014b) carried out a more detailed study of their previous work. They assessed the destroyed exergy in the different components of this offshore platform. Results indicate that, in the separation train, production heaters account for 19.6 MW (75%) of the destroyed exergy in this system. In the gas compression train, the destroyed exergy in compressors is 1.1 MW (35.7%) and in the gas coolers is 1.8 MW (56.6%) of the total destroyed exergy. The combustion chamber of the gas turbine presents the highest destroyed exergy of the gas turbine, 7.9 MW (79.2%). In the carbon capture system, the desorber destroys 8.3 MW of exergy (61.5%).

In 2014, Nguyen (NGUYEN, 2014) published its thesis which deals with the modelling, analyzing and optimization of offshore platforms taken into account energy and exergy concepts. Some results have already been discussed in this section. One of the conclusions of this thesis highlights the impact of the variation of field composition and operation conditions in the performance of the offshore platforms, and the difficulty to define generic improvements to increase the energy performance of the offshore installations.

In 2015, Carranza and Oliveira (CARRANZA SÁNCHEZ; OLIVEIRA JR, 2015b) assessed the performance of a floating, production, storage and offloading FPSO offshore platform. Analyzed FPSO platform has the field and operation features of a Santos Basin-Brazil offshore installation for oil production, and consists of the following systems: separation train, vapor recovery unit, main compressors, gas dehydration unit, CO_2 removal unit, gas export compressors, gas/CO_2 injection compressors, and gas turbine. In this study, an evaluation of the exergy performance of the FPSO is carried out and the main goal is to investigate the influence of three operating modes on the following criteria: exergy efficiency, specific exergy consumption, renewability exergy index, CO_2 emissions and CO_2 emissions normalized to exergy of the product streams of the plant. In the operational Mode 1 (maximum water/CO_2 in the well stream), all gas is sent through the bypass of the CO_2 removal system and it is injected into the production wells; in the Mode 2 (50% BS&W), part of the gas is treated in the CO_2 removal system to be exported, and the other part is injected in the production wells; and in the Mode 3 (maximum oil/gas in the well stream), all gas is exported and the removed CO_2 is injected in the well. Simulations of the processing and utility plants in the FPSO were carried out using the software Aspen HYSYS®. Results show that the power demand is 14.8 MW for Mode 1, 18.3 MW for Mode 2, and 44.2 MW for Mode 3. Exergy efficiency is 13.0%, 24.5%, and 23.9%, for Modes 1, 2, and 3, respectively. CO_2 emissions normalized to exergy of the product streams of the plant is 1.65 [kg_{CO2}/GJ_b] for Mode 1, 0.69 [kg_{CO2}/GJ_b] for Mode 2, and 0.65 [kg_{CO2}/GJ_b] for Mode 3. They concluded that operational mode 1 has the lowest exergy performance considering the performance indicators used in this study. Operational mode 3 has lower specific exergy consumption in comparison with the other modes. It indicates that the mode 3 might be the best exergy scenario for the operation of the FPSO.

Barrera, Bazzo and Kami (BARRERA; BAZZO; KAMI, 2015) investigated the exergy performance analysis of a Brazilian FPSO and the use of Organic Rankine Cycles ORCs as strategy for recovering the heat in the exhaust gases of the gas turbines. The studied plant includes separation train, gas compression train, oil export system, and gas turbine system for the power generation. The exergy efficiency of the plant is calculated as 12.5%, and the energy consumption per standard cubic meter of exported oil is 19.44 MJ/m^3. An analysis of the exergy destruction within each subsystem shows the most of exergy is destroyed in gas turbines, followed by the separation plant, the gas injection system, and the water injection system. The integration of ORC in the FPSO showed an increment in the exergy efficiency of

about 14%-20%. They concluded that ORC integration may have a great potential for savings in fuel consumption.

Carranza et al. (CARRANZA SANCHEZ et al., 2015) conducted an investigation into the energy and exergy performance of the systems of a FPSO operating in three production modes. The FPSO platform and operation modes used are the same as studied in (CARRANZA SÁNCHEZ; OLIVEIRA JR, 2015b). The power consumption, heat requirement, and thermal exergy were derived for the whole plant. Additionally, the distribution of power consumption, destroyed exergy, SED and exergy efficiency was evaluated for the different systems of the FPSO. Results showed that the main exergy-destroying processes (in descending order) are, for Mode 1: Main Compressors A, Main Compressors B, and Combined Compressors; while the ones for Mode 2 are Separation Process, Main Compressors A, and the injection sections of the Main Compressors B; and the ones for the Mode 3 are Main Compressors B, Separation Process, and Main Compressors A. The results show that it is not simple to predict a generic pattern to characterize the energy and exergy parameters of the systems in their operating modes. They concluded, among other things, that Mode 3 has the highest power, heat and thermal exergy consumption, while Mode 1 has the highest *specific exergy destruction* indicator for FPSO, which leads to conclude that the metric plays an important role in the FPSO assessment.

Ortiz and Gallo (ORTIZ; GALLO, 2015) applied the First and Second Law of the Thermodynamics to analyze the CO_2 compression system in a FPSO. They also implemented the gas turbine model in order to study the power demand of the compression train. Simulations were performed using Aspen HYSYS® and gas turbine characteristics were obtained from Thermoflex® database. Three different well-fluid compositions for different stages of the field were assessed. Irreversibilities and exergy efficiency were calculated for compressors, heat exchangers and gas turbine. Results indicate that gas turbines are the main exergy destructors, while compressors and heat exchangers irreversibilities are about a third part of the gas turbines exergy destruction. Total destroyed exergy is 65.1 MW, 68.4 MW, and 60.3 MW for Cases 1, 2, and 3, respectively. Exergy efficiency for compressors varies significantly for the three cases.

Table 6 summarizes some results of the previous literature review.

Table 6. Summary of the literature review related to exergy application to offshore platforms.

Authors/year	Description	Results
Oliveira and Van Hombeeck 1997	Analyzed offshore plant: separation, compression and pumping systems.	Useful exergetic effect: 4.4 MW Exergy efficiency: 9.7% Exergy consumption in heating operations in the separation process is very important.
Voldsund et al. 2010	Analyzed offshore plant: process plant (separation, re-compression and injection trains, and export pumping).	Destroyed exergy in process plan: 12 MW Exergy efficiency of process plant: 36% Injection train is the main exergy destructor in the platform.
Voldsund et al. 2012	Analyzed offshore plant: separation, re-compression and injection trains, and export pumping, fuel gas system and anti-surge system. Case 1: reference, Case 2: increased compressor efficiencies, Case 3: No anti-surge system	Power Consumption [MW]: *Case 1: 23.9, Case 2: 23.1, Case 3: 20.3* Destructed Exergy [MW]: *Case 1: 16.1, Case 2: 15.5, Case 3: 12.6* Exergetic Efficiency [%]: *Case 1: 32, Case 2: 33, Case 3: 38*
Voldsund et al. 2013a	Analyzed offshore plant: separation, re-compression and injection trains, and export pumping, fuel gas system and production manifold.	Exergy efficiency: 13% Specific exergy consumption: 179 kWh/Sm^3 Power Consumption [MW]: 23.8 Destroyed Exergy [MW]: 20.7
Nguyen et al. 2013	Analyzed offshore plant: production manifold, separation, oil pumping and export, gas recompression and purification, gas compression and exportation, waste water treatment, seawater injection, power generation and heat recovery, HVAC, miscellaneous utilities.	Destroyed exergy [MW]: between 68 and 84 Largest exergy destruction system: gas turbine and water recovery system with 62-65% Specific exergy destruction [MJ/t_{rf}]: 253-670
Voldsund et al. 2013b, 2014	Analyzed offshore platforms: Platform A, Platform B, Platform C, Platform D. Analyzed offshore systems: production manifold, separation train, oil and condensate treatment, recompression train, gas treatment, condensate treatment, fuel gas system, produced water treatment, and seawater injection.	Exergy exported [MW]: Platform A: 1400, Platform B: 11000, Platform C: 12600, Platform D: 2190 Power exergy consumption [MW]: Platform A: 24.6, Platform B: 5.5, Platform C: 29.8, Platform D: 23.3 Heat exergy consumption [MW]: Platform A: 0, Platform B: 0.3, Platform C: 4.7, Platform D: 0.9 More than 27% of exergy destruction takes place in the gas treatment system. At least 16% of exergy destruction occurs in the manifold production system.
Voldsund et al. 2013c	Analyzed offshore platforms: Platform A, Platform B, Platform C, and Platform D from Voldsund et al. 2013b	*SEU* [MJ/Sm^3o.e]: Platform A: 667, Platform B: 20, Platform C: 136, Platform D: 371 *SED* [MJ/Sm^3o.e]: Platform A: 162, Platform B: 17, Platform C: 20, Platform D: 84

Table 6. Continued

Authors/year	Description	Some results
Barrera et al. 2013	Analyzed offshore platform: Base case: separation, compression, oil pumping, and gas turbine systems. Case 1: HR for power generation Case 2: HR for cold supplying Case 3: HR for power and cold	Exergetic Efficiency [%]: *Base Case: 96.25, Case 1: 96.75, Case 2: 96.32, Case 3: 96.79*
Nguyen et al. 2014a	Analyzed offshore platform: North Sea platform in early-life, plateau, and end-life stages.	Well-streams exergy [MW]: Early-life: 10700, Plateau: 14900, End-life: 3800 Exported exergy [MW]: Early-life: 9620, Plateau: 14100, End-life: 3940 Destroyed exergy [MW]: Early-life: 65, Plateau: 64, End-life: 58 SED [kWh/Sm^3o.e]: Early-life: 70, Plateau: 50, End-life: 210
Nguyen et al. 2014b	Analyzed offshore platforms: Platform A, Platform B, Platform C, and Platform D from Voldsund et al. 2013b	Exergy efficiency [%]: *Component-by-component* model: Platform A: 17.9, B: 1.7, C: 26.8, D: 29.6 *Tsatsaronis and Cziesla* model (on mass basis): Platform A: 48.1, B: 39.0, C: 53.9, D: 38.8 *Cornelissen-Rian-Ertesvåg* model: Platform A: 70.9, B: 84.2, C: 71.0, D: 33.2 *Kotas* model: Platform A: 12.7, B: -215, C: 20.6, D: 23.6
Carranza and Oliveira 2014a, 2015a	Analyzed offshore platform: separation, compression, pumping and gas turbine systems. Case 1: with CCS and Case 2: without CCS.	Destroyed exergy [MW]: Case 1: 39.0, Case 2: 53.5 Exergy efficiency [%]: Case 1: 12.1, Case 2: 9.3 Separation train exergy destroyed [MW]: Case 1: 27.1, Case 2: 26.2 CCS exergy destroyed [MW]: Case 1: -, Case 2: 14.1
Carranza and Oliveira 2014b	Analyzed offshore platform: Case 2 from Carranza and Oliveira 2015	Main exergy destruction by component In decreasing order [MW]: Separation train: Heaters, supplementary burner, mixers. Gas compression train: coolers, compressors, mixers. Gas turbine: combustion chamber, turbine, compressor, mixer, generator. CCS: Desorber, Cooler-6, absorber, Cooler-5, heat exchanger. CO_2 compression and pumping train: Coolers, compressors, pump.
Carranza and Oliveira 2015b	Analyzed offshore platform: FPSO in three operational modes. Systems: separation train, vapor recovery unit, main compressors, gas/CO_2 injection compressors, gas export compressors, gas turbine.	Exergy efficiency [%]: Mode 1: 13.0, Mode 2: 24.5, Mode 3: 23.9 SEC_{volume} [MW/Sm^3o.e]: Mode 1: 898, Mode 2: 434, Mode 3: 411 Normalized CO_2 emissions [kg_{CO2}/GJ_b]: Mode 1: 1.65, Mode 2: 0.69, Mode 3: 0.65
Barrera, Bazzo and Kami 2015	Analyzed offshore platform: FPSO Systems: separation plant, gas boosting, gas injection, gas turbines, and seawater.	Exergy efficiency [%]: ORC not incorporate: 12.5% ORC incorporate: 12.5%-14.5% SEU_{volume} saving: 15%-20%

Table 6. Continued

Authors/year	Description	Some results
Carranza et al. 2015	Analyzed offshore platform: FPSO in three operational modes. Systems: separation train, vapor recovery unit, main compressors, gas/CO_2 injection compressors, gas export compressors, gas turbine.	Main exergy destructors (in descending order): Mode 1: Main Compressors A, Main Compressors B, and Combined Compressors. Mode 2: Separation Process, Main Compressors A, and the injection section of the Main Compressors B. Mode 3: Main Compressors B, Separation Process, and Main Compressors A.
Ortiz and Gallo 2015	Analyzed offshore platform: FPSO CO_2 compression and gas turbines systems	Destroyed exergy [MW]: Case 1: 65.1, Case 2: 68.4, Case 3: 60.3

Source: Compiled by the author

2.5 Carbon Capture and Storage (CCS) and its application to offshore platforms

A few research results have been published on application of carbon dioxide capture in offshore platforms. In 1997, Falk-Pedersen and Dannström (FALK-PEDERSEN; DANNSTRÖM, 1997) published their study on the separation of carbon dioxide from offshore gas turbine exhaust. They analyzed the heat recovery and power generation processes on an offshore platform. The research included the production of steam, the CO_2 capture and disposal system, and the flue gas for recycling. This study concluded that the amine process utilizing membrane is the best process to CO_2 capture; and the use of a combined cycle with 40% recycling of exhaust gas is the desirable alternative to generate power and to increase the CO_2 concentration entering the absorber.

Hetland et al. (HETLAND et al., 2009) performed a conceptual design study in order to assess the integration of a combined cycle power plant (540 MW_e) with a post-combustion CO_2 capture process operating in offshore conditions. This study emphasized the development of an optimized conceptual design within the structural constraints, and it assessed the relation between the capture unit efficiency and dynamic behavior induced by the sea. It was concluded that the gas separation system is accountable for nine percentage points of efficiency (fuel penalty) reducing the net power capacity to 450 MW_e (net electric efficiency: 45%).

Kvamsdal et al. (KVAMSDAL et al., 2010) developed a study on minimizing the process water consumption in a natural gas-fired power plant with post-combustion CO_2 capture process aimed at offshore operations. The results showed that the neutral water balance is

achieved by controlling the temperature in the top part of the absorber and minimizing the temperature variations in the absorber.

Some studies were found related to exergy analysis of CO_2 capture system. Petrakopolou et al. (PETRAKOPOULOU et al., 2012), Schach et al. (SCHACH et al., 2010) , Amrollahi et al (AMROLLAHI; ERTESVÅG; BOLLAND, 2011), and Yang and Zhai (YANG; ZHAI, 2010) have applied the exergy concept to study CO_2 capture technology in power plants: combined cycle power plants, coal-fired power plants and natural gas-fired power plant.

2.6 Motivation to the implementation of exergy analysis and carbon capture and storage system in offshore platforms.

Some aspects that highlight the motivation for the development of this research are presented in the following paragraphs. These aspects describe the contribution and novelty that this research presents in comparison with other studies.

A first aspect worth noting is that few studies have been developed in the application of exergy analysis for the study of offshore platforms. Similarly, there are a small number of studies focused on the capture and storage of CO_2 produced by power generation systems in the offshore industry. Additionally, even fewer studies have considered simultaneously these two topics for evaluating the performance of offshore oil and gas production facilities. This was an aspect that largely motivated the development of this research.

Secondly, existing studies on exergy analyses of offshore platforms have mainly focused on fixed platforms. Despite having similar systems of processing, FPSO offshore units are used for storing the produced oil, besides operating in locations that may be different from that of fixed platforms. These differences can impact the energy demand of gas injection, gas export or oil disposal processes, and hence, of the installation performance.

Thirdly, most reported studies on the issue of exergy analysis of offshore platforms have been for installations located in the North Sea. The FPSO studied in this work operates in Brazil, and it is characterized by other operating conditions: different composition of the well streams, different product specifications, and different modes of operation, mainly.

Finally, the oil and gas has established clear guidelines to encourage measurement and assessment of energy and environmental performance of their processing facilities, and then the integration of exergy analysis and capture and storage of CO_2 was identified as a line interesting to identify potential improvements for energy use and environmental impact mitigation on offshore platforms.

3 METHODOLOGY

In Figure 5, the general methodology used in this study is presented. This flow chart represents the thesis framework and workflow. The methodology includes the procedure to calculate the exergy and environmental performance, and finally, the analysis and discussion of the Reference FPSO and the FPSO with CCS.

Figure 5. Flow chart of the general methodology used in this study.

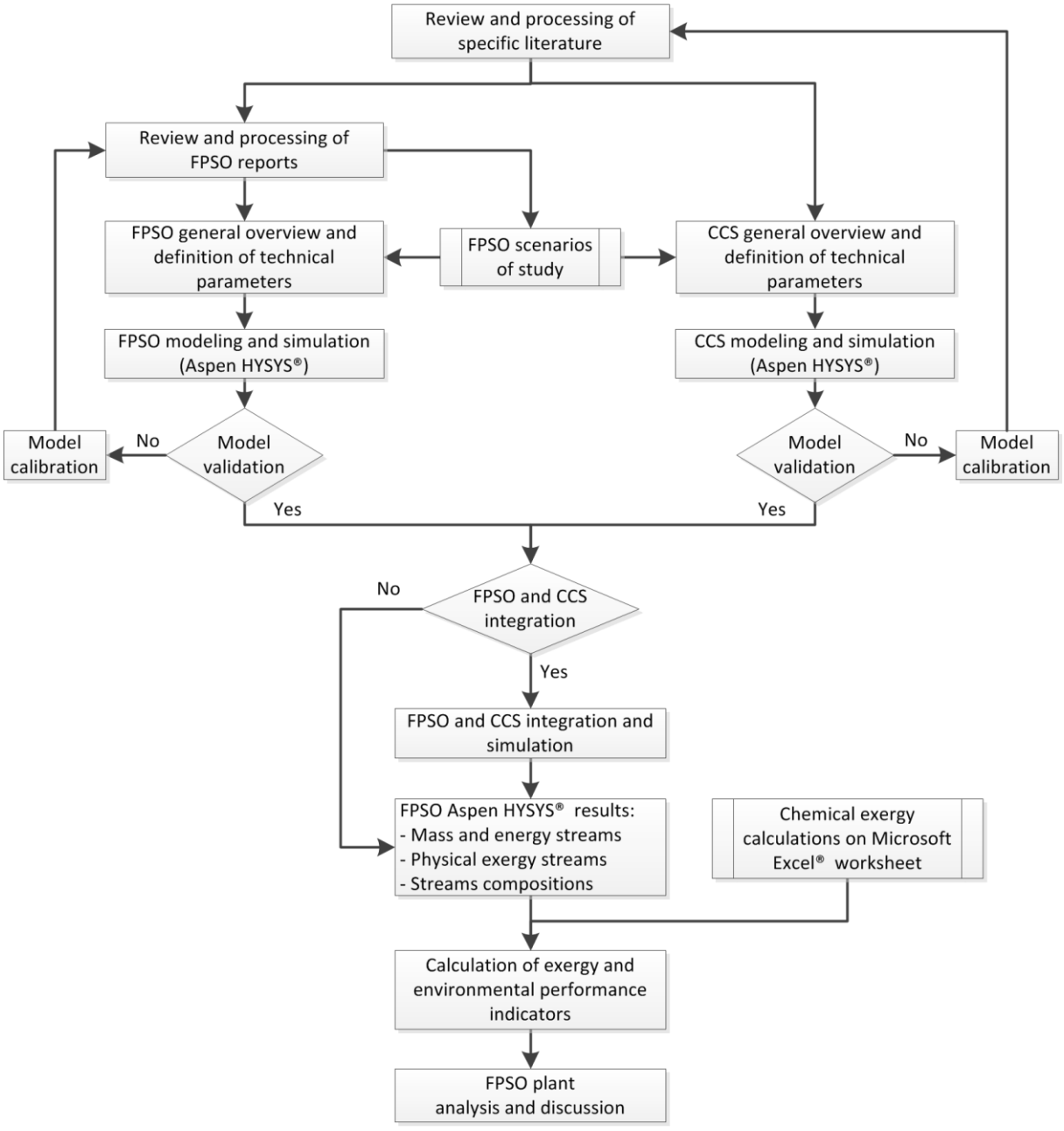

Source: Author´s elaboration.

The methodology begins by the specific literature review and processing in order to understand the surface operations in FPSO plants. According with Figure 5, specific literature is complemented by technical reports of the FPSO operator, hence, a general overview of the FPSO is made and its main technical parameters are defined (left side in Figure 5). Different scenarios of study are also established from the information of the technical reports. The following step is related to the developing of the FPSO model and its simulation. This last step was developed considering different details of the process as pressure losses and adjusting the minimum temperature differences in the heat exchangers, setting the minimum temperature of the gas cooled in coolers, among others. After modeling and simulation, the validation of the model is done by comparison with results of simulations developed by the operator of the FPSO. Similar steps were performed for modeling and simulation of the CCS system (right side in Figure 5). Depending on the analyzed scenario, FPSO integration with CCS was performed. This integration required detailed and manual iteration work to adjust the parameters of the two simulations, especially, adjusting the additional fuel in the CCS and the mass flow of the monoethanolamine solution to adjust the carbon capture efficiency value to 90%. Then, mass flow, energy, physical exergy, and composition data of different streams provided by Aspen HYSYS® were processed in order to calculate exergy and environmental performance indicator. An additional and manual routine for chemical exergy calculation was made by using an Excel® worksheet. Finally, the analysis and discussion of the FPSO performance were carried out.

3.1 The Reference FPSO

Figure 6 presents a simplified scheme of the Reference FPSO studied in this thesis. It includes a processing plant and a utility plant. The processing plant has basically a separation train and a compression system, whereas the utility plant has two gas turbines systems to supply the electric demand and the mechanical power for CO_2 compressors. Other systems such as the Hot Water System and the Cooling Water System were modeled and simulated. The molecular sieves of the gas dehydration system and the membranes of the CO_2 removal unit were not modeled in detail, and their operations were simplified to an ideal splitting process.

Flare and gas lift systems were not considered in this study. As can be seen in the Figure 6, gas, CO_2 or water may be injected to enhance the oil recovery or increase the oil production of the reservoir, methods commonly named Enhance Oil Recovery EOR, and substituted for the term Improved Oil Recovery IOR (ROSA; CARVALHO; XAVIER, 2006). A brief description of the different systems that make up the plant is presented in the next sections.

Figure 6. Simplified scheme of the FPSO reference plant.

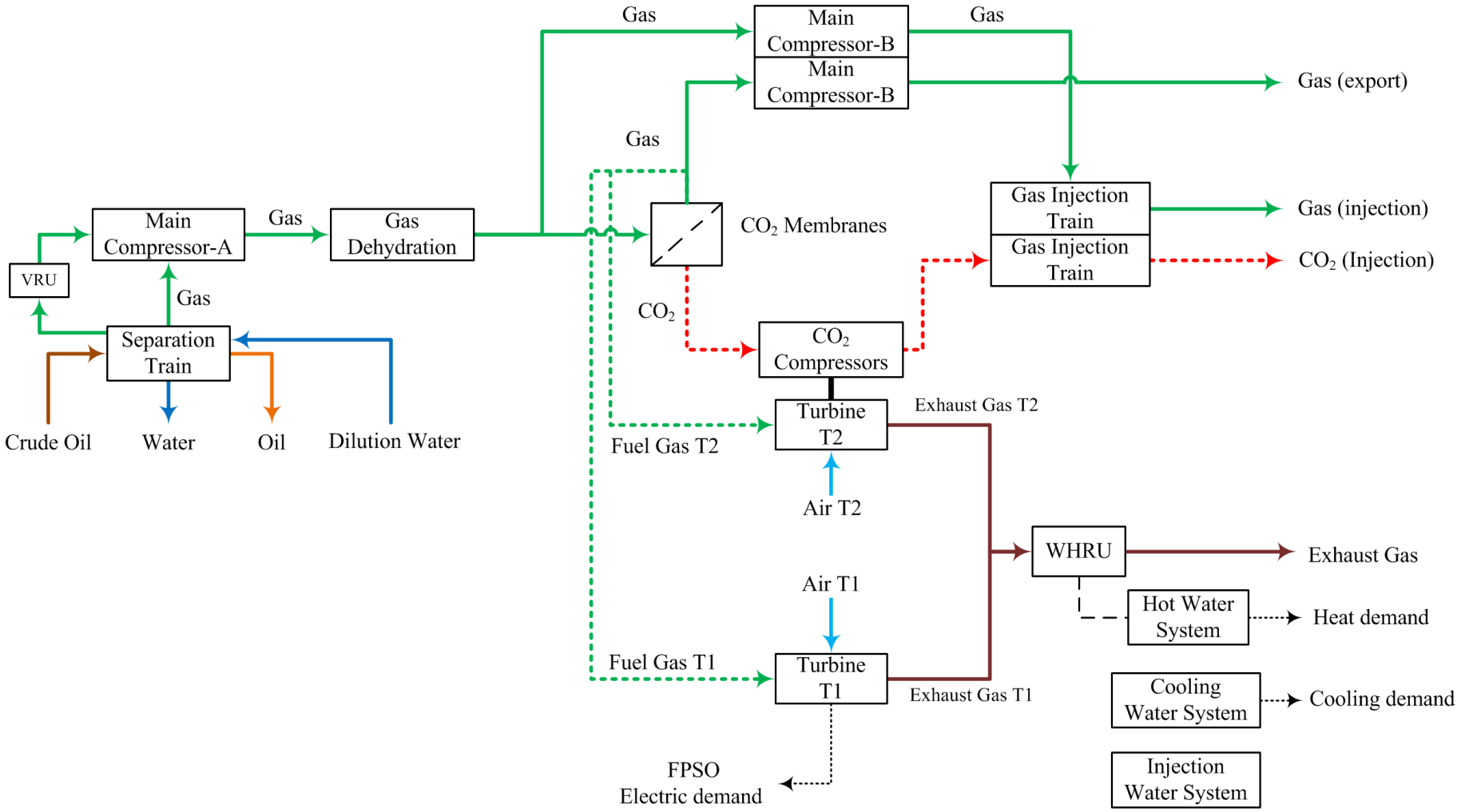

Source: Author´s elaboration.

3.1.1 Separation Train

In the *Separation Train*, the crude oil is separated into oil, gas and water. The oil is stored, the gas is treated and can be exported or injected, and the water is treated and rejected to the sea. Dilution water is used to improve the oil purity by the reduction of the salt content to a suitable low level. The separation train is composed of three separation stages. The first stage separates the three phases at approximately 20 °C and 1500 kPa, by means of a free-water knockout (*FWKO*) separator, which limits the processing capacity of the *FPSO* to 151000 bpd at standard conditions. The separated gas in the first stage is sent directly to the *Main Compressors A (MC-A).* The temperature of the separated oil from the first separator is increased by using two heaters. In the first heater, the oil stream is pre-heated through the treated oil from the third separation stage, and in the second heater, the oil is heated up to 90 °C through the hot water from the Hot Water System. The second separation stage is operating at 770 kPa. The gas separated in this stage is sent to the second stage of the *Vapor Recovery Unit VRU* to be compressed and routed to the *MC-A*. The oil stream from this separator is mixed with dilution water to increase the water content to 5% for allowing the oil desalinization (not simulated in details). The process in the third separation stage takes place at 236 kPa. The separated gas is sent to the first stage of the *VRU* and then is directed to the *MC-A*. The separated or processed oil is recirculated to heat the oil from the first separator, and finally, sent to the storage at 60 °C and 423 kPa. The separated water from the three separation processes is sent to discharge. A simplified scheme of the separation train is presented in Figure 7.

Figure 7. Simplified scheme of the separation train.

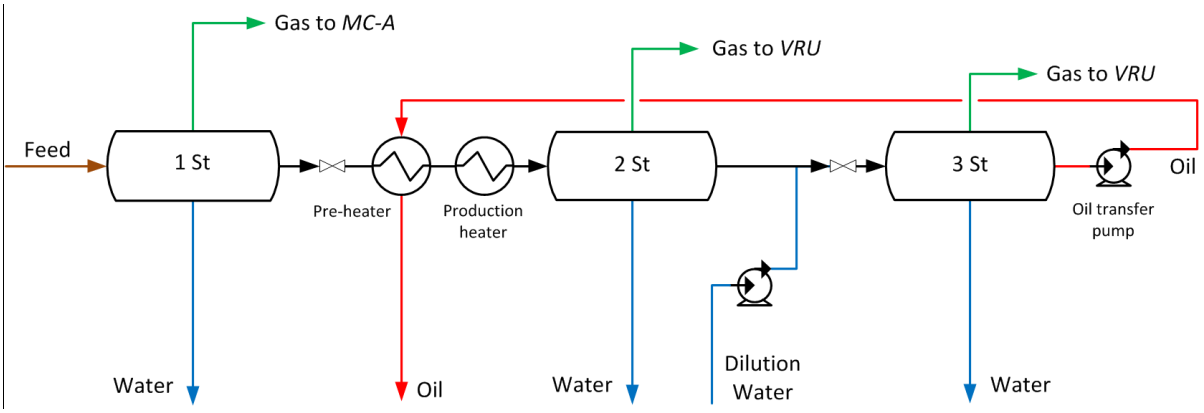

Source: Author´s elaboration.

3.1.2 Vapor Recovery Unit *VRU*

The *Vapor Recovery Unit* is used to recover the separated gas from the first and second stages of the separation train. *VRU* consists of two stage compressors with their corresponding cooling and scrubbing stages as presented in Figure 8. Scrubbers are two-phase separators used to recover liquids condensed in coolers. Gas from the second stage of the Separation Train enters the *VRU* at about 85 °C and 236 kPa, and the gas from the third stage is recovered at approximately 90 °C and 770 kPa. Temperature for the cooling stages is 40 °C. The final compression pressure is 1550 kPa and the gas is cooled at 40 °C and directed to the *MC-A*.

Figure 8. Simplified scheme of the *VRU*.

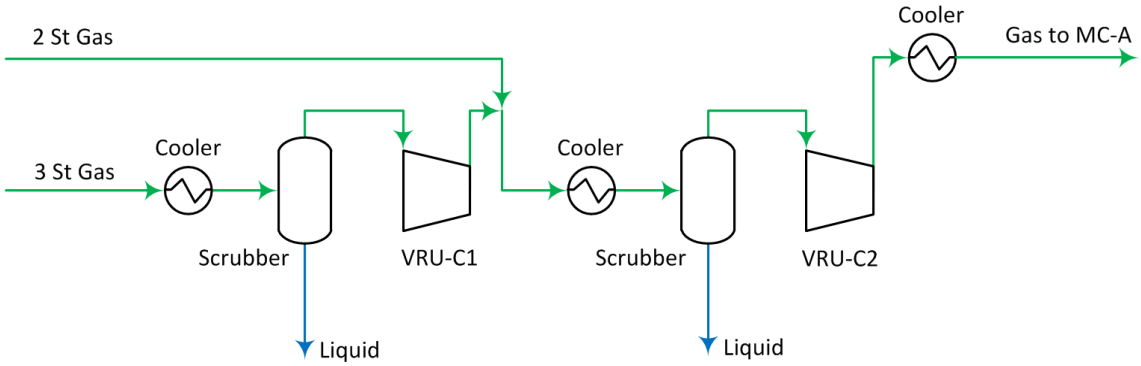

Source: Author´s elaboration.

3.1.3 Main Gas Compressors-A

Gas processing includes treatment and compression processes to meet operational and delivery specifications. A simplified scheme of the MC-A is shown in Figure 9.

Figure 9. Simplified scheme of the *MC-A*.

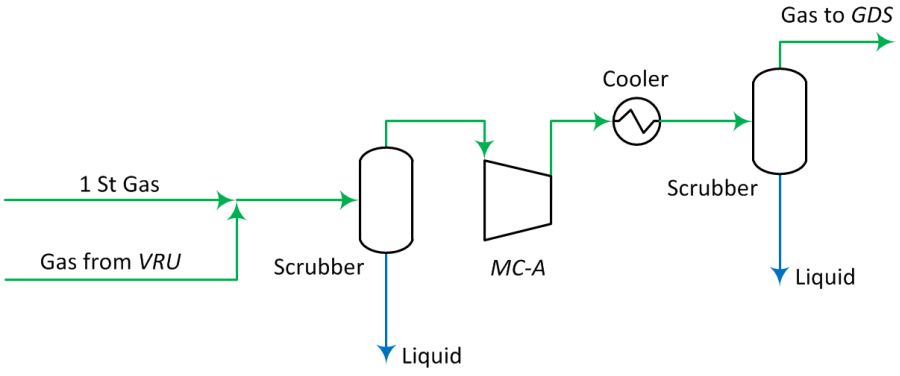

Source: Author´s elaboration.

First, gas from the first stage of the *Separation Train* and gas from *VRU* enters the Main Gas Compression Unit, specifically the *MC-A*. Before entering the compressors, the gas is treated in the scrubbers to remove any presence of liquid. The discharge pressure of these compressors is 7944 kPa, and then, the compressed gas is routed to the coolers to be cooled to 40 °C. Finally, a separator is used to remove the liquid fraction.

3.1.4 Gas Dehydration System

The gas treatment serves to meet the specifications in the produced gas to be used as fuel gas, gas for exportation, or gas for injection. The Gas Dehydration System *GDS* is one of the systems employed for gas treatment and it is used to reduce the water content of the gas. "Dehydration is often necessary to prevent the formation of gas hydrates, which may plug high-pressure processing equipment or pipelines at high pressure and at temperatures considerably higher than 0 °C" (MANNING; THOMPSON, 1995). The gas stream from *MC-A* is cooled down in a heat exchanger to about 26 °C by the treated cool gas from the Gas Dew Point System. After the cooling process, a gas coalescer filter removes the condensate from the gas stream. To reach a water content of 1 ppm_v, molecular sieves are utilized for the dehydration. This dehydration process by desiccant bed for water was not modeled in detail and a splitter unit was used instead to represent this separation process. A simplified scheme of the *GDS* is presented in Figure 10.

Figure 10. Simplified scheme of Gas Dehydration System.

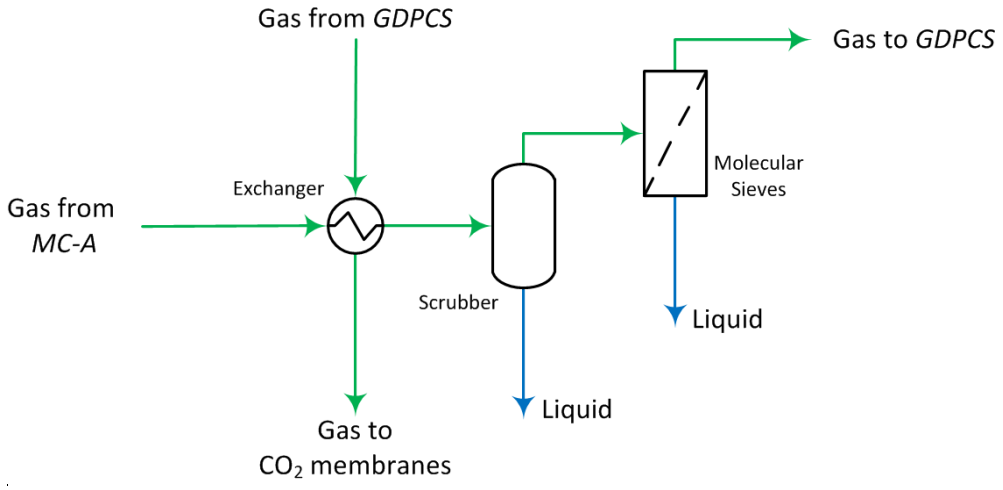

Source: Author´s elaboration.

The modeling of molecular sieves was simplified due to the lack of detailed information of the process; for this reason, a splitter unit was used to simulate the separation. In order to consider the heat demand of the regeneration process, a quantity of water is estimated and used for this propose in the hot water system.

3.1.5 Gas Dew Point Control System

The Gas Dew Point Control System *GDPCS* is the second system employed for gas treatment and its simplified scheme is shown in Figure 11. First, the gas stream from *GDS* is cooled down in the Gas/Liquid exchanger to around 21°C. Next, the gas stream is expanded in a valve to dew point conditions: about 5336 kPa and 10°C. These conditions allow the condensation and separation of part of the hydrocarbons in the gas. Then, the condensate is separated and the specified gas is then sent to the *GDS* exchanger, and then, for the CO_2 membranes. Finally, the cool mixture from the Gas/Liquid exchanger is directed to the *VRU* where it is recycled into the second *VRU* stage.

Figure 11. Simplified scheme of Gas Dew Point Control System.

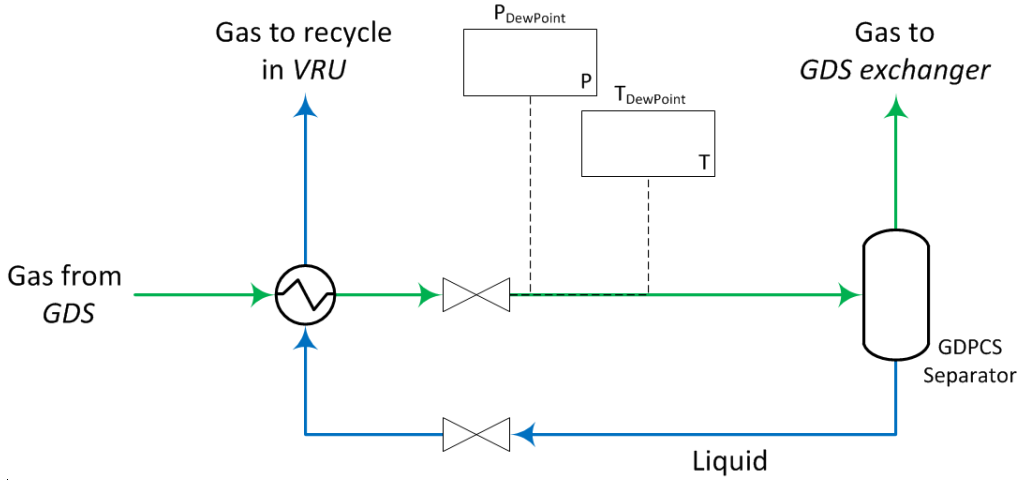

Source: Author´s elaboration.

3.1.6 CO_2 Removal System

The CO_2 removal system is represented in Figure 12. Gas from the *GDS* exchanger is routed to the CO_2 treatment process. Depending on the operation mode, all or part of the gas must be sent through the by-pass of the membranes to be compressed and injected into the wells. Gas for CO_2 removal is heated up to 60°C according to membrane requirements. In the CO_2 membranes, the CO_2 content of the gas stream must be reduced to 3% molar to be compressed and exported or to be used as gas fuel in the gas turbines. Separated CO_2 is assumed to have a

molar composition of 100% of CO_2, and it is directed to the CO_2 compressors to be injected in wells. This CO_2 removal process was not modeled in detail and an ideal splitting unit was used instead to represent the membrane technology.

Figure 12. Simplified scheme of the CO_2 removal system.

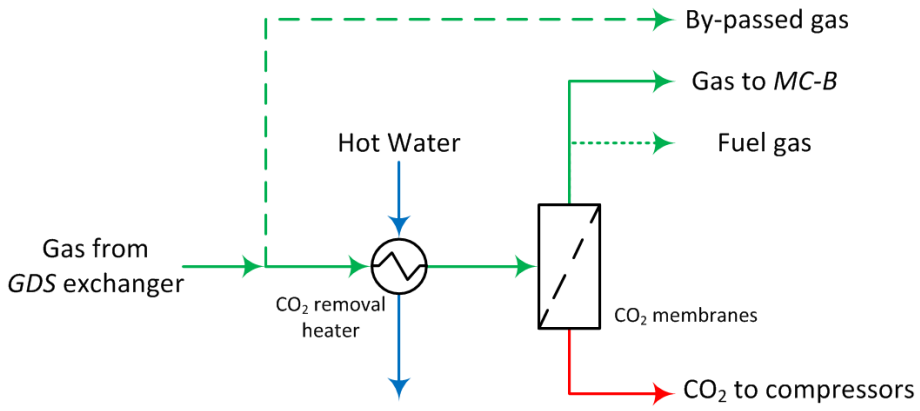

Source: Author´s elaboration.

3.1.7 Main Gas Compressors B (Exportation gas compression)

Main compression train *MC-B* consists of two compression stages, each one with its scrubbing and cooling processes. A simplified scheme is shown in Figure 13.

Figure 13. Simplified scheme of the *MC-B*.

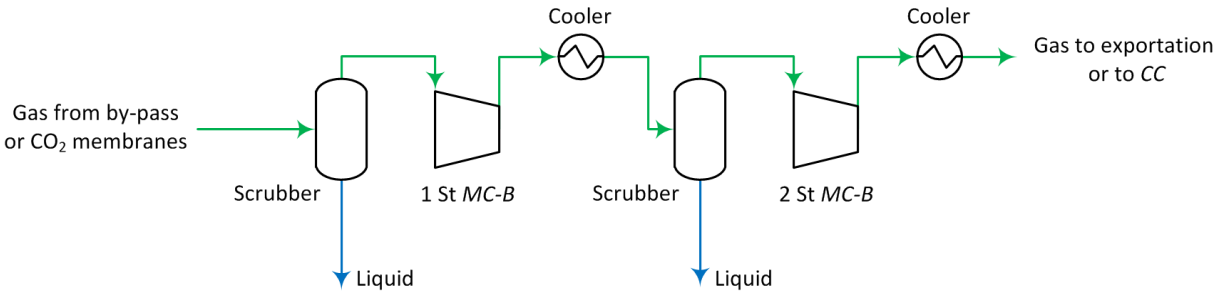

Source: Author´s elaboration.

Firstly, the gas from by-pass or CO_2 membranes is treated in a scrubber to prevent any liquid from entering compressor. Gas inlet pressure in the first compression stage (1 St *MC-B*) has a maximum pressure of 5300 kPa when it was by-passed, or 4752 kPa when the gas from CO_2 removal unit is compressed. Next, the gas pressure is increased to 10960 kPa, and the compressed gas is cooled down to 40°C to separate the condensate in the scrubber. Then, the cooled gas is compressed in the second stage (2 St *MC-B*) to reach a pressure of 25000 kPa

which is the requirement for exportation purpose. The discharged gas stream from the second compressor is cooled down to 40°C depending on the gas composition. When the FPSO operates in gas injection mode, the compressed gas in the *MC-B* is routed to the gas injection train.

3.1.8 CO_2 Compression System

The CO_2 stream from the membranes is compressed in the CO_2 Compression System CO_2-CT to be further injected in the wells. This compression train consists of four compression stages, see Figure 14. Each compression stage has a scrubber to guarantee that no liquid will be sent to the compressor, and a gas cooler after the compressor to ensure a gas temperature of 40°C. These compressors are mechanically powered by gas turbines. At the first stage, the inlet pressure and temperature are 400 kPa and 37°C, respectively. Injection pressure of the CO_2 stream depends on the gas volume flow and gas composition according to the supplied data by the FPSO operator. As the assumed CO_2 content of the CO_2 stream is 100%, the injection pressure is about 20000 kPa, with some variations due to the volume flow of the CO_2 stream. This pressure injection level implies that the projected CO_2-CT is sufficient to inject the CO_2 stream, and additional compression in *the Gas Compression Train* is not required.

Figure 14. Simplified scheme of the CO_2 Compression System.

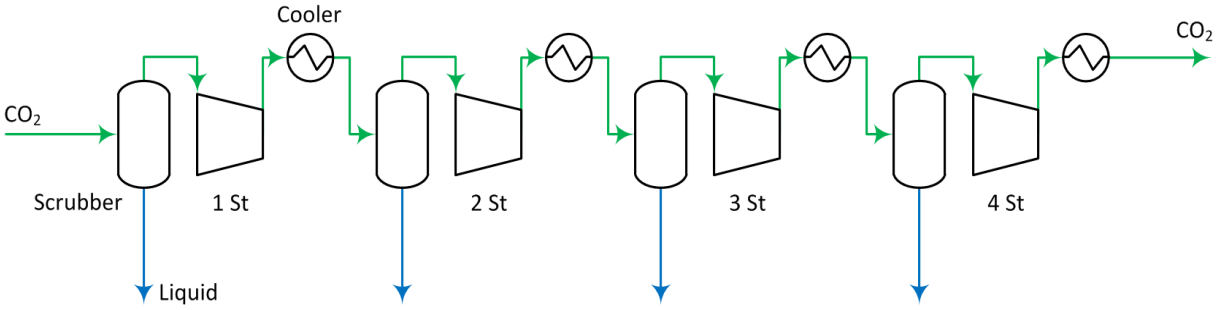

Source: Author´s elaboration.

3.1.9 Gas Injection Train

The Gas Injection Train *GIT* receives the gas from *MC-B*. First, the gas enters the scrubber at 25000 kPa and 40°C. This temperature may change depending on gas composition. Gas from scrubber is directed to the compressor where its pressure is increased to the injection pressure value which has a maximum value of 55000 kPa. This pressure may have lower values than 55000 kPa in accordance with the gas stream volume flow and composition; see Table 18 (APPENDIX A). A final stage of cooling allows reducing the gas temperature to 40°C or

higher depending on the gas composition. A simplified scheme of this system is shown in Figure 15.

Figure 15. Simplified scheme of the Gas Injection Train GIT.

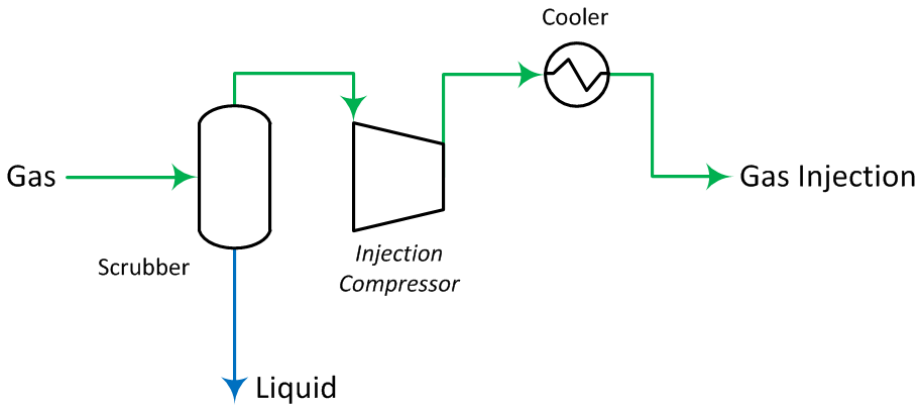

Source: Author´s elaboration.

3.1.10 Gas Turbine System

The utility plant is composed by gas turbines *GT*. These are used to generate the electricity demand of the FPSO. Gas turbines were modelled according to scheme presented in Figure 16 (SADDIQ et al., 2015; YOUNG; WILCOCK, 2002). Considering its widespread use in the offshore industry (FORECAST INTERNATIONAL, 2011), a LM2500® General Electric gas turbine was taken as reference in order to calibrate the gas turbine model. LM2500® features and operation data were taken from specific literature (BROOKS, 2006; MCCARRICK; MACKENZIE, 2011) and GateCycle™ software (GE ENERGY, 2013). It was very important to develop the gas turbine models in Aspen HYSYS® in order to obtain flexibility in the simulation convergence (power demand of consumers and the power supply of the gas turbine system).

Air for gas turbines was modeled as a mixture of dry air and moisture. In line with the gas turbine specifications for the FPSO project in Santos basin - Brazil, site conditions are assumed as: 25 ºC, 101.325 kPa, and 80% relative humidity. Humid air composition is calculated taking into account the following species: nitrogen, oxygen and water (PULKRABEK; WILLARD, 2004).

Compressed air in the compressor section is sent to the combustion chamber *CC* and a fraction of 17.8% the compressed air flow is directed to the turbine blades for cooling. In the

combustion chamber, the fuel gas treated from the CO_2 removal unit is burned with air, which results in the production of hot exhaust gases at combustor exit temperature. The chemical reactions to simulate combustion process in Aspen HYSYS® were defined and adjusted based on typical stoichiometric coefficients for different hydrocarbon reactions (TURNS, 2000).

Hot gases from combustor are mixed with cooling air to reach the rotor inlet temperature. Next, hot gases are expanded in the turbine section generating power which is used to drive the compressor section and to generate electric power by means of the electric generator. It was considered a power factor of 0.8 and a generator efficiency of 0.96. Exhaust gas are routed to the waste heat recovery unit in the hot water system.

CO_2 compressors are mechanically powered by a gas turbine. The used model for this gas turbine is the same for the turbines used for electric generation. Exhaust gases from the gas turbine for CO_2 compressors are directed to the hot water system. Mechanical coupling losses were neglected.

Figure 16. Simplified scheme of Gas Turbine and Hot Water System.

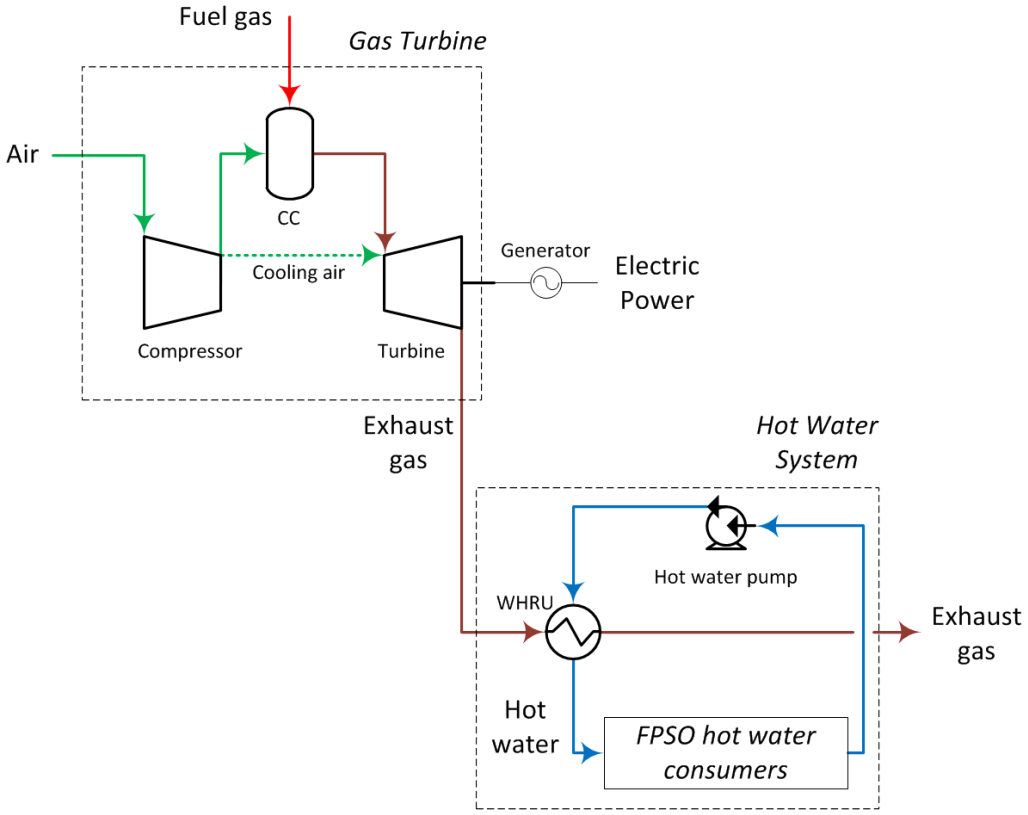

Source: Author´s elaboration.

3.1.11 Hot Water System

Hot water system HWS is a closed system coupled to gas turbines according to the scheme shown in the Figure 16. In the Waste Heat Recovery Unit *WHRU*, heat is recovered from the exhaust gases from gas turbines, and pressured water at about 100 ºC is heated to 130 ºC in order to be sent to the hot water consumers: production heaters, dilution water heater, and CO_2 removal heater.

3.1.12 Cooling Water System

Cooling water system CWS consists of a closed system of cooling water and a seawater cooling system, see Figure 17. Seawater at 25°C is pumped to the heat exchanger where the cooling water from cooling water pump is cooled down to 35°C, and then, the seawater at around 45°C is rejected to the sea. Next, cool water is routed to the FPSO coolers to remove heat and it backs to the cooling water pump.

Figure 17. Simplified scheme of the Cooling Water System.

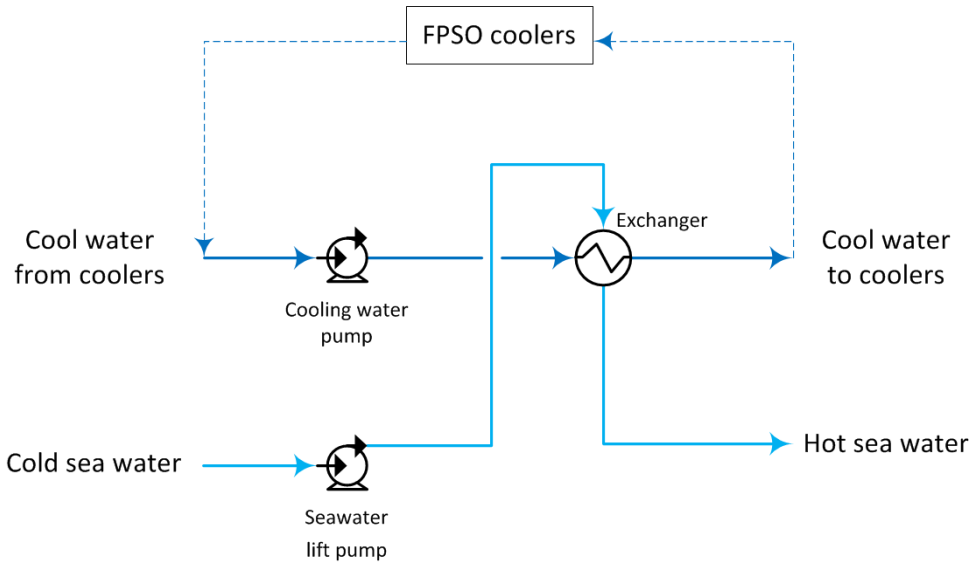

Source: Author´s elaboration.

3.1.13 Water Injection System

A simplified scheme of the water injection system WIS is presented in Figure 18. For model and simulation purposes, treatment processes such as sulphate removal, membrane cleaning, and deaeration were not considered. The injection pump system increases the water pressure from 101.3 to 24500 kPa to be injected in injection wells. The maximum injection capacity is 28600 m^3/d, but this capacity varies with the FPSO operation mode.

Figure 18. Simplified scheme of the Water Injection System.

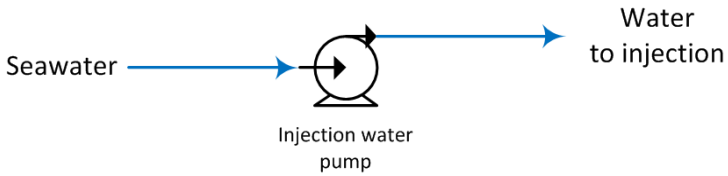

Source: Author´s elaboration.

3.2 The plant with Carbon Capture and Storage System

Releases of gaseous emissions are unavoidable in the oil and gas production process. On FPSOs, CO_2-emissions occur mainly from the combustion of gas for power generation purposes. In order to mitigate the environmental impact of the FPSO, a carbon capture and storage system *CCS* has been considered, and it was expected to reduce the CO_2 emissions by about 90%. Captured CO_2 is then injected and stored in wells with the aim to enhance oil recovery processes.

A simplified scheme of the Reference FPSO integrated to a carbon capture and storage system *CCS* is presented in Figure 19. CO_2 capture and storage system consists of CO_2 capture process and CO_2 compression train. Gray blocks indicate the specific processes related to *CCS*. It was assumed that flue gases from turbines *T1* and *T2* are sent to the *CCS* system. After the *WHRU*, exhaust gases still have a considerable amount of exergy to be recovered. Then, a second waste heat recovery unit *CCS WHRU* is used to provide the heat demand in the *CCS* desorber column. Electric demand of the CCS consumers is provided by the gas turbine *T1*.

The CO_2 capture process is based on a chemical absorption system with monoethanolamine (MEA) to remove the CO_2 from flue gases. It has two main sections: absorption and desorption. In the absorption section, CO_2 is removed from flue gases using the CO_2-lean liquid chemical absorbent *LEAN-MEA*, whereas in the desorption section the CO_2-rich liquid chemical absorbent *RICH-MEA* is regenerated by heating.

The CO_2 compression train consists of four compression stages. Each stage has a scrubber to remove any liquid, and a discharge cooler to reduce the CO_2 temperature to 40°C depending on the injected stream pressure.

Figure 19. Simplified scheme of the FPSO plant with CCS.

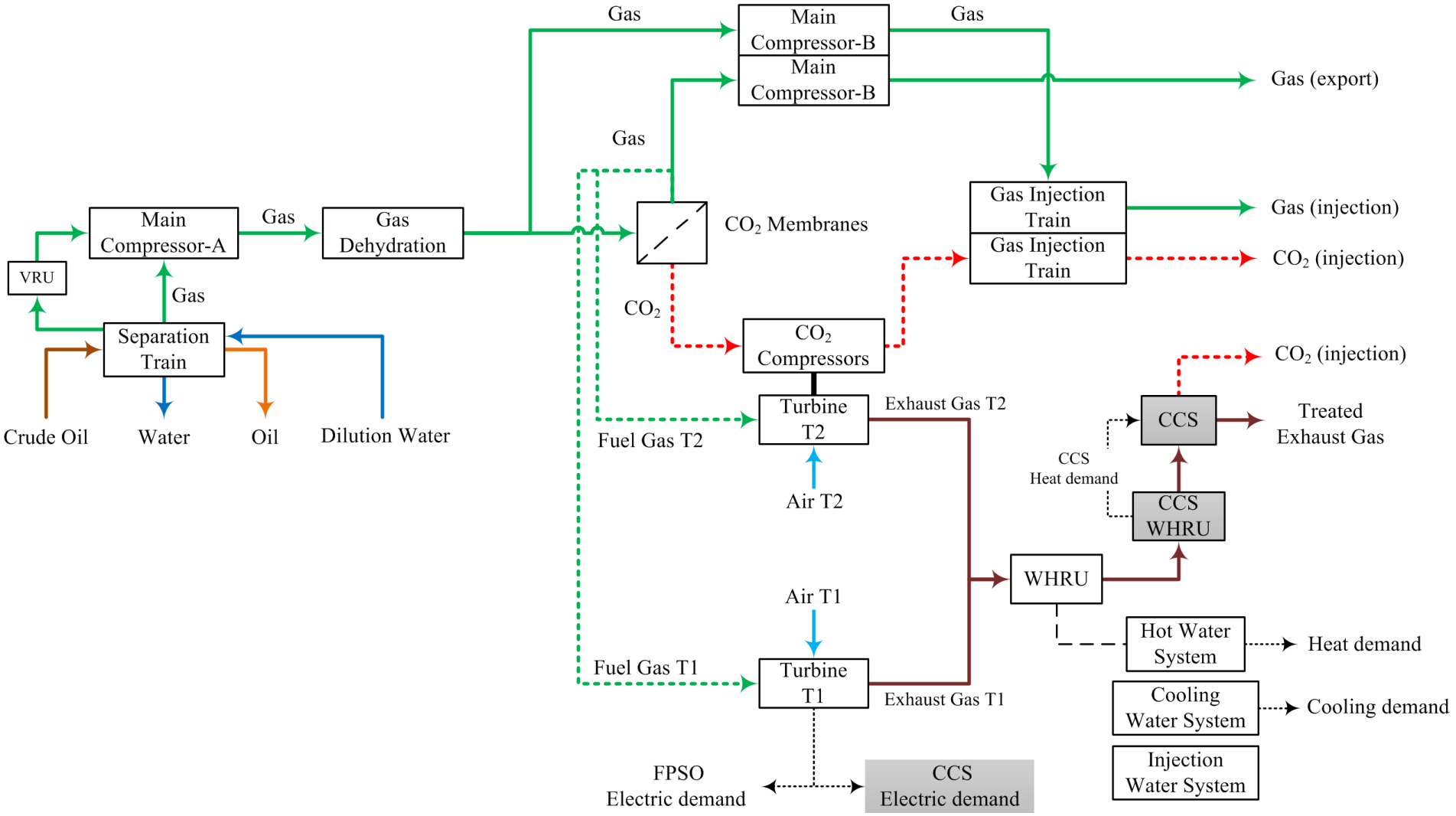

Source: Author´s elaboration.

Figure 20. Scheme of the Carbon Capture and Storage System.

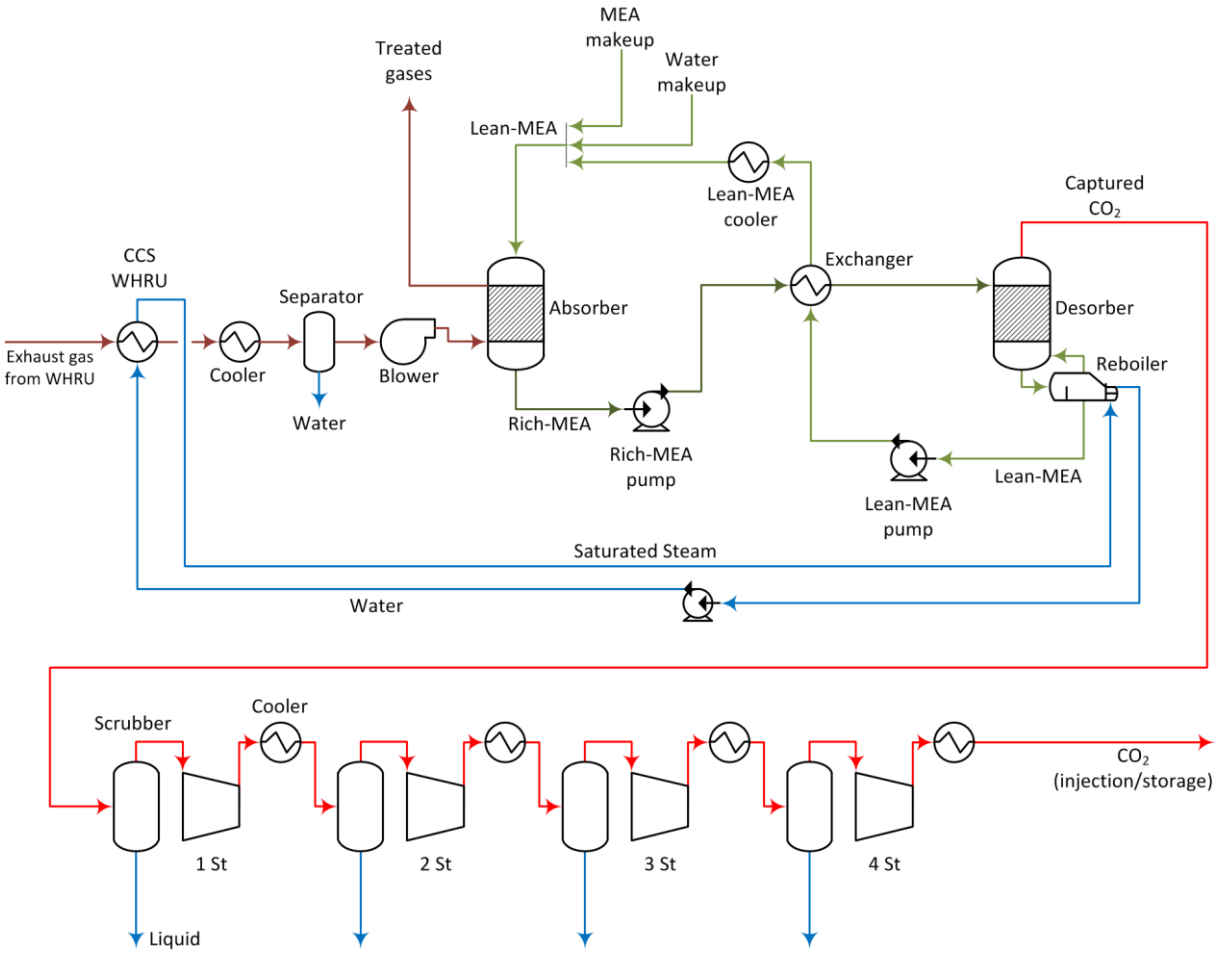

Source: Author´s elaboration.

Figure 20 shows a more detailed scheme of the *CCS*. Exhaust gases are directed from the *WHRU* to the *CCS WHRU* in order to recovery energy and to generate saturated steam which will be utilized in the reboiler. Next, these gases are routed to the cooler where temperature is lowered to condense some of the water. In the separator, condensate water and flue gas are separated. This gas dehydration operation increases the CO_2 molar fraction in the gas to ease the carbon dioxide absorption, which is favored with higher CO_2 contents and low temperatures. The blower slightly pressurizes flue gas, and then, it is directed to the *Absorber* to be treated. The flue gas enters the absorber column from the bottom stage and flows up through to the column. In the *Absorber*, CO_2 is separated from the flue gas by passing the flue gas through an aqueous solution of MEA (*Lean MEA*) that enters from the top of the column. The treated gases are vented to the atmosphere from the top of the column. The solution rich in CO_2 (*Rich-MEA*) leaves from the bottom of the *Absorber* and is directed to the *Rich-MEA* pump, where is pumped to the heat *Exchanger* for energy recover. In the heat *Exchanger*,

Rich-MEA is heated to 120ºC and then is directed to the top side of the *Desorber* column. Desorption process uses heat from the reboiler allowing that CO_2 to be separated and the aqueous solution of MEA turns to be the *Lean-MEA* solvent. *Lean-MEA* from *Desorber* unit is pumped to the *Exchanger* to heat the *Rich-MEA*, and then, an additional cooling process is necessary in order to enhance the absorption process. Next, water makeup and MEA makeup are used to replace fluid losses and the MEA solvent is again ready to enter the *Absorber* and to begin the capture cycle. Captured CO_2 from the capture system is routed to the compression train to be injected and stored. The compression train includes four compression stages, with a separator and a cooler.

3.3 Well-fluid compositions

The composition of the well-fluid is an important factor considered in this study. Four well-fluids were considered in the simulations. The molar composition for the four well-fluids is shown in the Table 7. This is the reference composition for this study. C_4 and C_5 includes the nC_4 and iC_4, and the nC_5 and iC_5 hydrocarbons, respectively.

Table 7. Molar composition [%] of well-fluids used in this study.

	Fluid 1	Fluid 2	Fluid 3	Fluid 4
CO_2	8.24	16.00	26.08	0.86
N_2	0.37	0.49	0.33	0.39
C_1- C_4	65.92	63.82	50.26	77.88
C_5- C_{12}	11.97	10.29	10.78	10.33
C_{13}-C_{19}	5.88	4.67	4.60	4.48
C_{20+}	7.62	4.73	7.95	6.06
MW C_{20+}	536	581	486	481
SG C_{20+}	0.9594	0.9587	0.9616	0.9380

Source: Author´s elaboration. Data of typical FPSO operation in Brazil.

3.4 Operation modes

The FPSO studied in this work has a distinctive feature: it must be flexible and should be able to operate in any of the three operation modes at any time based on the production needs or changes in composition over the life of the field. These operation modes are related to the possibility to export or inject the produced gas. Then, the three operation modes are studied: Mode 1 where all gas is injected, Mode 2 where all gas is exported, and Mode 3 where one part of the gas is injected and the other is exported.

In the operation mode 1 – Mode 1 – all gas is injected, see Figure 21. The gas injection operation is practiced to enhance the oil recovery (Enhance Oil Recovery EOR). Except for a small fraction of gas to be treated and used as fuel (green dotted line), dehydrated gas bypasses the *CO_2 membranes* unit and is directly sent to the *Main Compressors-B* and after to the *Gas injection train* to reach the pressure required for injection purposes. Lines in gray indicate that the stream is disabled.

Figure 21. Simplified scheme of the operation mode 1.

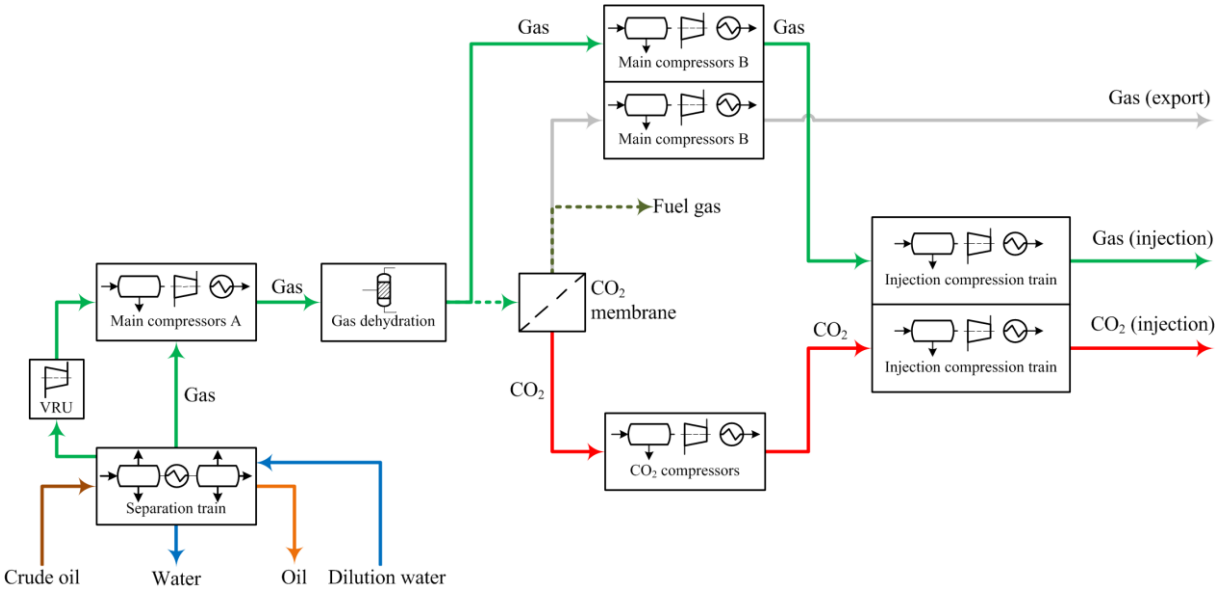

Source: Author´s elaboration.

In the operation mode 2 – Mode 2 – all gas is exported, see Figure 22. All dehydrated gas is treated in the *CO_2 membranes unit* in order to be exported, except for the part used as fuel for the gas turbines. The separated gas in this unit is then compressed in the *Main Compressors-B* for export purposes. Separated CO_2 is compressed in *CO_2 Compressors* and, depending on the composition and volume flow rate, it may be additionally compressed in a section of the *Gas injection train* to be injected increasing the percentage of the oil that is recovered (EOR).

Figure 22. Simplified scheme of the operation mode 2.

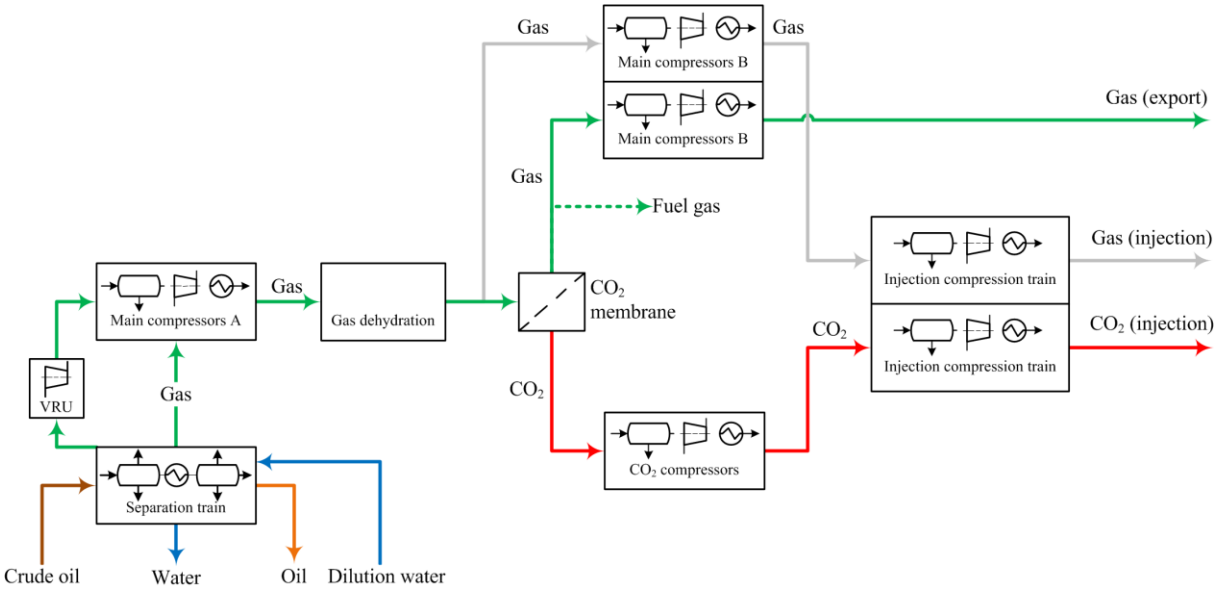

Source: Author´s elaboration.

Figure 23. Simplified scheme of the operation mode 3.

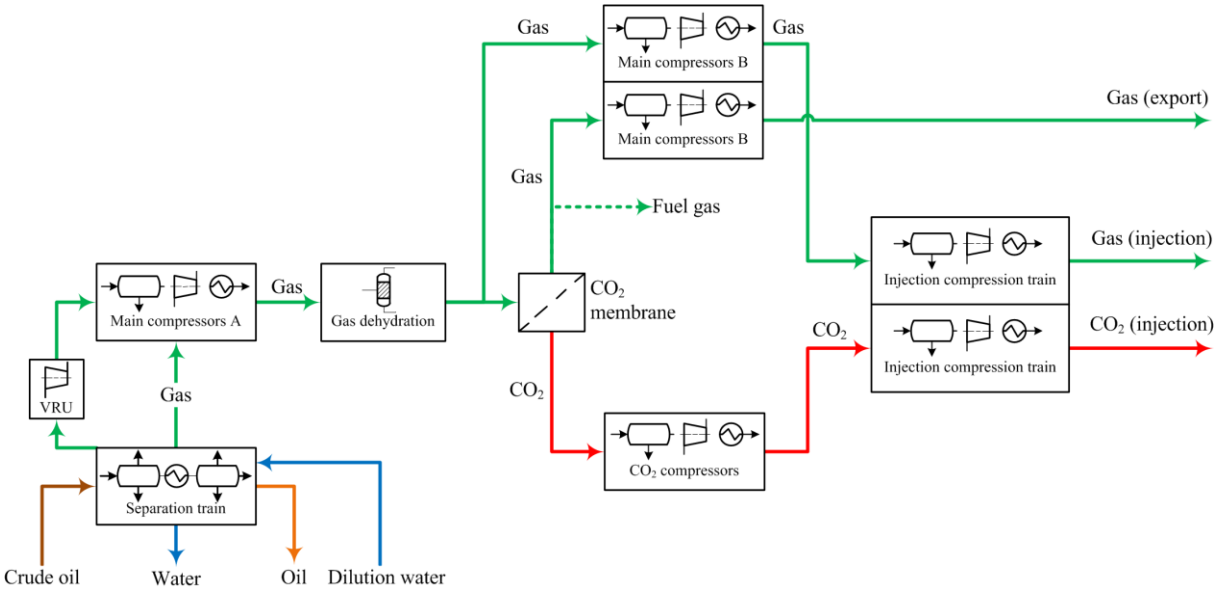

Source: Author´s elaboration.

In the operation mode 3 – Mode 3 – the FPSO operates with partial gas injection (50% of the gas flow rate from the *GDPCS*) and partial gas exportation (slightly lower than 50% of the gas flow rate from the *GDPCS*), see Figure 23. A fraction of the dehydrated gas is sent to the *CO_2 membrane*, while the remaining dehydrated gas is processed directly through a section of the *Main Compressors-B*, and then to a section of the *Gas injection train* for further

compression and injection in the wells. The treated gas in the *CO_2 membrane* is mainly used for export purposes and a slight quantity is used as fuel gas in the gas turbines. Gas to export is compressed in a section of the *Main Compressors-B* to the export pressure. The CO_2 removed in the membrane unit is compressed in the *CO_2 Compressors* and in a section of the *Gas injection train* in order to be injected into the well.

3.5 The scenarios considered

Considering the two plants described, the four well-fluid compositions, and the three operating modes, different scenarios are established to carry out exergetic and environmental assessments of the platform. Figure 24 shows these factors and how they are structured in order to define the study scenarios.

Figure 24. Factors considered for scenarios definition.

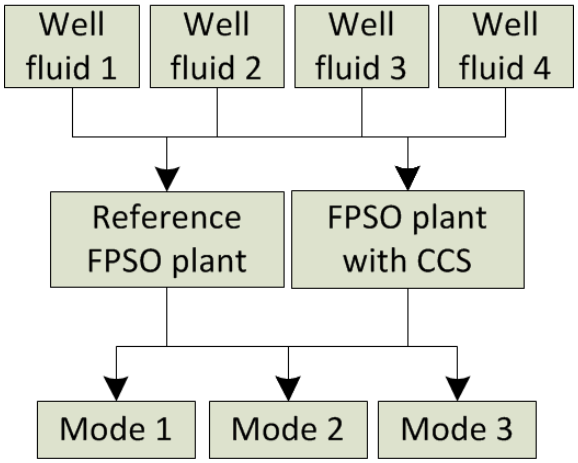

Source: Author´s elaboration.

Well-fluids presented in Table 7 represent the crude oil in the first stage of oil production. At this stage, it is possible that all gas is exported, but gas injection may be required to enhance the oil production. These are conditions that are associated with operator decisions. In order to consider these possibilities, the three operation modes were studied to determinate how the performance of the plant changes when operation mode are switched. Table 8 shows the twenty-four scenarios studied.

Table 8. Scenarios considered in this study.

		Fluid 1	Fluid 2	Fluid 3	Fluid 4
Reference FPSO plant	Mode 1	*1*	*2*	*3*	*4*
	Mode 2	*5*	*6*	*7*	*8*
	Mode 3	*9*	*10*	*11*	*12*
FPSO plant with CCS	Mode 1	*13*	*14*	*15*	*16*
	Mode 2	*17*	*18*	*19*	*20*
	Mode 3	*21*	*22*	*23*	*24*

Source: Author´s elaboration.

3.6 Exergy concepts and exergy performance indicators

This section presents the concepts and details for calculating the exergy of each stream. The exergy of a material flow, on a time-rated basis $\dot{B}$, can be divided into four distinct components: kinetic exergy (k), potential exergy (p), physical exergy (ph), and chemical exergy (ch), according to eq.(1):

$$\dot{B} = \dot{B}_k + \dot{B}_p + \dot{B}_{ph} + \dot{B}_{ch}. \quad (1)$$

Kinetic and potential components of exergy streams are considered negligible in this study. Equation (2) presents the specific physical exergy:

$$b_{ph} = (h - h_0) - T_0(s - s_0), \quad (2)$$

where h is the specific enthalpy, s is the specific entropy, and the subscript 0 refers to the restricted dead state. The chemical exergy of a mixture per mole of the gas mixture is given by eq.(3):

$$b_{ch} = \sum_i x_i b_{ch}^i + \bar{R}T_0 \sum_i x_i \ln x_i \gamma_i, \quad (3)$$

where x_i is the mole fraction of the i-th component in the mixture, b_{ch}^i is the chemical exergy of the i-th component, and γ_i is the activity coefficient of the i-th component, and it is taken as 1 for petroleum components (RIVERO et al., 1999; SILVA et al., 2014). Chemical exergy for different components presented in Table 7 was taken from Szargut (SZARGUT, 1988), except for the chemical exergy of the C20+ pseudo-component of petroleum, which was estimated by means of eq.(4) (SZARGUT, 1988):

$$b_{ch} = \beta \cdot LHV, \quad (4)$$

where β is the ratio of the chemical exergy to the lower heating value LHV. β was estimated as a function of the atomic ratio of carbon to hydrogen H/C according to eq.(5):

$$\beta = 1.0406 + 0.0144 \cdot \frac{H}{C}. \quad (5)$$

Lower heating value and the atomic ratio of carbon to hydrogen were calculated by means of eqs.(6) and (7), respectively (RIAZI, 2005):

$$LHV = 55.5 - 14.4 \cdot SG - 0.32 \cdot S\% \ \left[\frac{MJ}{kg}\right], \quad (6)$$

where SG is the specific gravity and $S\%$ is the sulfur wt% in the fuel.

$$H/C = {}^{11.9147}\Big/\left(8.7743\times10^{-10} \cdot \epsilon \cdot {T_b}^{-0.98445} \cdot SG^{-18.2753}\right), \quad (7)$$

where T_b is the boiling temperature and ϵ is given by eq.(8):

$$\epsilon = exp(7.176\times10^{-3} \cdot T_b + 30.06242 \cdot SG - 7.35\times10^{-3} \cdot T_b \cdot SG). \quad (8)$$

Physical exergy calculations were performed by implementing Aspen HYSYS® calculation routines developed by Abdollahi-Demneh et al. (ABDOLLAHI-DEMNEH et al., 2011), see APPENDIX C, while chemical exergy calculations were calculated by means of Microsoft Excel worksheets, see APPENDIX D.

Oil and gas industry proposes several energy-based performance indicators for understanding, assessing and analyzing the performance of its operations and activities. Comparing operation must be done carefully and taking into account well-defined metric due to the presence of many factors related to oilfield composition, oilfield lifetime, gas/oil final destination, among others. Absolute and specific energy consumption indicators are commonly used in this industry, but the specific indicators have a great interest to compare the performance of the facilities operations (INTERNATIONAL ASSOCIATION OF OIL AND GAS

PRODUCERS; THE GLOBAL OIL AND GAS INDUSTRY ASSOCIATION FOR ENVIRONMENTAL AND SOCIAL ISSUES, 2013).

The literature in the field of exergy presents several indicators used to assess the exergy-based performance of energy conversion processes. In this study, the following references have been especially reviewed. Szargut (SZARGUT, 1988) and Kotas (KOTAS, 1995) propose useful expressions for assessing the exergy performance of different processes. Other books such as Oliveira (OLIVEIRA JR, 2013), Rivero (RIVERO, 1999), and Dincer and Rosen (DINCER; ROSEN, 2007) have applied the exergy concept to assess the oil and gas industry. Oliveira applied the exergy method to an offshore platform, while Rivero carried out an exergy assessment in the petroleum refining and petrochemical industry, and Dincer and Rosen used the exergy method to evaluate crude oil distillation systems. The report of the IPIECA and IOGP (INTERNATIONAL ASSOCIATION OF OIL AND GAS PRODUCERS; THE GLOBAL OIL AND GAS INDUSTRY ASSOCIATION FOR ENVIRONMENTAL AND SOCIAL ISSUES, 2013) proposes several energy indicators accepted by IOGP member companies, and suggests the use of the exergy concept to take into account the energy quality of products and resources. Other performance indicators have been reviewed and taken from the recent works of Nguyen et al. (NGUYEN et al., 2014a) and Voldsund et al. (VOLDSUND et al., 2013c).

Offshore primary petroleum processing plant is mainly a separation process associated with a series of treatment and conditioning operations for the final disposal of products (oil/gas/water): transport, storage, or direct use in the plant. In separation processes, a performance criterion used to assess its exergy behavior is known as the rational efficiency $\eta_{B,sep}$. The rational efficiency is analogous to exergy efficiency and $\eta_{B,sep}$ is expressed by means of eq.(9) for a separation process (KOTAS, 1995). This expression was used to evaluate the overall performance.

$$\eta_{B,sep} = \frac{\sum \dot{B}_{prod} - \dot{B}_{mix}}{\sum \dot{B}_h^Q + \dot{W}_{in}}, \tag{9}$$

where the numerator $\left(\sum \dot{B}_{prod} - \dot{B}_{mix}\right)$ is the *Useful exergy effect*, or also called *Desired output of the process*, *Exergy product*, or *Exergy output flow rate*. *Useful exergy effect* is

calculated as the difference between the exergy flow rate of the separated products $\sum \dot{B}_{prod}$ (oil, gas, and water), and the exergy flow rate of the mixture $\dot{B}_{mix}$ (well-fluid). The denominator $\left(\sum \dot{B}_h^Q + \dot{W}_{in}\right)$ is the exergy input rate of the separation process where $\dot{B}_h^Q$ is the thermal exergy rate associated with the heating required for the separation, and $\dot{W}_{in}$ is the exergy inlet rate related to shaft power needed for the separation.

Exergy efficiency is the first performance indicator used to assess the overall FPSO performance, and it is calculated by means of eq.(10), which is an equation adapted for the whole plant from eq.(9):

$$\eta_{B,FPSO} = \frac{Useful\ exergy\ effect}{\dot{B}_{fuel}}, \tag{10}$$

In this equation, $\dot{B}_{fuel}$ is the exergy flow rate of the fuel utilized in the gas turbine system and it is considered the exergy input or the exergy consumption of the FPSO. A more detailed equation for the FPSO exergy efficiency calculation is presented in eq.(19) considering the FPSO control volume.

Destroyed exergy flow rate $\dot{B}_d$ is an important exergy concept used to determinate how much is the lost work capacity in a thermodynamic process. The exergy balance of a control volume in steady-state steady-flow process may be expressed by means of eq.(11) (KOTAS, 1995):

$$\dot{B}_d = \sum_{in} \dot{B}_i - \sum_{out} \dot{B}_i + \sum \dot{B}^Q - \dot{W}, \tag{11}$$

where $\sum_{in} \dot{B}_i$ and $\sum_{out} \dot{B}_i$ are the sum of exergy flow rates of the streams i in the inlet and the outlet of the system, respectively, $\sum \dot{B}^Q$ is the sum of thermal exergies, and $\dot{W}$ is the power crossing the boundary of the control volume.

In addition to destroyed exergy, *relative exergy destruction* ϵ for FPSO systems is calculated to identify the contribution of each FPSO system to the total exergy destruction $\dot{B}_d$. *Relative exergy destruction* is given by the ratio between the destroyed exergy of system *i*, $\dot{B}_{d,i}$, and total destroyed exergy $\dot{B}_d$ in the FPSO according to eq.(12) (KOTAS, 1995):

$$\epsilon = \frac{\dot{B}_{d,i}}{\dot{B}_d} \tag{12}$$

There are other performance indicators that, based on exergy destruction and exergy consumption, are analogous to specific energy consumption described in (INTERNATIONAL ASSOCIATION OF OIL AND GAS PRODUCERS; THE GLOBAL OIL AND GAS INDUSTRY ASSOCIATION FOR ENVIRONMENTAL AND SOCIAL ISSUES, 2013). These indicators are: *specific exergy destruction SED* and *specific exergy consumption SEC*, and were presented by Voldsund et al. (VOLDSUND et al., 2013c). *Specific exergy destruction* is expressed as the ratio between the destroyed exergy in a system of the FPSO and the standard equivalent oil volume of the products of the FPSO, SED_{vol}, see eq.(13). Separated oil for stock purposes and the exported gas are used to calculate the standard equivalent oil. It may as well be calculated by unit of exported exergy or exergy into the products, SED_b, see eq.(14).

$$SED_{vol} = \frac{\dot{B}_d}{\dot{V}_{o.e.,prod}} \tag{13}$$

$$SED_b = \frac{\dot{B}_d}{\dot{B}_{prod}} \tag{14}$$

Eqs.(15) and (16) present two expressions for s*pecific exergy consumption* SEC. In the numerator, $\dot{B}_{fuel}$ indicates the exergy consumed in the FPSO, while the denominator may be expressed in terms of the standard oil equivalent produced in the facility or the exergy flow rate of the products.

$$SEC_{vol} = \frac{\dot{B}_{fuel}}{\dot{V}_{o.e.,prod}} \tag{15}$$

$$SEC_b = \frac{\dot{B}_{fuel}}{\dot{B}_{prod}} \tag{16}$$

3.7 Environmental performance indicators

As reported by IOGP (INTERNATIONAL ASSOCIATION OF OIL&GAS PRODUCERS, 2015), the following pollutants are predicted to be the most important emissions in the oil and

gas industry: Carbon dioxide (CO_2); Methane (CH_4), Greenhouse Gas (GHG), Non-Methane Volatile Organic Compounds (NMVOCs), Sulphur dioxide (SO_2), and Nitrogen oxides (NO_x). In this work, the environmental analysis is only based on the CO_2 emissions. In the FPSO, these emissions occur mainly from the combustion processes in the gas turbines. *Combustion emissions* is one of the three categories defined for oil and gas industry, while the other two categories are *vented emissions* and *fugitive emissions* (GLOBAL OIL AND GAS INDUSTRY ASSOCIATION FOR ENVIRONMENTAL AND SOCIAL ISSUES; THE AMERICAN PETROLEUM INSTITUTE; INTERNATIONAL ASSOCIATION OF OIL AND GAS PRODUCERS, 2011).

In this study, *Total CO_2 emissions* and *CO_2 normalized to hydrocarbons production* $CO_{2,norm}$ (CO_2 e*missions per unit of production*) are calculated in order to assess the environmental performance of the FPSO. These two environmental indicators satisfy several features proposed by OECD about an indicator as: "*a parameter, or a value derived from parameters, which points to, provides information about, describes the state of a phenomenon/environment/area, with a significance extending beyond that directly associated with a parameter value*" (ORGANISATION FOR ECONOMIC CO-OPERATION AND DEVELOPMENT, 1993). *CO_2 emissions* and *CO_2 normalized* allow the comparison of oil and gas companies and its operations in order to improve their performance. *CO_2 normalized* is derived from eq.(17) as:

$$CO_{2,norm} = \frac{\dot{m}_{CO2}}{\dot{m}_{prod}} \tag{17}$$

Environmental indicators may include the exergy concept, and the application of exergy to evaluate the environmental impact was recommended by Gong and Wall (GONG; WALL, 2001). In order to measure the ratio between carbon emissions and exergy content of separated products, other environmental performance indicator used in this work is the *CO_2 normalized to exergy of the product streams,* $CO_{2,prod}$, see eq.(18). Smaller values of the $CO_{2,prod}$ indicator happen when the carbon emissions are lower and the exergy into the products is higher.

$$CO_{2,prod} = \frac{\dot{m}_{CO2}}{\dot{B}_{prod}} \tag{18}$$

3.8 FPSO model and simulation/calculation parameters

3.8.1 Reference FPSO model

In this section, the control volumes for FPSO and its systems are shown and detailed. Moreover, the expressions for calculating the *Destroyed Exergy* $\dot{B}_d$ in different systems are presented for each control volume in order to describe the interaction of the different streams.

FPSO model studied in this work is represented by the control volume presented in Figure 25, and this scheme represents the reference offshore plant. The studied control volume has six inlet streams (Crude Oil, Dilution Water, Air for Gas Turbines, Fuel Gas, Seawater 1, and Seawater 2) and nine outlet streams (Oil, Gas (export), Gas (injection), CO_2 (injection), Fuel Gas, Water, Exhaust gases, Hot seawater, and Water for injection). Additionally, an electric power stream $\dot{W}_{Aux}$ leaves the control volume in order to be utilized in secondary processes of the FPSO that are not modelled in this study.

Figure 25. Simplified scheme of the FPSO model.

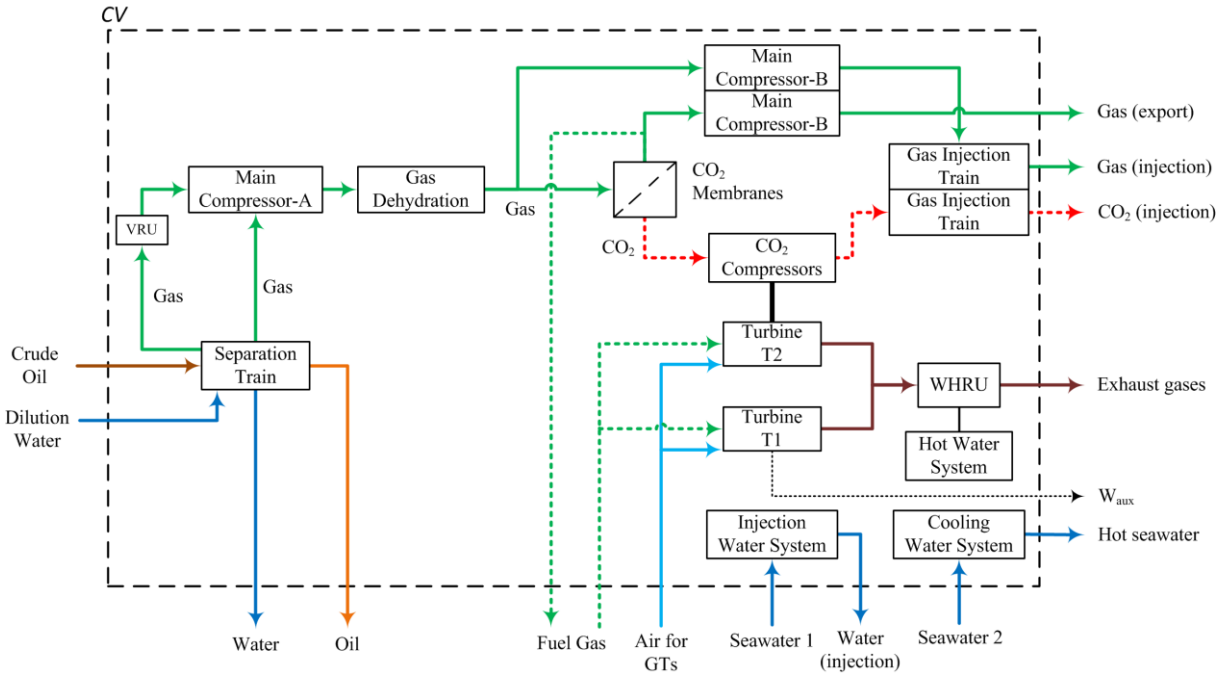

Source: Author´s elaboration.

It is interesting to note that Fuel Gas stream is considered as inlet and outlet, and this consideration is necessary to have the exergy consumption term $\dot{B}_{fuel}$ in the denominator of the exergy efficiency expression, see eq.(10). For the overall process of the FPSO, the *Useful exergy effect* is given by eq.(19):

$$Useful\ exergy\ effect = \left[\dot{B}_{oil} + \dot{B}_{Gas\ (export)} + \dot{B}_{Gas\ (injection)} + \dot{B}_{CO2\ (injection)} + \dot{B}_{Fuel\ Gas} + \dot{B}_{water} - \dot{B}_{Crude\ Oil} - \dot{B}_{Dilution\ Water}\right] + \left(\dot{B}_{Water\ (injection)} - \dot{B}_{Seawater\ 1}\right) + \dot{W}_{aux}. \quad (19)$$

In eq.(19), the term in brackets represents the portion of the *Useful exergy effect* related to the separation of the crude oil into oil, gas and water, as claimed by Kotas (KOTAS, 1995). In addition, the term in parenthesis is the part associated with the useful effect given by the water injection process, while $\dot{W}_{aux}$ is the auxiliary power generated for supplying the secondary electric demand of the FPSO.

Based on Figure 25, destroyed exergy of the reference FPSO may be calculated utilizing eq.(20):

$$\dot{B}_d = \left[\dot{B}_{Crude\ Oil} + \dot{B}_{Dilution\ Water} + \dot{B}_{Fuel\ Gas} + \dot{B}_{Seawater\ 1} + \dot{B}_{Seawater\ 2} + \dot{B}_{Air\ for\ GTs}\right] - \left[\dot{B}_{oil} + \dot{B}_{water} + \dot{B}_{Fuel\ Gas} + \dot{B}_{Gas\ (export)} + \dot{B}_{Gas\ (injection)} + \dot{B}_{CO2\ (injection)} + \dot{B}_{Water\ (injection)} + \dot{B}_{Hot\ seawater} + \dot{B}_{Exhaust\ gases}\right] - \dot{W}_{aux} \quad (20)$$

Seven control volumes have been defined with the aim of making a more detailed analysis of the reference FPSO systems. These control volumes (in dotted lines) are: *CV 1* (Separation train), *CV 2:* (Compression Train), *CV 3:* (Gas turbine GT1), *CV 4:* (Gas turbine GT2), *CV 5:* (Hot water system), *CV 6:* (Cooling water system), and *CV 7:* (Injection water system). Figure 26 shows the control volumes.

Figure 26. Control volumes for the FPSO model.

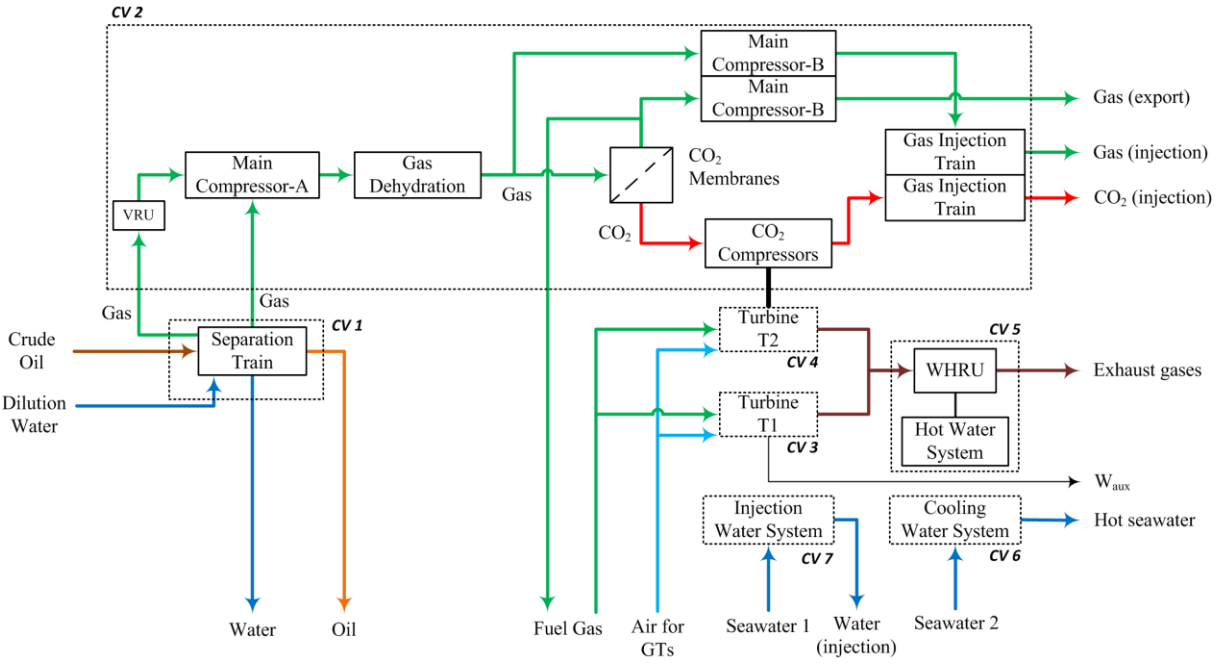

Source: Author´s elaboration.

A simplified scheme of the control volume of the Separation Train (*CV 1*) is presented in Figure 27. This figure shows the mass and power streams considered in the exergy analysis. Hot water is used to supply the exergy for heating of the separated oil and the dilution water.

Figure 27. Simplified scheme of the control volume *CV 1* - Separation Train.

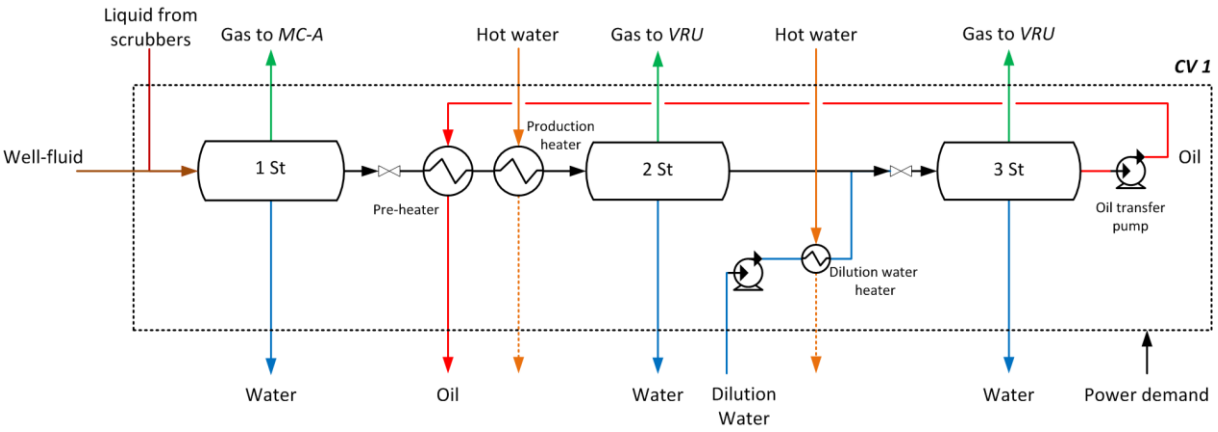

Source: Author´s elaboration.

The exergy balance for the Separation Train system is given by eq.(21). $\dot{B}_{d-ST}$ is the destroyed exergy in the Separation Train, and $\dot{W}_{ST}$ is the power demanded by the pumps in

this system. Well-fluid and crude-oil are terms that are used to define the fluid that will be processed in the separation train. These terms will be used indistinctly.

$$\dot{B}_{d-ST} = \left[\dot{B}_{Well-fluid} + \dot{B}_{Dilution\ Water} + \sum \dot{B}_{Hot\ water\ \ to\ ST} + \sum \dot{B}_{Liquid\ from\ scrubbers}\right] - \left[\dot{B}_{Gas\ to\ MC-A} + \sum \dot{B}_{Gas\ to\ VRU} + \dot{B}_{Oil} + \sum \dot{B}_{Water} + \sum \dot{B}_{Hot\ water\ \ from\ ST}\right] + \dot{W}_{ST} \quad (21)$$

Figure 28 presents the simplified control volume for the exergy analysis in the Compression Train. As indicated in this figure, there are export and injection gas outlet streams which depend on the operation mode. Fuel gas is the sum of the fuel streams for gas turbines GT1 and GT2. Hot water stream is mainly used for heating of the gas to be treated in the CO_2 membrane unit. Cooling water is used to reduce the outlet gas temperature of the different compressors. Finally, power demand is related to power consumption for driving all compressors.

Figure 28. Simplified control volume for Compression Train.

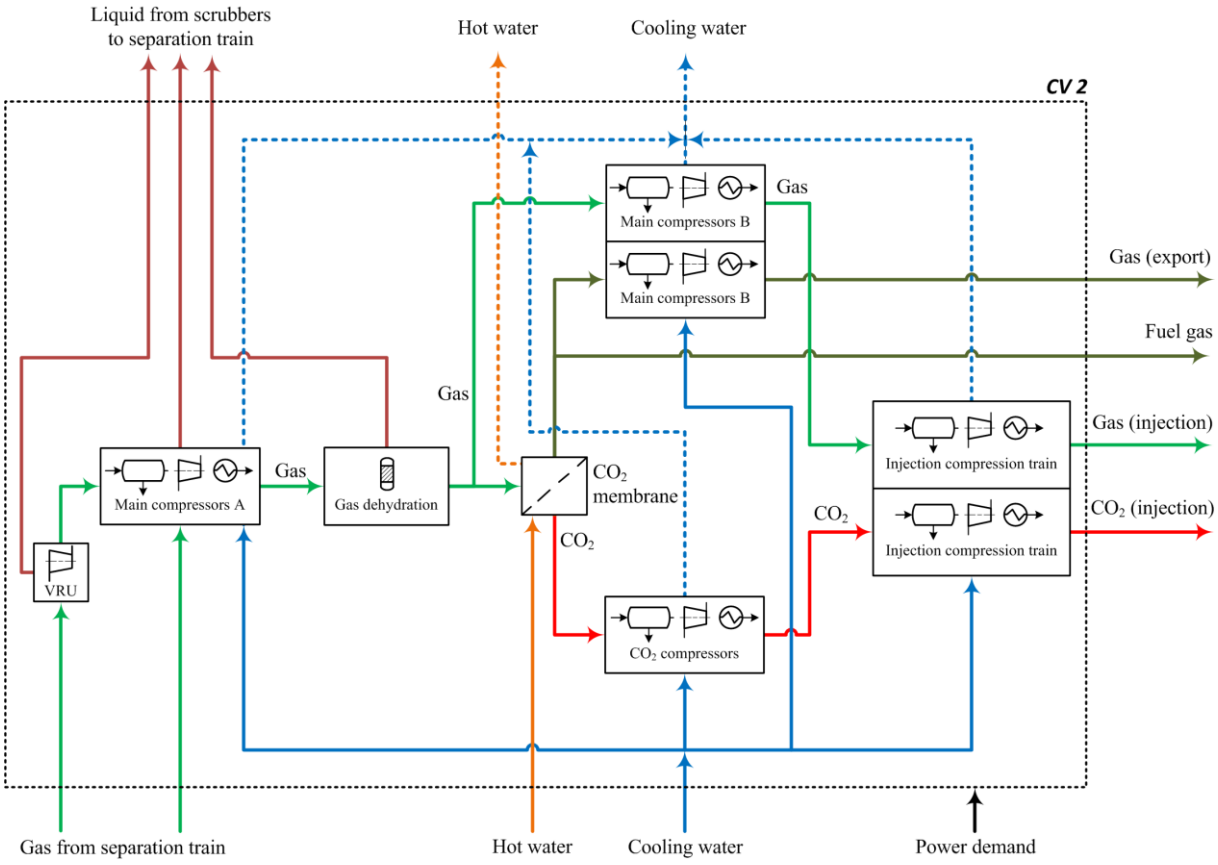

Source: Author´s elaboration.

The exergy balance for the Compression Train system (*CV 2*) is given by eq.(22). $\dot{B}_{d-CT}$ is the destroyed exergy in the Compression Train, and $\dot{W}_{CT}$ is the total power consumption of the compressors.

$$\dot{B}_{d-CT} = \left[\sum \dot{B}_{Gas\ from\ ST} + \sum \dot{B}_{Hot\ water\ \ to\ CT} + \sum \dot{B}_{Cooling\ water\ \ to\ CT}\right] - \left[\dot{B}_{Gas\ (export)} + \dot{B}_{Gas\ (injection)} + \dot{B}_{Fuel\ Gas} + \dot{B}_{CO2\ (injection)} + \sum \dot{B}_{Hot\ water\ \ from\ CT} + \sum \dot{B}_{Cooling\ water\ from\ CT} + \sum \dot{B}_{Liquid\ from\ scrubbers}\ \right] + \dot{W}_{CT} \quad (22)$$

Control volumes for Gas Turbines (*CV 3 and CV 4*) and Hot Water System (*CV 5*) are presented in Figure 29. These systems are coupled to recover part of the exergy content of the exhaust gases from gas turbines and produce hot water. The fuel gas is heated to 60 ºC in the heat exchangers by means of hot water from the WHRU.

Figure 29. Simplified control volume for Gas Turbines and Hot Water System.

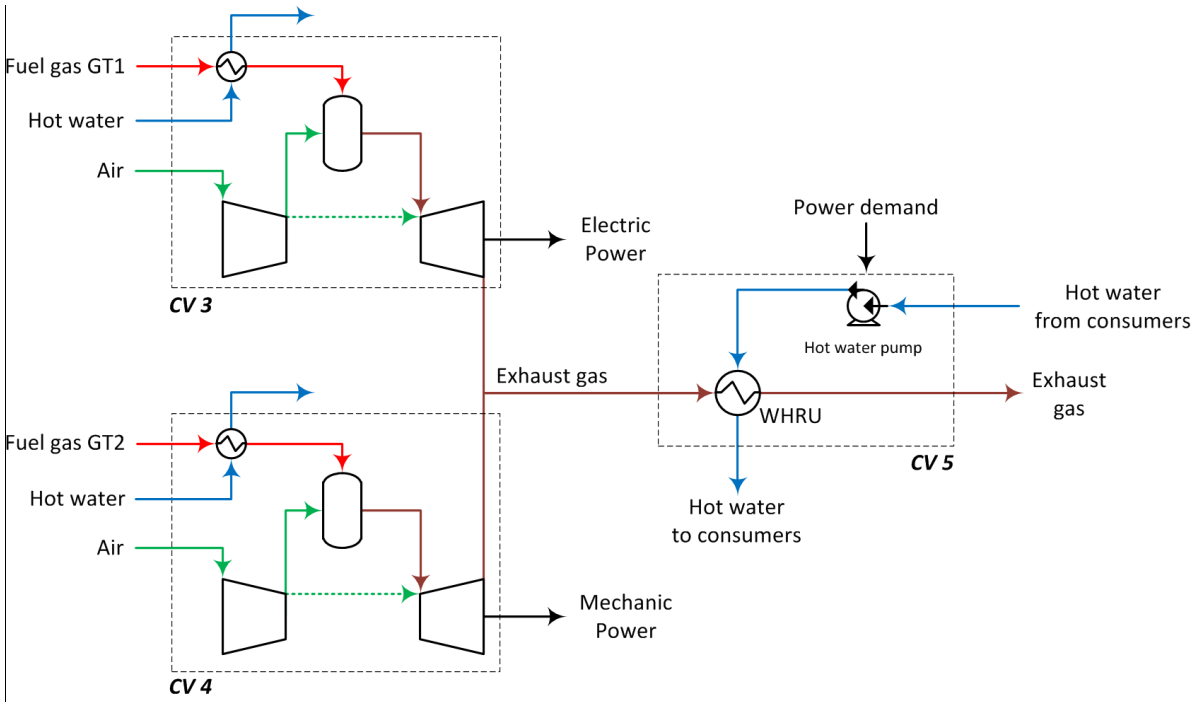

Source: Author´s elaboration.

The exergy balances for the gas turbine GT1, gas turbine GT2, and hot water system are presented in eqs.(23), (24), and (25), respectively. $\dot{B}_{d-GT1}$, $\dot{B}_{d-GT2}$, and $\dot{B}_{d-HWS}$ represent the destroyed exergy in GT1, GT2, and HWS, respectively. $\dot{W}_{GT1}$ is the electric power generated

by GT1, while $\dot{W}_{GT2}$ is the mechanical power generated by GT2 which is used for driving the CO_2 compressors. $\dot{W}_{HWS}$ is the power demand of the hot water pump.

$$\dot{B}_{d-GT1} = \left[\sum \dot{B}_{Fuel\ Gas\ GT1} + \sum \dot{B}_{Air\ to\ GT1} + \sum \dot{B}_{Hot\ water\ \ to\ GT1\ heater}\right] - \left[\dot{B}_{Exh-gas\ GT1} + \dot{B}_{Hot\ water\ \ from\ GT1\ heater}\right] - \dot{W}_{GT1} \quad (23)$$

$$\dot{B}_{d-GT2} = \left[\sum \dot{B}_{Fuel\ Gas\ GT2} + \sum \dot{B}_{Air\ to\ GT2} + \sum \dot{B}_{Hot\ water\ \ to\ GT2\ heater}\right] - \left[\dot{B}_{Exh-gas\ GT2} + \dot{B}_{Hot\ water\ \ from\ GT2\ heater}\right] - \dot{W}_{GT2} \quad (24)$$

$$\dot{B}_{d-HWS} = \left[\dot{B}_{Exh-gas\ GT1} + \dot{B}_{Exh-gas\ GT2} + \dot{B}_{Hot\ water\ from\ consumers}\right] - \left[\dot{B}_{Exh-gas} + \dot{B}_{Hot\ water\ \ to\ consumers}\right] + \dot{W}_{HWS} \quad (25)$$

Figure 30 shows the control volume used to analyze the Cooling Water System (*CV 6*). There are two water flows: one is the cooling water flow and the other one is the sea water flow. The exergy balance for this systems is given in eq.(26). $\dot{B}_{d-CWS}$ is the destroyed exergy, and $\dot{W}_{CWS}$ represents the power consumption in the cooling water and the seawater lift pumps.

Figure 30. Simplified control volume for Cooling Water System.

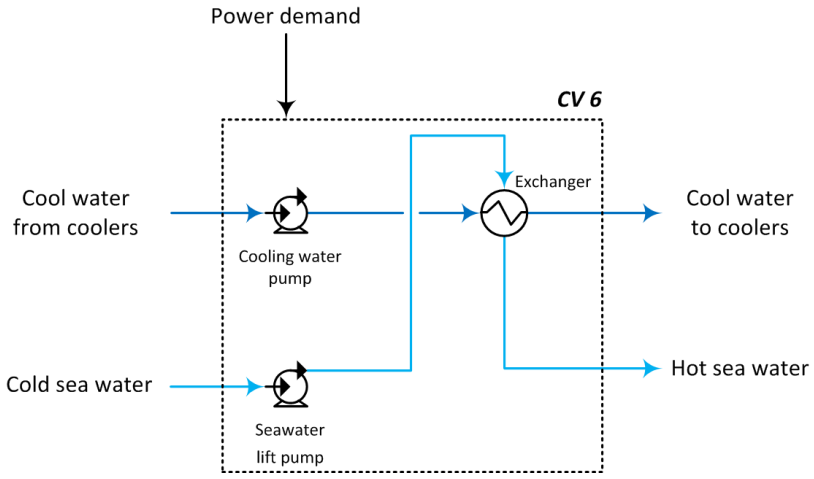

Source: Author´s elaboration.

$$\dot{B}_{d-CWS} = \left[\dot{B}_{Cool\ water\ from\ coolers} + \dot{B}_{Cold\ sea\ water}\right] - \left[\dot{B}_{Cool\ water\ to\ coolers} + \dot{B}_{Hot\ water\ \ to\ consumers}\right] + \dot{W}_{CWS} \quad (26)$$

The control volume for the Injection Water System (*CV 7*) is shown in Figure 31. The exergy balance is given in eq.(27). In this equation, $\dot{B}_{d-IWS}$ is the destroyed exergy in the system, and $\dot{W}_{IWS}$ is the power demand of the injection water pump.

$$\dot{B}_{d-IWS} = \dot{B}_{Sea\ water} - \dot{B}_{Water\ to\ injection} + \dot{W}_{IWS} \quad (27)$$

Figure 31. Simplified control volume for Injection Water System.

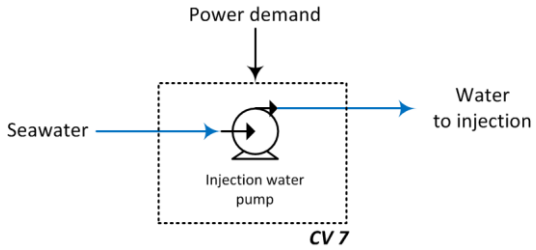

Source: Author´s elaboration.

The comparison of the different scenarios established in the previous chapter must be achieved taking into account the same production parameter. In this work, the maximum liquid capacity is defined by the processing capacity of the Free-water Knockout FWKO, 24000 m^3/d (150956 bpd), and this parameter was fixed for all simulation scenarios. Table 9 shows the maximum capacities of the operations in the FPSO.

Table 9. Maximum capacities of the FPSO operations.

Stream	Capacity	Unit	Operation
Liquid	24000	m^3/d	Processing
	150956	bpd	
Natural gas	6000000	Sm^3/d	Movement and treatment
Oil	24000	m^3/d	Storage
	150956	bpd	
Water (produced)	19000	m^3/d	Treatment
Water (injected)	28500	m^3/d	Injection

Source: Author´s elaboration. Data of typical FPSO operation.

Parameters and restrictions are established based on the values for typical Brazilian FPSO plants and on specialized and technical literature. Table 10 gives some of the main operation parameters and restriction values used in this work.

Table 10. Operation parameter and restriction conditions of the studied FPSO.

SEPARATION TRAIN		
Well-fluid temperature	20	°C
Well-fluid pressure	1.5	MPa
MC-A		
Compressors discharge pressure	8	MPa
Compressors adiabatic efficiency	75	%
MC-B		
Gas exportation pressure	24.5	MPa
Compressors adiabatic efficiency	75	%
GIT/CO_2-CT		
Gas exportation pressure	About 55	MPa
Compressors adiabatic efficiency	75	%
GAS TURBINE		
Overall efficiency	33.6	%
Turbine isentropic efficiency	91.11	%
Compressor isentropic efficiency	88.57	%
Compressor pressure ratio	17.98	
Compressor outlet temperature	432	°C
$\dot{m}_{air}/\dot{m}_{fuel}$ in the combustor	38.6	
$\dot{m}_{air}/\dot{m}_{fuel}$ in the gas turbine	46.9	
Turbine cooling air fraction	17.8	%
Combustor exit temperature	1156	°C
RIT	1125	°C
Turbine outlet pressure	106.2	kPa
$\dot{W}_{aux}/\dot{W}_{Processing\ plant\ power\ demand}$	25	%
Power factor	0.8	
Generator efficiency	0.96	
PUMPS		
Pumps adiabatic efficiency	75	%

Source: Author´s elaboration. Data of typical FPSO operation. Data for Gas turbine from Author´s modelling and simulation.

Pumps, gas compressors, and blower are powered by electrical motors. The factors showed in Table 11 were considered to calculate the electrical demand.

Table 11. Factors for electrical motors

Power range		Factor
If *Machine Power* is < 22 *bkW*	then	$kW \geq bkW$ x **1.25**
If 22 $bkW \leq$ *Machine Power* $\leq$ 55 *bkW*	then	$kW \geq bkW$ x **1.15**
If *Machine Power* is $\geq$ 55 *bkW*	then	$kW \geq bkW$ x **1.10**

Source: Author´s elaboration. Data of typical FPSO operation.

3.8.2 FPSO with CCS model

The FPSO with CCS model is represented by the control volume shown in Figure 32. This model is similar to the Reference FPSO model, but it includes the CCS system and its input and output streams. The details of the control volume for the CCS are described in Figure 33.

Figure 32. Simplified scheme of the control volume for the FPSO with CCS model.

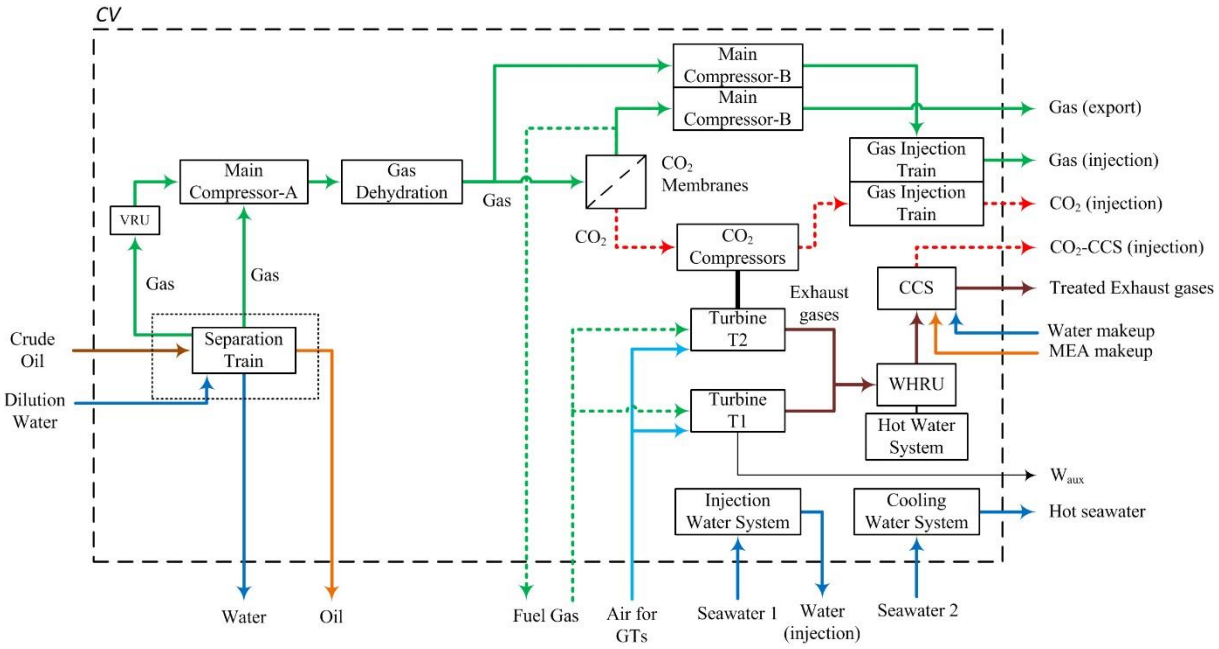

Source: Author´s elaboration.

As can be seen in Figure 33, exhaust gases from WHRU are sent to the CCS. The ranges of temperature of these exhaust gases are 377.1-388.8 °C for the well-fluid F1, 400.5-414.5 °C for the well-fluid F2, 384.4-389.5 °C for the well-fluid F3, and 409.8-414.8 °C for the well-fluid F4. These relatively high temperatures allow identification of exergy potential to be used to improve the use of the energy resources. Then, in order to satisfy the energy demand in the CCS, a second waste heat recovery unit is used to recover part of the exhaust gas exergy content. The CCS WHRU generates saturated steam at 140 °C which is used in the reboiler process. Exhaust gases from CCS-WHRU enter in the cooler to reduce their temperature at 40 °C which produces the reduction of the water content. The condensed water is drained in the separator. Exhaust gases from separator is sent to the blower where the gas pressure is increased from 101.8 kPa to 103.3 kPa to be introduced in the absorber column.

The absorber and desorber columns have been simulated with 12 and 20 equilibrium stages, respectively. Two pumps are used to transport the rich MEA solution and the lean MEA solution in the capture cycle. Discharge pressure of these pumps is 250 kPa. A heat exchanger is used to heat the rich MEA solution to the desorber, and the temperature of heated rich MEA solution is 104.3 °C. In the desorber, the established reflux ratio is 0.3 and the fixed reboiler temperature is 120 °C. Makeup water and makeup MEA are used to replace fluid losses. In this study, the CO_2 removal is about 90 %. The calculated energy consumption in the reboiler process are in the range of 3747-3756 kJ/kg_{CO2} for the well-fluid F1, 3761-3769 kJ/kg_{CO2} for the well-fluid F2, 3749-3769 kJ/kg_{CO2} for the well-fluid F3, and 3760-3787 kJ/kg_{CO2} for the well-fluid F4.

Figure 33. Simplified scheme of the control volume for CCS system.

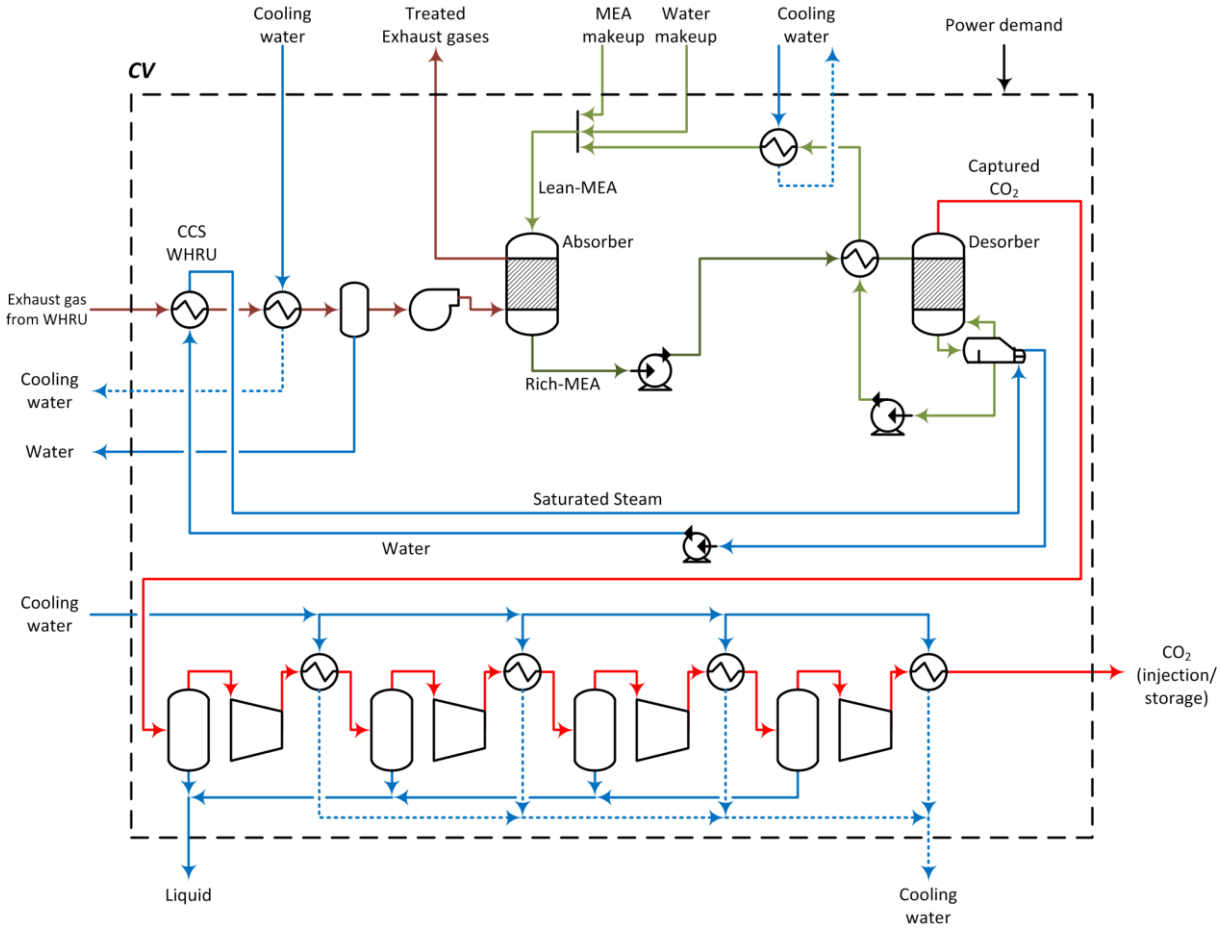

Source: Author´s elaboration.

Based on Figure 32, destroyed exergy of the reference FPSO with CCS may be calculated utilizing eq.(28):

$$\dot{B}_d = \left[\dot{B}_{Crude\ Oil} + \dot{B}_{Dilution\ Water} + \dot{B}_{Fuel\ Gas} + \dot{B}_{Seawater\ 1} + \dot{B}_{Seawater\ 2} + \dot{B}_{Air\ for\ GTs} + \dot{B}_{Water-makeup} + \dot{B}_{Mea-makeup}\right] - \left[\dot{B}_{oil} + \dot{B}_{water} + \dot{B}_{Fuel\ Gas} + \dot{B}_{Gas\ (export)} + \dot{B}_{Gas\ (injection)} + \dot{B}_{CO2\ (injection)} + \dot{B}_{Water\ (injection)} + \dot{B}_{Hot\ seawater} + \dot{B}_{Treated\ Exhaust\ gases} + \dot{B}_{CO2-CCS\ (injection)}\right] - \dot{W}_{aux} \quad (28)$$

The exergy balance for the CCS system, Figure 33, is given in eq.(29). In this equation, $\dot{B}_{d-CCS}$ is the destroyed exergy in the system, and $\dot{W}_{CCS}$ is the power demand of the CCS.

$$\dot{B}_{d-CCS} = \left[\dot{B}_{Exhaust\ gas\ from\ WHRU} + \sum \dot{B}_{Cooling\ water-inlet} + \dot{B}_{Water-makeup} + \dot{B}_{Mea-makeup}\right] - \left[\dot{B}_{Treated\ Exhaust\ gases} + \sum \dot{B}_{Cooling\ water-outlet} + \dot{B}_{water} + \dot{B}_{liquid} + \dot{B}_{CO2-CCS\ (injection)}\right] + \dot{W}_{CCS} \quad (29)$$

4 RESULTS AND DISCUSSION

Molar fractions for some components of the four simulated well-fluids are presented in Figure 34. As mentioned previously, these compositions are based on the first oilfield production stage. The blue bar indicates the sum of the molar fractions for methane C_1, ethane C_2, propane C_3, and butane C_4, which are considered as light hydrocarbon gases (JONES; MATTHEWS; RICHERS, 2000). The red bar shows the composition of the carbon dioxide CO_2, and the green bar presents the molar fraction of the hydrocarbon-plus fraction C_{20+}. The purple bar is the sum of medium and heavy components from C_5 to C_{20+}. In addition, this research found that when light hydrocarbon gases are summed with CO_2 (C_1-C_4 + CO_2), an idea of the power of the compressors may be predicted, as will be discussed later in the analysis of the *MC-A*. The cyan bar shows this value.

From the Figure 34 it can see that the well-fluid F2 has the lowest molar fraction of C_{20+} (4.8%) and C_5-C_{20+} components (19.7%), but has the highest molar content of C_1-C_4 + CO_2 (79.8%). Well-fluid F3 has the highest C_{20+} (8.0%) and CO_2 (26.1%) content, and the lowest level of light hydrocarbon gases (50.1 %). Well-fluid F4 exhibits the highest level of light hydrocarbon gases (77.9%) and the lowest CO_2 content (0.9%). It can be said that the fluid F1 has molar fraction values (light hydrocarbon gases (65.9%), CO_2 (8.2%), and C_{20+} (7.6%)) that are closest to the average of the four studied fluids: light hydrocarbon gases (mean 64.5%), CO_2 (mean 12.8%) and C_{20+} (mean 6.6%). In addition, F1 has the highest content of C_5-C_{20+} components (25.5%) and the lowest content of C_1-C_4 + CO_2.

Molar fraction patterns for different components presented in Figure 34 are defined below (in descending order):

- C_1-C_4: F4>F1>F2>F3
- CO_2: F3>F2>F1>F4
- C_{20+}: F3>F1>F4>F2
- C_5-C_{20+}: F1>F3>F4>F2
- C_1-C_4+CO_2: F2>F4>F3>F1

It is interesting to mention that the variability in the composition leads to both separation and power demand may have different behavior patterns as will be explained later in this chapter.

This makes it difficult to make a simple prediction of the plant performance, which is one of the contributions of the present work.

Figure 34. Molar fraction [%] of C_1-C_4, CO_2, C_{20+}, C_5-C_{20+}, and C_1-C_4+CO_2 for simulated well-fluids.

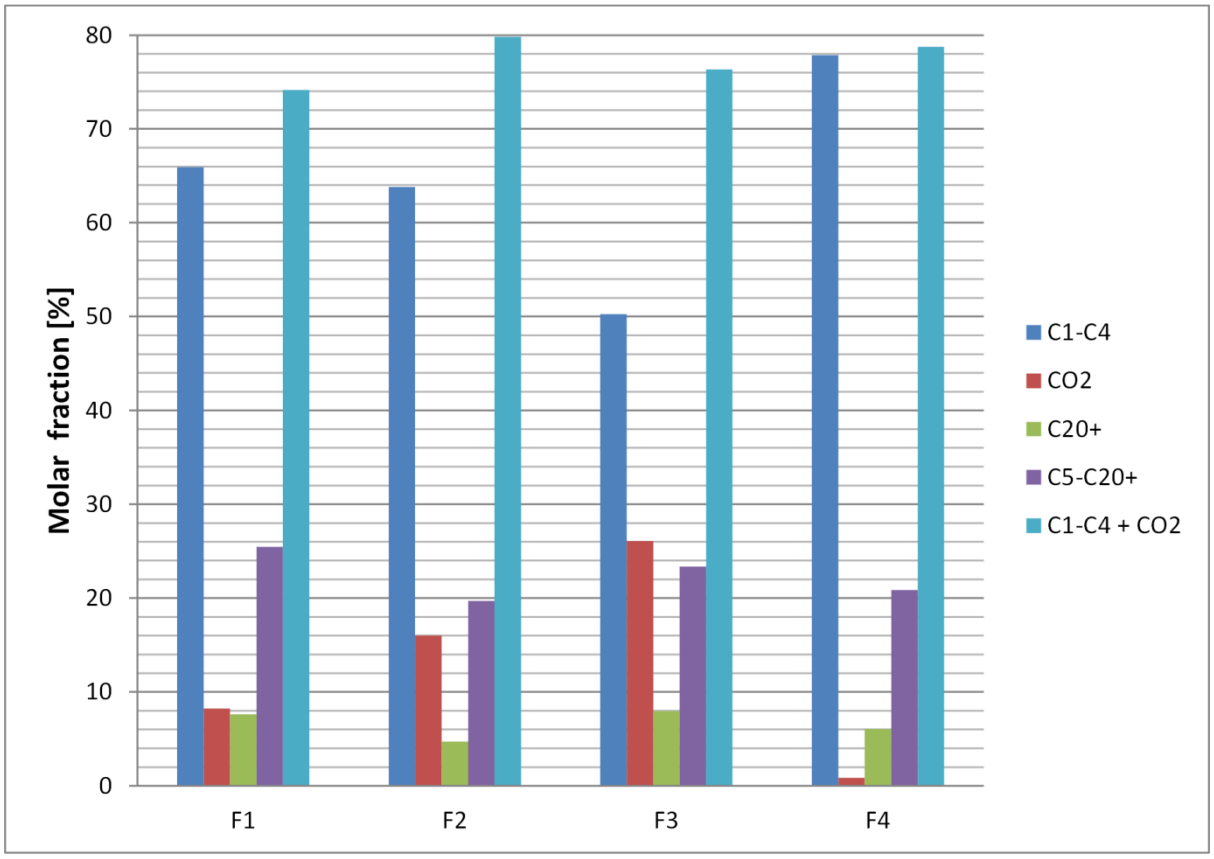

4.1 Volume flow rates

This section shows the results of volume flow rates of the more representative streams of the FPSO. Analysis focuses to understanding and interpreting of the pattern of the results and their relationship with parameters such as well-fluid composition and operational mode.

The well-fluid enters the first separator at 20°C and 1500 kPa, and it is processed in the separation train with a maximum processing capacity of about 151000 bpd. With this restriction, the volume flow rates for the Crude Oil stream obtained from the simulations are shown in Figure 35. Results are the same for the Reference FPSO and for the FPSO with CCS, in the three operation modes, since the processes of the CCS (e.g. CCS gas consumption) have no influence on the separation process. It is possible to observe that the

flow rate of Crude Oil only varies according to the processed fluid, and it can be seen from the Figure 35 that the well-fluid F4 allows the highest processing capacity, whereas well-fluid F3 has the lowest one. The variation between maximum and minimum processing capacity is about 5%. Additionally, it can be seen that it is not possible to establish a pattern that relates the molar fraction of any component in Figure 34 with the volume flow rate of the Oil Crude in Figure 35.

Figure 35. Volume flow rate [Sbpd] of the *Crude Oil* for Reference FPSO and FPSO with CCS.

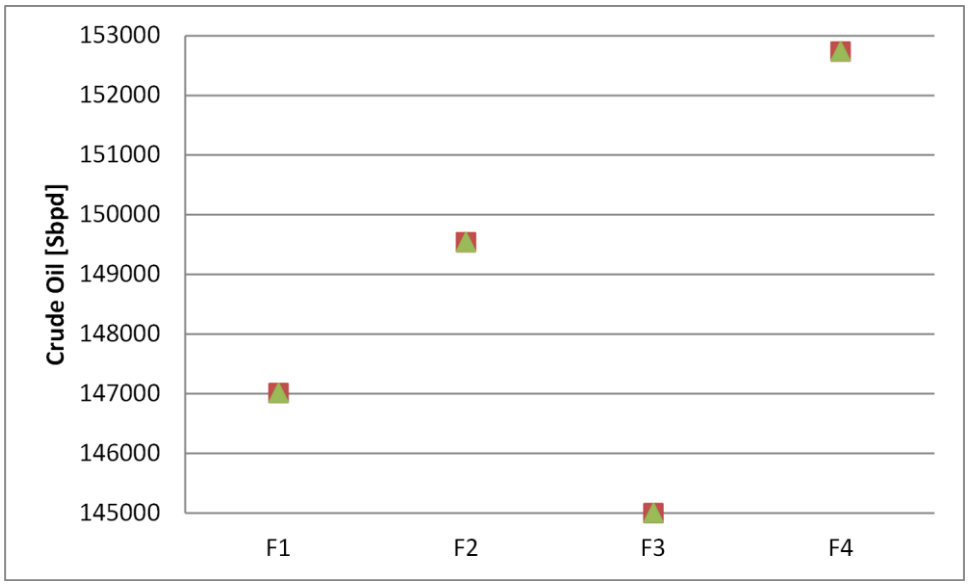

Figure 36. Volume flow rate [Sbpd] of the *Oil* for Reference FPSO and FPSO with CCS.

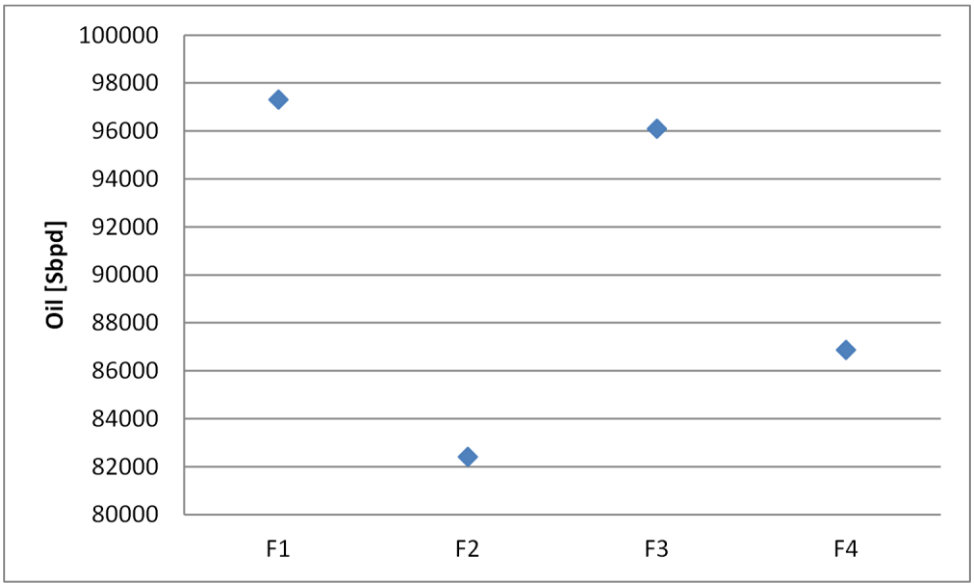

Figure 36 presents the results of volume flow rate for oil processed in the separation train. These results are the same for Modes 1, 2, and 3, as well as for Reference FPSO and FPSO with CCS. A detailed composition of the oil stream is provided in
Table 19 (APPENDIX B) for well-fluids F1, F2, F3, and F4. The pattern of the Oil volume flow rate (F1>F3>F4>F2) coincides with the pattern of C_5-C_{20+} heavy hydrocarbon components showed in Figure 34. Volume flow rate of the Oil stream is 66%, 55%, 66%, and 57% of the Crude Oil flow rate for well-fluids F1, F2, F3, and F4, respectively.

Gas flow rate compressed in the Main Compressors-A is shown in Figure 37. These results are unchanged when the CCS is implemented in the Reference FPSO, because the gas consumption of the CCS only affects the process after the CO_2 membranes. The pattern of the results is seen to be consistent with that defined by of sum of the light hydrocarbon gases and CO_2 in well-fluids (F2>F4>F3>F1), see Figure 34. As shown in Figure 37, well-fluid F2 presents the maximum value of volume flow rate; on the contrary, F1 has the minimum gas flow value. Flow rates for well-fluids F2, F3, and F4 are 26%, 4%, and 16%, respectively, higher than F1.

Figure 37. Volume flow rate [Sm^3/d] in the *Main Compressors-A* for Reference FPSO and FPSO with CCS.

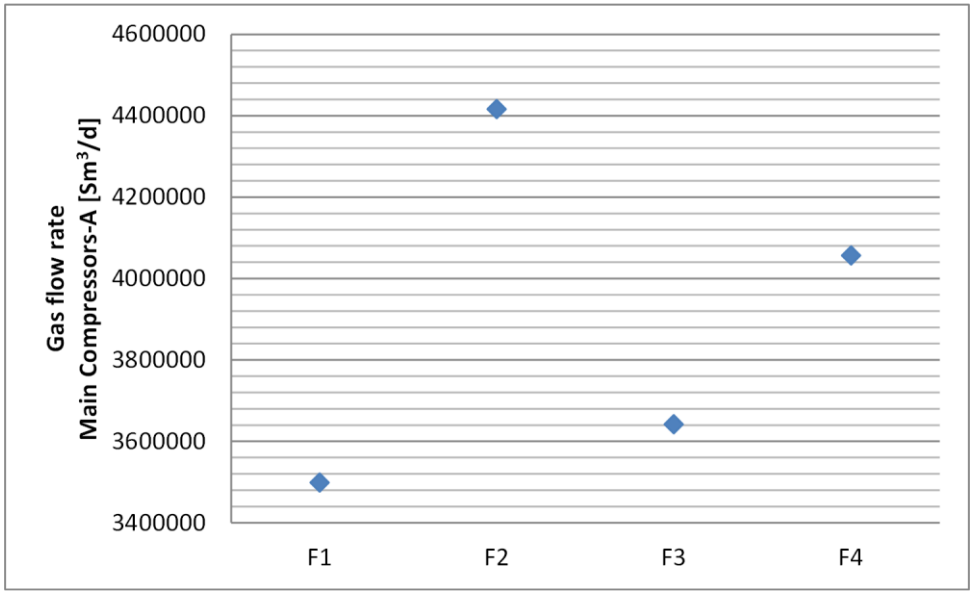

Gas export flow results are presented in Figure 38. Mode 1 does not export gas, therefore, gas flow values are zero. Higher results in Mode 2 in comparison with Mode 3 may be explained by the fact that Mode 2 is exclusively used to export all gas. Slight differences are founded between Reference FPSO and FPSO with CCS. For example, in Mode 2, FPSO with CCS exports 1.6% (avg. for all well-fluids) less gas that Reference FPSO, while in Mode 3, gas exportation in FPSO with CCS is 3.6% (avg. for all well-fluids) lower than Reference FPSO. These differences can be explained by the higher fuel consumption in the operation modes when FPSO has the CCS.

For a fixed operation mode, gas export values for the different well-fluids have the following descending order: F4>F2>F1>F3. This pattern does not match the one shown in Figure 37 for the gas flow rate of the Main Compressors-A. This divergence may be mainly explained by means of the results of volume flow rate of the CO_2 removed in the CO_2 removal system, see Figure 39. Gas export flow pattern is approximately the result of the difference between gas flow of MC-A and the sum of CO_2 removed and Fuel Gas flow rates. For well-fluid F3, the high value of CO_2 flow has a noticeable influence on the reduction of Gas export flow rate.

Figure 38. Volume flow rate [Sm^3/d] of the *Gas export* for Reference FPSO and FPSO with CCS.

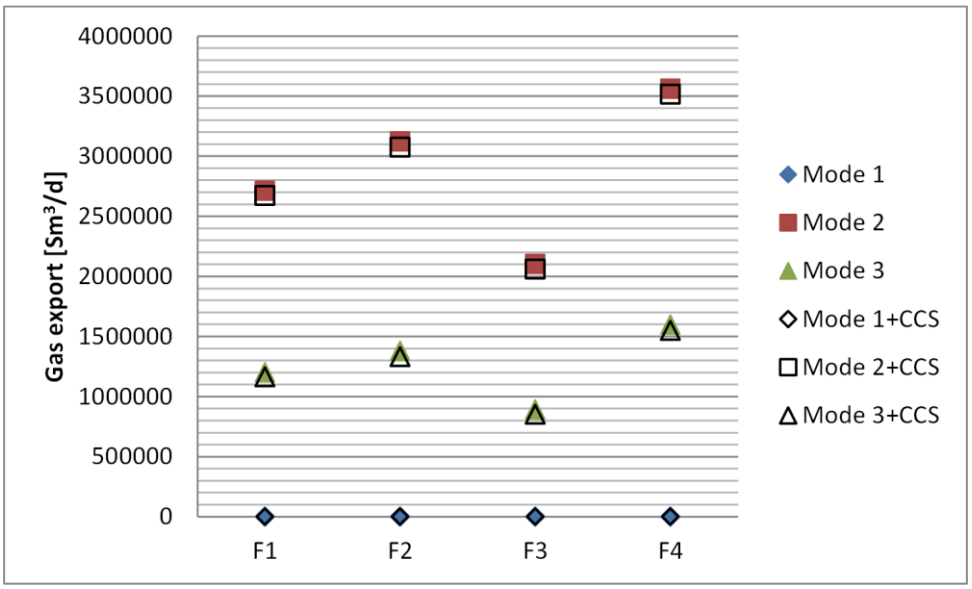

Figure 39. Volume flow rate [Sm^3/d] of the *CO_2 removed* for Reference FPSO.

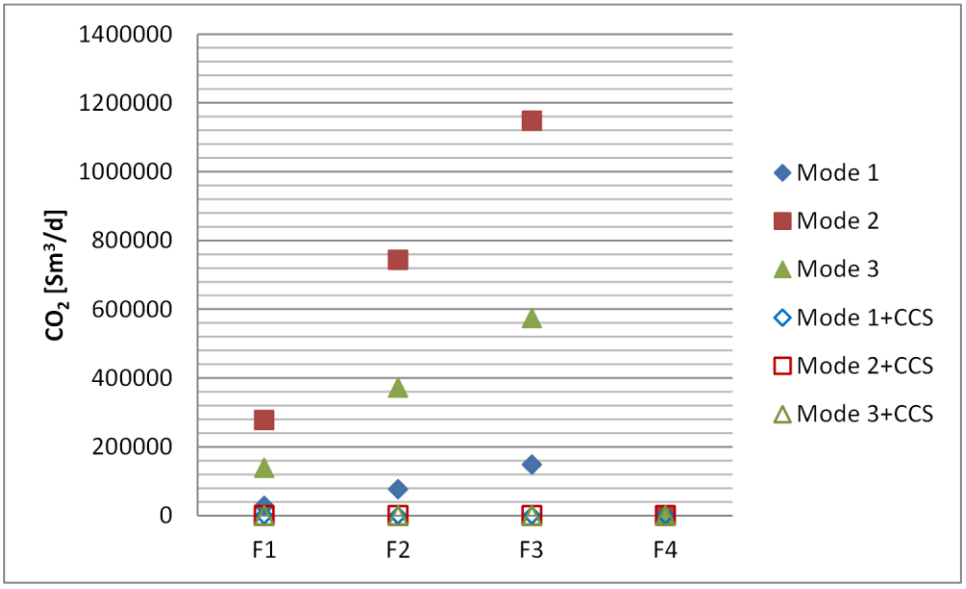

The results of the volume flow rate of the separated oil and exported gas are mixed in a single flow stream called *oil equivalent processed* at standard conditions. Figure 40 shows the results for the Reference FPSO. Results for FPSO with CCS (not shown) have a similar pattern except for slight differences (max. 0.3%) in scenarios of Modes 2 and 3, giving lower values than the Reference FPSO. These differences are due to the slight reduction of the amount of gas for export as a consequence of the increase of the fuel gas demand in the gas turbines which provide the additional power consumed in the CCS.

Figure 40. Volume flow rate [Sbpd] of the *oil equivalent processed* for Reference FPSO.

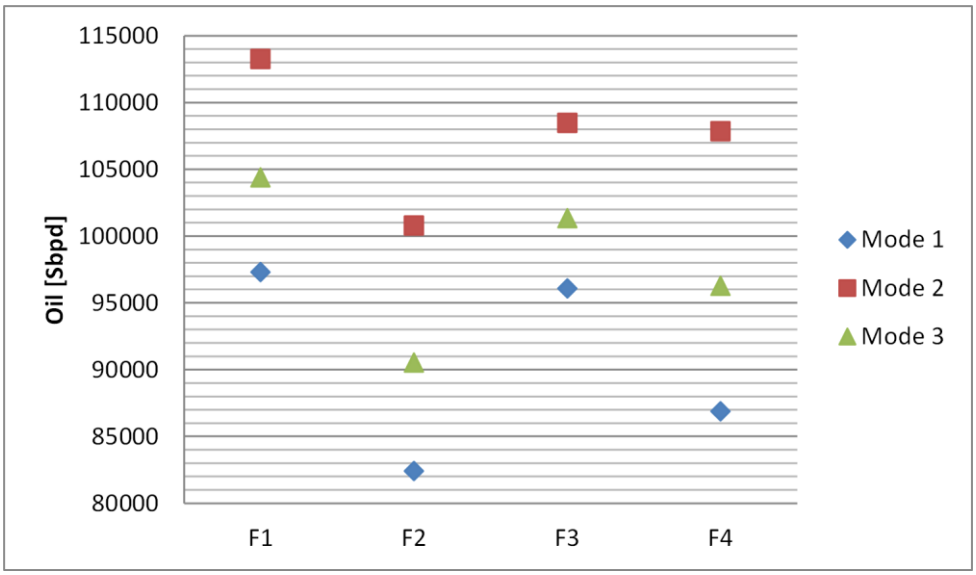

Fuel gas consumption for different scenarios is presented in Figure 41. Because FPSO with CCS plant has an additional power demand, the fuel gas consumption is higher than that in the Reference FPSO. Taking into account the average value for the three operational modes, well-fluid F1 has a fuel gas consumption value 12.6% lower in Reference FPSO in comparison with FPSO with CCS, while F2, F3, and F4, are 13.0%, 12.5%, and 13.6% lower, respectively.

For a fixed well-fluid composition, Reference FPSO shows that in well-fluids F1, F2, and F3, fuel gas consumptions are in the descending order: Mode 2>Mode 3>Mode 1, which is in accordance with the power demand explained in the next section. On the contrary, for well-fluid F4 the descending order is Mode 1>Mode 3>Mode 2, which indicates that, in absence of CO_2 removal and compression operations, gas injection operation is relevant in the fuel gas demand. In order to clarify the influence of the CO_2 compression operation in the total fuel consumption, Figure 42 and Figure 43 show the behavior of the fuel gas consumption for gas turbines GT1 and GT2, respectively.

Figure 41. Volume flow rate [Sm^3/d] of the *Fuel Gas* for Reference FPSO and FPSO with CCS.

As can be observed in Figure 42, for well-fluids F2, F3, and F4, the fuel gas consumption in the GT1 is higher in the Mode 1 followed by Mode 3 and Mode 2. In the case of well-fluid F1, all values are very close. As seen in Figure 41, values of fuel gas are higher in FPSO with CCS in comparison with Reference FPSO.

Figure 42. Volume flow rate [Sm^3/d] of the Fuel Gas consumption in Gas Turbine GT1 for Reference FPSO and FPSO with CCS.

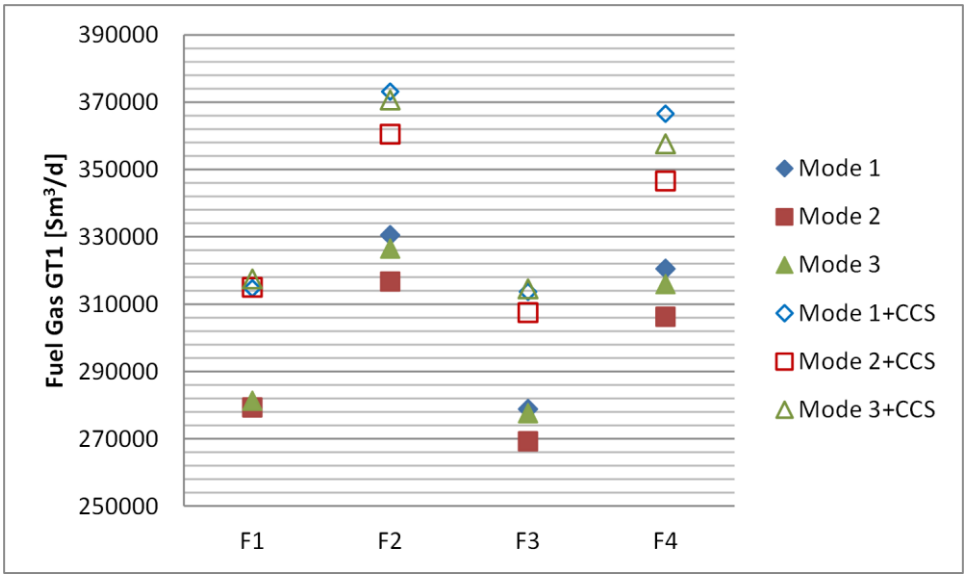

Figure 43 shows the fuel gas consumption in the gas turbine GT2 used for driving CO_2 compressors. The fuel gas pattern is similar to the CO_2 molar fraction pattern showed in Figure 34, and for a fixed well-fluid, the volume flow rate is higher in the Mode 2 followed by Mode 3 and Mode 1. Mode 2 requires the treatment of all gas for export purposes; therefore, more CO_2 is separated and compressed to be injected.

Figure 43. Volume flow rate [Sm^3/d] of the Fuel Gas consumption in Gas Turbine GT2 for Reference FPSO and FPSO with CCS.

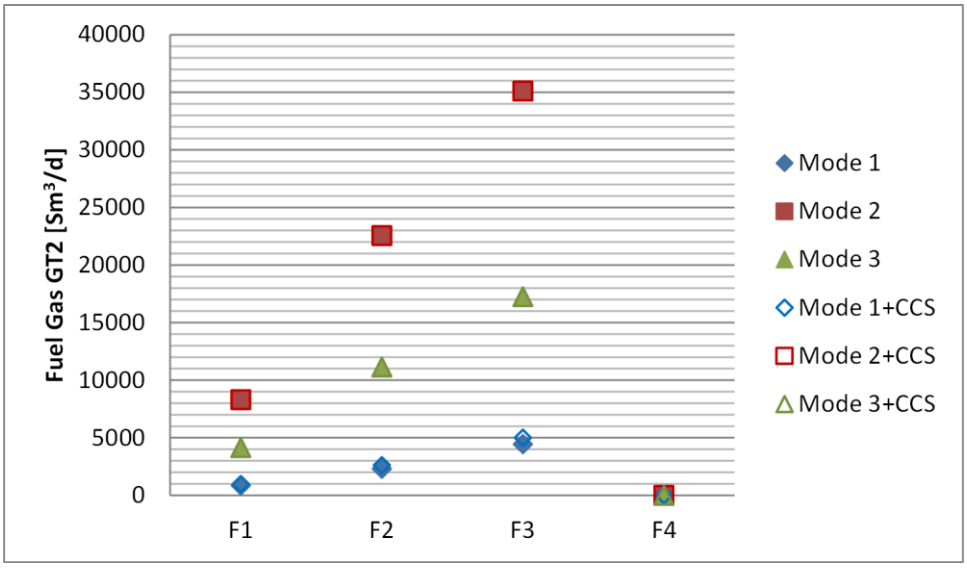

4.2 Power demand

In this section, results of power demand of whole FPSO and different systems is presented and analyzed. In the exergy analysis, power demand is an essential variable due to its influence in the exergy consumption of the plant, and in consequence, in the overall exergy and environmental performance.

FPSO power demand indicates the overall electric power consumed by different fluid machines in the processing plant. Basically, compressors and pumps are the electrical consumers used in the FPSO model, except for the FPSO with CCS which uses additionally a blower for flue gas movement.

Figure 44 presents the results of the total power demand of the FPSO for the different studied scenarios. Power demand has a similar pattern for Reference FPSO as well as FPSO with CCS. For a fixed operation mode, this pattern is, in descending order, as follows: F2>F4>F1>F3. Additionally, power demand in FPSO with CCS is 13.3% higher than in Reference FPSO as a consequence of the power consumption in the blower, pumps and compressors of the carbon capture system.

Figure 44. Power demand of the FPSO.

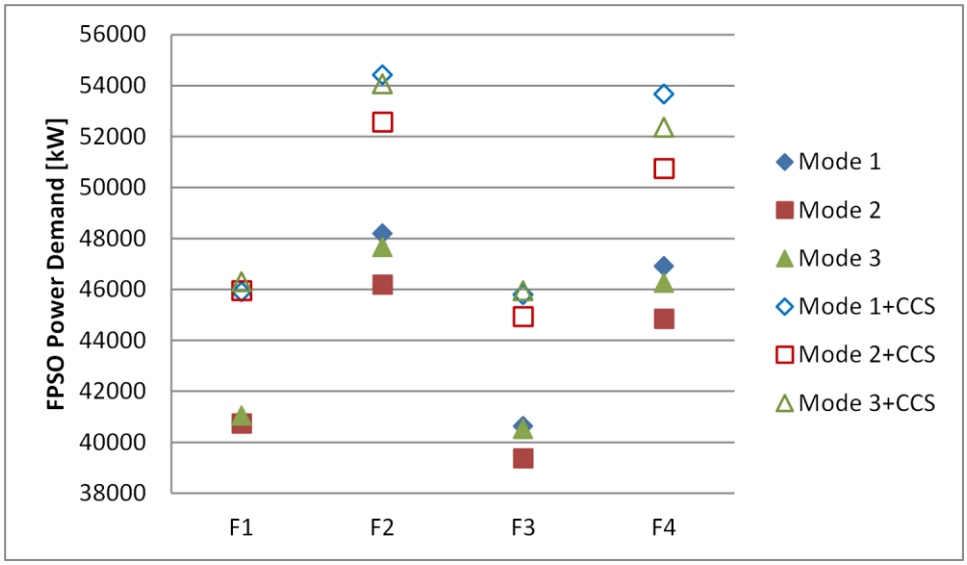

When the pattern is analyzed based on a fixed well-fluid, it is interesting to note that the power demand in descending order is mainly given by: Mode 1>Mode 3>Mode 2. These values of power demand present a dispersion that varies depending on the well-fluid and the

FPSO plant. As well-fluid F1 has minimal dispersion of the power demand for the three operation modes, well-fluid F4 in the FPSO with CCS has the maximum. Variations in the dispersion of the power demand are mainly related to the electric consumption in the compressors, which is not readily predicted, but there is another important consumer: the water injection pumps. These pump systems consume 8289 kW, 11841 kW, and 10065 kW, for Modes 1, 2, and 3, respectively.

Power demand in some compression trains is presented in the next figures in order to compare the contribution of each operation in the gas compression processes. The first compression systems presented are those with highest power consumption: Main Compressors-A MC-A, Main Compressors-B, MC-B (for exportation), Gas injection train GIT, CO_2 injection, and Carbon capture and storage systems CCS. After, vapor recovery unit, water injection pumps, separation train pumps, hot water system pumps, and cooling water system pumps will be analyzed.

Power consumption of Main Compressors-A is presented in Figure 45. The power demand pattern given by F2>F4>F3>F1 is directly related to the volume flow rate of the MC-A in Figure 37, therefore power demand is correlated with the C_1-C_4+CO_2 molar fraction pattern in Figure 34. Power demand for well-fluids F2, F3, and F4 are 27%, 6%, and 17% higher than F1.

Figure 45. Power demand of the Main Compressors-A *MC-A*.

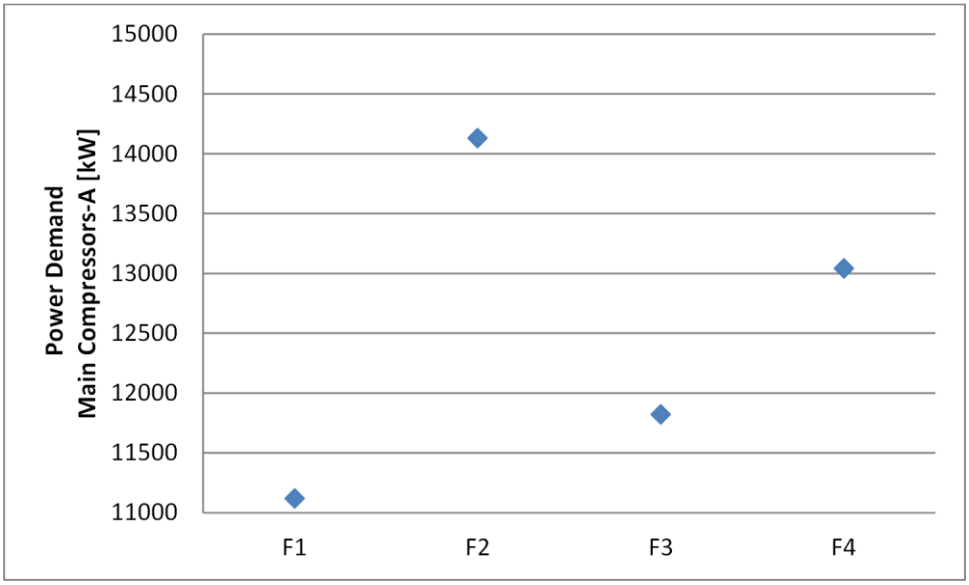

Results of the power demand of the Main Compressors-B shown in Figure 46, consider the electric power of the MC-B section used exclusively for gas exportation process, see Figure 22. Mode 1 (all gas is injected) does not have power consumption for exportation purposes. Power demand of MC-B presents the pattern F4>F2>F1>F3 which obviously is the same pattern of the volume flow rate of the gas exportation. As mentioned previously, light hydrocarbon gases and CO_2 content in the well-fluid are relevant in the MC-B power demand. For all well-fluids, power demand for Mode 3 is approximately the 44 percent of the power consumption in Mode 2. Power requirements of MC-B in Mode 2 for well-fluids F1, F2, and F4, are 26.8%, 45.5%, and 52.4% greater than F3; whereas in Mode 3, the power consumption for F1, F2, and F4 are 32.4%, 51.5%, and 60.9% higher than F3. There are slight variations in MC-B power demand of Reference FPSO and FPSO with CCS. In Mode 2, power demand in Reference FPSO is 1.6% less, on average, than FPSO with CCS, whereas in Mode 3, this value is 3.6%.

Figure 46. Power demand of the Main Compressors-B *MC-B* (for gas exportation).

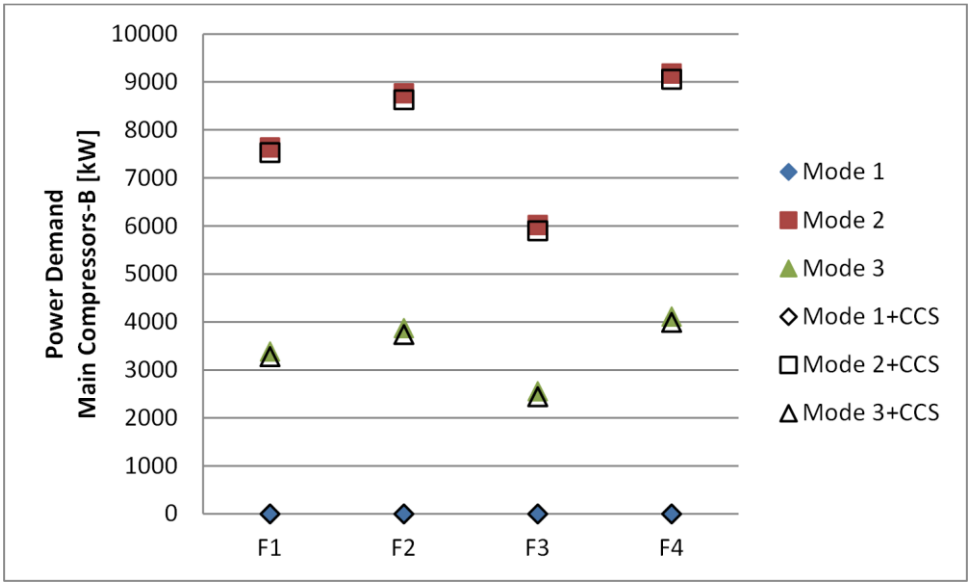

The results obtained for power demand of Gas injection train GIT can be seen in Figure 47. This power consumption includes the power demand of the MC-B section destined for gas injection purposes and the power demand of the gas injection compressors, see Figure 21.

Figure 47. Power demand of Gas injection train *GIT*.

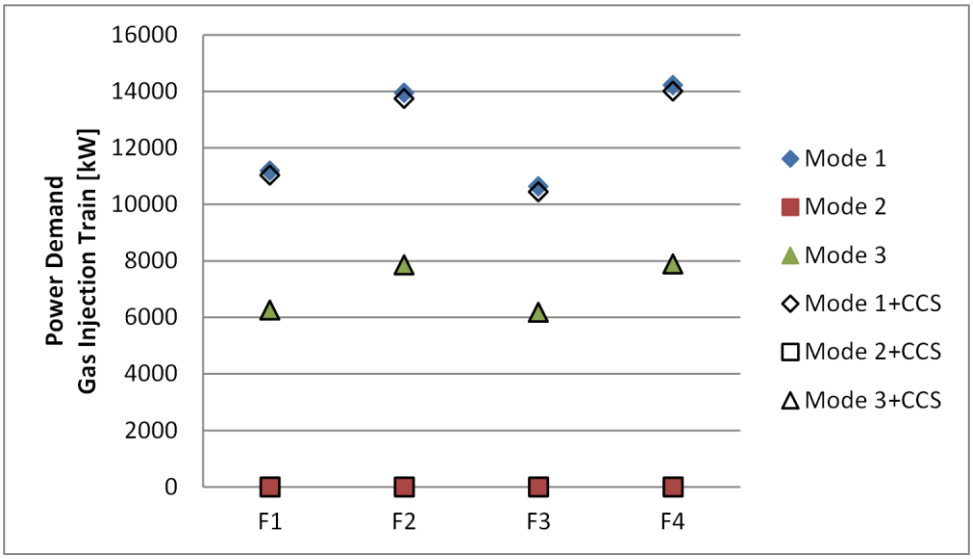

Mode 3 power demand results in lower values in comparison with Mode 1. For all well-fluids, power demand for Mode 3 is, on average, about 56% of the power consumption in Mode 1. As shown in Figure 47, Mode 2 (all gas is exported) does not have power consumption for the gas injection train.

No differences were obtained for power demand in the Mode 3 for Reference FPSO and FPSO with CCS, however, in Mode 1, slight differences may be observed. For this mode, all production fluids demand 1.6% (on average) less power in FPSO with CCS than in Reference FPSO.

In spite power demand pattern for Modes 1 and 3 is F4>F2>F1>F3, this pattern is not clearly defined as in the case of MC-B because no significant differences were found between power demand for well-fluids F1 and F3, and for well-fluids F2 and F4, especially, in Mode 3. Furthermore, it is interesting to note that the injected gas has approximately the same composition of the MC-A, and consequently the expected pattern could be F2>F4>F3>F1; however, the gas injection train pattern is different due to the influence of the required injection pressure. Table 12 presents the injection pressure for the studied scenarios, which was interpolated from the Table 18 (APPENDIX A) as a function of the gas volume flow rate and CO_2 molar fraction. From the data in this table, it is apparent that the injection pressure pattern for gas may explain the relative increment of the injection power demand for well-

fluid F4 in comparison with F2 and, similarly, the relative increment of F1 in comparison with F3, giving as result the pattern in Figure 47.

Table 12. Required injection pressures for studied scenarios in Reference FPSO and FPSO with CCS [kPa].

		Fluid 1	Fluid 2	Fluid 3	Fluid 4	Pattern for injection pressure
Mode 1	Gas	49911	48889	44026	52220	F4>F1>F2>F3
	CO_2	20400	20400	20400	-	F1=F2=F3
Mode 2	Gas	-	-	-	-	-
	CO_2	20562	21856	23342	-	F3>F2>F1
Mode 3	Gas	50388	49691	44828	52753	F4>F1>F2>F3
	CO_2	20400	20752	21341	-	F3>F2>F1

Power demand of the CO_2 compressor train is presented in Figure 48. The behavior of this power consumption (F3>F2>F1) is coherent with CO_2 molar fraction (Figure 34) of well-fluids and with volume flow rate of CO_2 removed in the membranes (Figure 39). As indicated by the results, well-fluid F4 has low content of CO_2 and for that reason CO_2 membranes unit is not used. No differences were obtained for power demand of Modes 2 and 3 in Reference FPSO and FPSO with CCS, while in Mode 1, the results for Reference FPSO are 12.7% (on average) lower than power consumption in FPSO with CCS.

Figure 48. Power demand of CO_2 compressor train *CO2-CT*.

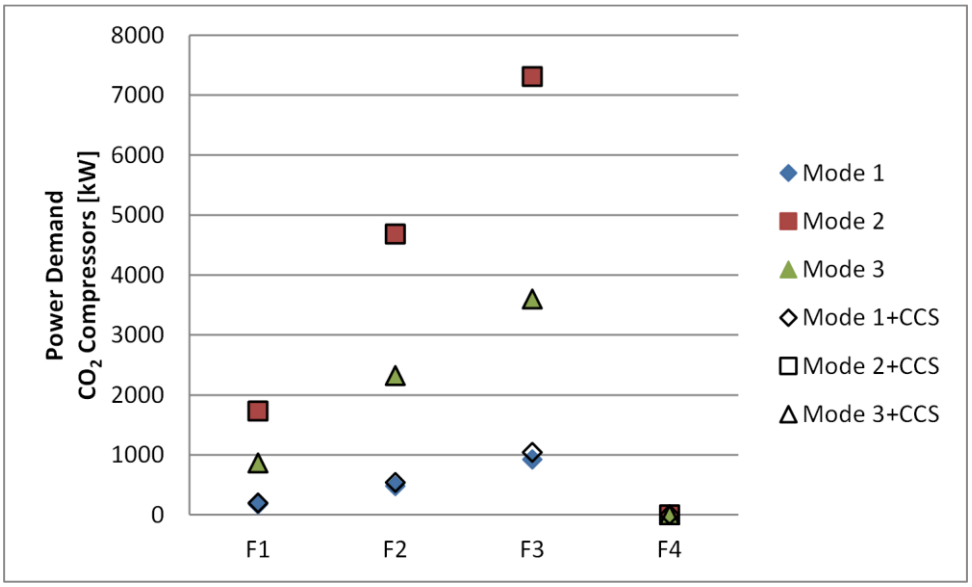

In addition, it may be seen in Figure 48 that, in Mode 2, the power demand of CO_2 compressors for F1, F2, and F3, is 9.9, 9.8, and 7.9 times higher than power demand in Mode 1; whereas in Mode 3, power consumption of these well-fluids is 5.0, 4.9, and 3.9 times higher than in Mode 1.

Figure 49 and Figure 50 summarizes the power consumption of the Gas Compression Train including and not including the power demand of the CO_2-CT, respectively.

Figure 49. Power consumption of the Gas Compression Train (MC-A+MC-B+GIT+VRU).

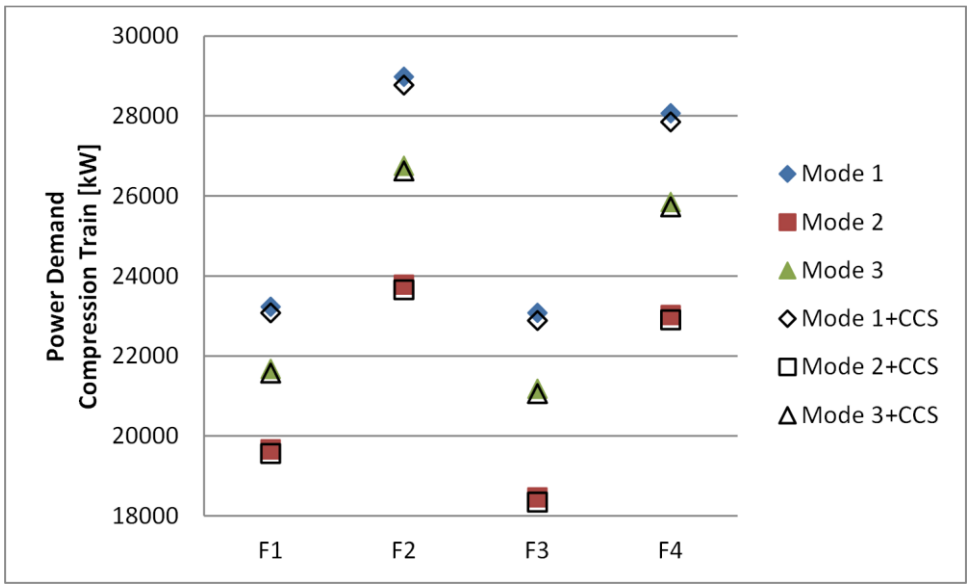

Figure 50. Power consumption of the Gas Compression Train (MC-A+MC-B+GIT+VRU+ CO_2-CT).

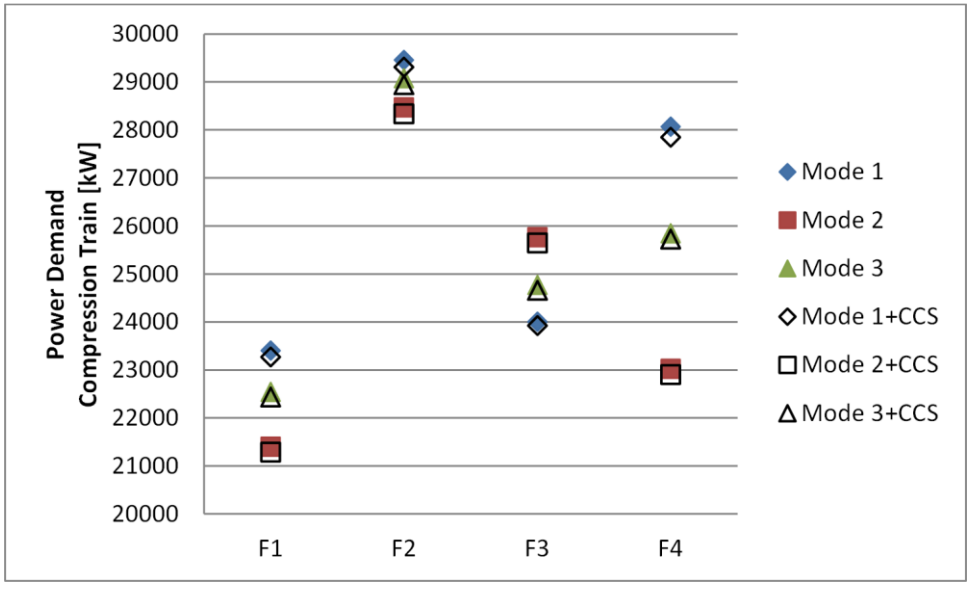

The behavior of the power consumption showed in Figure 49 is associated with the pattern of consumption of the MC-A (Figure 45), MC-B (Figure 46), GIT (Figure 47), and VRU (Figure 59). There is a considerable variation in the pattern of the power demand in Mode 2 when the CO_2-CT is taken into account.

As seen in Figure 50, Mode 2 presents the highest power demand when the well-fluid F3 is processed; however, Mode 2 is the lowest value in Figure 49. These findings suggest a noticeable influence of the CO_2-CT in the power demand of the Compression Train.

The results obtained for power demand of the CCS are shown in Figure 51. CCS demand includes the power consumption of the following components: a blower for driving exhaust gases from gas turbine, two pumps for MEA solution recirculation, and a compression train for captured CO_2 injection and storage.

The power demand of CCS is related to the sum of fuel gas consumption in GT1 and GT2. More fuel gas implies more quantity of CO_2 to be captured, compressed and injected by means of the CO_2 compressors of the CCS. For example, the dispersion observed in the power demand for well-fluid F3 in Figure 51, is produced by the dispersion of the fuel gas in GT2, see Figure 43.

Figure 51. Power demand of CCS.

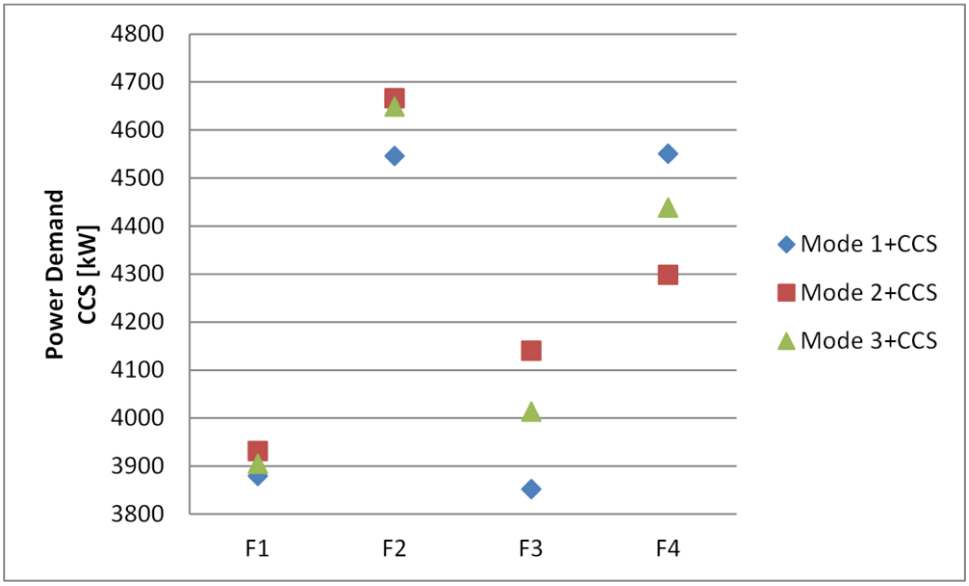

Also, it is important to note that the pattern of power demand of the well-fluid F4 is inverted regarding to F1, F2, and F3. This aspect may be explained by the absence of CO_2 compression train in the processing plant, therefore, the pattern is based on fuel gas consumption of GT1, see Figure 42. As shown in Table 13, power demand of CO_2 compressors constitutes 89.5% of the total power demand of the CCS, while the blower and the pumps demand 9.1%, and 1.4%, respectively.

Table 13. Power demand of CCS components [kW].

	F1	*F2*	*F3*	*F4*
	Blower			
Mode 1	333	416	353	405
Mode 2	359	426	382	383
Mode 3	356	424	369	395
	Pumps (Lean and Rich pumps)			
Mode 1	52	64	54	66
Mode 2	56	66	59	62
Mode 3	55	66	57	63
	CO_2 Compressors			
Mode 1	3262	4064	3444	4072
Mode 2	3517	4172	3699	3853
Mode 3	3493	4159	3587	3980

A comparison of power demand of different compressions trains previously discussed is shown in Figures 52-57. Additionally, power demand of the water injection system WIS was included and, as mentioned previously, this power has a fixed value for Mode 1 (8289 kW), Mode 2 (11841 kW), and Mode 3 (10065 kW). These figures complement the previous analysis and broaden the understanding of the FPSO behavior.

As can be seen from Figures 52-57, for each well-fluid, MC-A power demand is the same in all operational modes. For Reference FPSO operating in Mode 1, Figure 52 shows that MC-A demands similar power than GIT for well-fluids F1 and F2, while there are variations of about of 10% for F3 and F4. CO_2-CT power demand is less than 10% of the power consumption in MC-A or GIT. WIS has considerable power consumption and represents 74.6%, 58.7%, 70.1%, and 63.6% of the MC-A power for well-fluids F1, F2, F3, and F4, respectively.

Figure 52. Compressions trains power demand in Mode 1 – Reference FPSO.

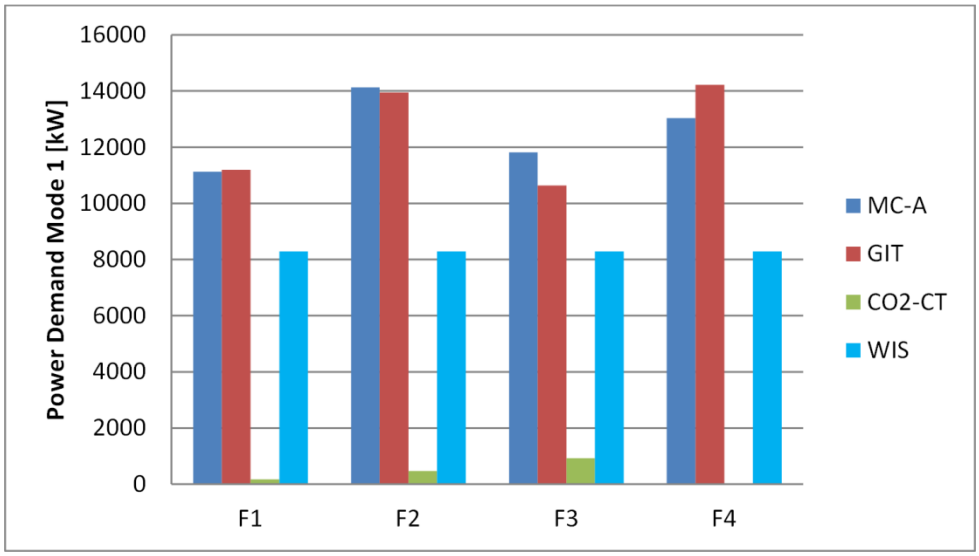

Figure 53 shows the results for Mode 1 in the FPSO with CCS. The influence of the CCS system is indicated by the orange bar, and the CCS power consumption is, on average, 33.6% of the MC-A power demand. All the other systems have power demands similar to those shown in Figure 52.

Figure 53. Compressions trains power demand in Mode 1 – FPSO with CCS.

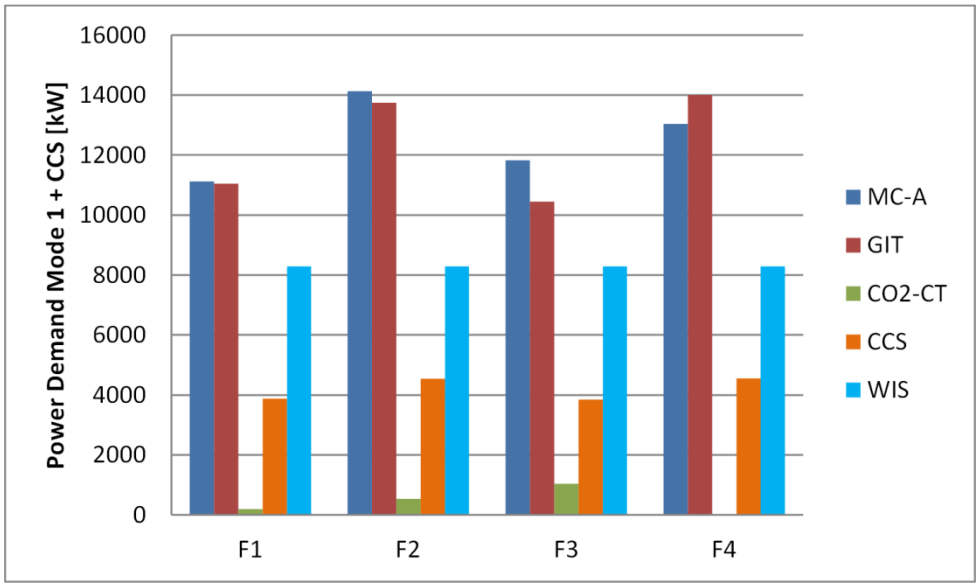

Figure 54 provides the results obtained for Reference FPSO operating in Mode 2. MC-B power consumption is 68.6%, 62.0%, 50.9%, and 70.3% of the MC-A power demand for F1, F2, F3, and F4, respectively.

Figure 54. Compressions trains power demand in Mode 2 – Reference FPSO.

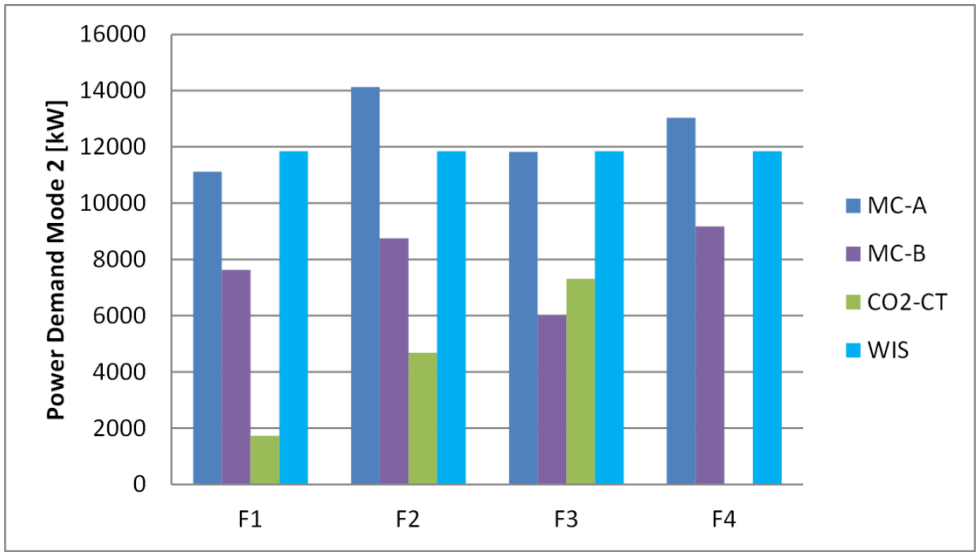

As mentioned previously, this operational mode has the highest CO_2-CT power demand in comparison with Modes 1 and 3. The CO_2-CT power consumption is 15.6%, 33.1%, and 61.8% of the MC-A power demand, for production fluids F1, F2, and F3, respectively. Also, it is interesting to note that WIS power consumption has a great influence in the overall power consumption. For well-fluid F1, WIS is 6.5% higher than MC-A; on the contrary, WIS is 16.2% and 9.2% lower than MC-A for F2 and F4, respectively. For production fluid F3, WIS and MC-A power consumptions are very similar.

Figure 55. Compressions trains power demand in Mode 2 – FPSO with CCS.

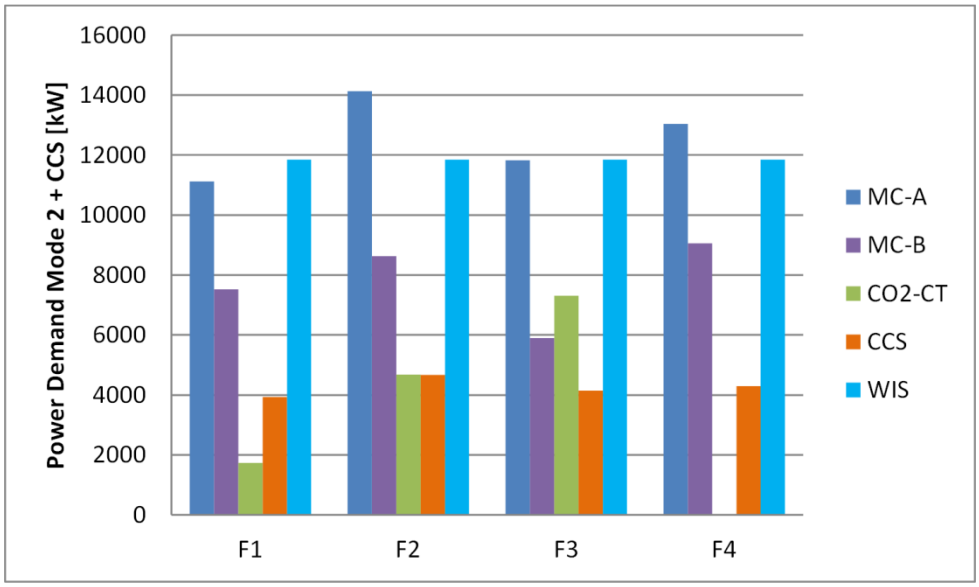

Results of power demand for FPSO with CCS operating in Mode 2 are presented in Figure 55. All systems exhibit similar values of power demand to those presented in Figure 54. The CCS power demand is, on average, 34% of the MC-A, for all well-fluids.

Figure 56 presents the results for Reference FPSO operating in Mode 3. As indicated by the results, MC-B power demand is 30.4%, 27.4%, 21.6%, and 31.5% of the demand in MC-A for F1, F2, F3, and F4, respectively; while GIT power consumption is, on average, 56.1% of the MC-A. In addition, CO_2-CT power demand represents 7.8%. 16.4%, and 30.4% of the power consumed by MC-A; and for WIS, the power demand is 90.5%, 71.2%, 85.1%, and 77.2% of the MC-A. In this operational mode, WIS is a predominant energy consumer system in comparison with MC-B and GIT systems.

Figure 56. Compressions trains power demand in Mode 3 – Reference FPSO.

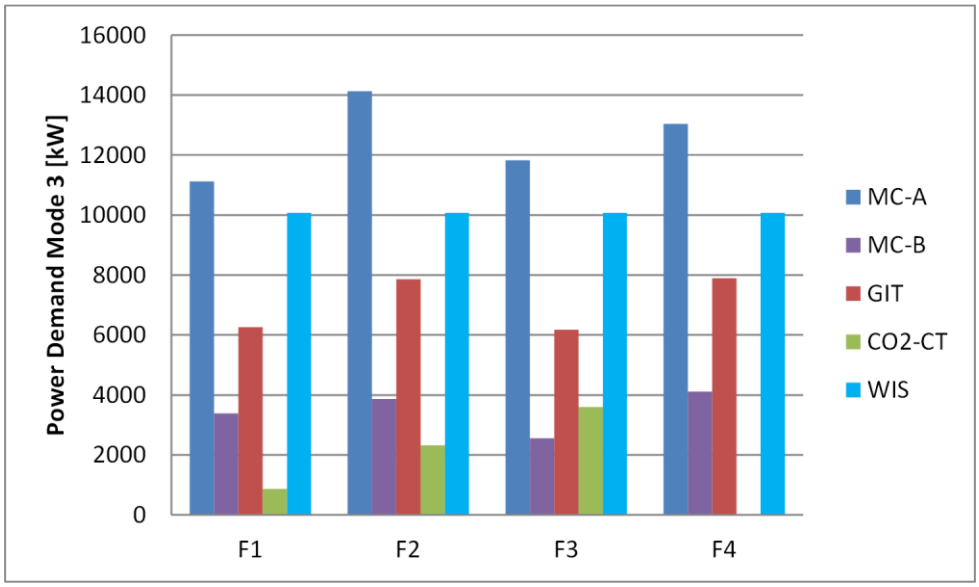

Results for FPSO with CCS in Mode 3 are presented in Figure 57. Similar to the previous cases, there are no considerable differences between power demand of the systems in Figure 57 and Figure 56. CCS power demand is, on average, 34% of the power consumed in MC-A.

As can be seen from Figures 53, 55, and 57, the power consumption of the CCS is, on average, 40% of the MC-A power demand. This value is equivalent to 8.6% (on average) of the total power demanded by FPSO, see Figure 44.

Figure 57. Compressions trains power demand in Mode 3 – FPSO with CCS.

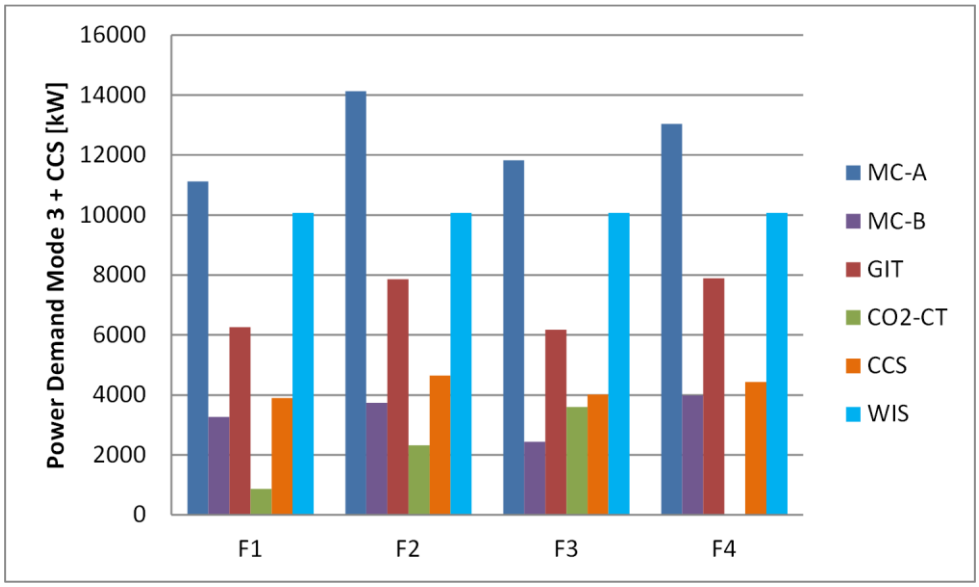

The following three figures give a description of the power demand for systems with lower consumption: separation train, vapor recovery unit VRU, cooling water system, and hot water system. The power demand of the separation train is shown in Figure 58. Results are the same for all operation modes and for Reference FPSO and FPSO with CCS. This is because there is no influence of either the mode of operation or the *CCS* in the separation process. These factors affect the process after *MC-A*. Separation train demands less than 0.32% of the total FPSO power demand. Moreover, the power demand pattern is given by F1>F3>F4>F2.

Figure 58. Power demand of Separation Train for Reference FPSO and FPSO with CCS.

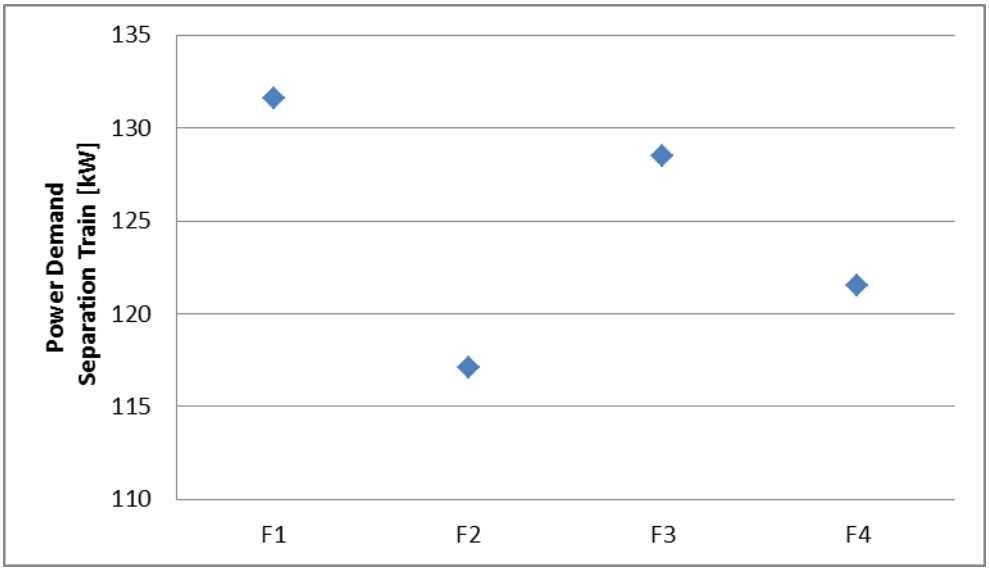

Figure 59 shows the results of the power demand in the VRU. A defined pattern of the VRU power consumption and its relation with the fraction molar of well-fluid components in Figure 34 cannot be identified for this system. Power demand for Modes 1, 2, and 3 is the same for each production fluid. From this figure, the VRU power demand pattern is given by: F1>F2>F4>F3. Additionally, there are not differences between power demand for Reference FPSO and FPSO with CCS.

Figure 59. Power demand of VRU for Reference FPSO and FPSO with CCS.

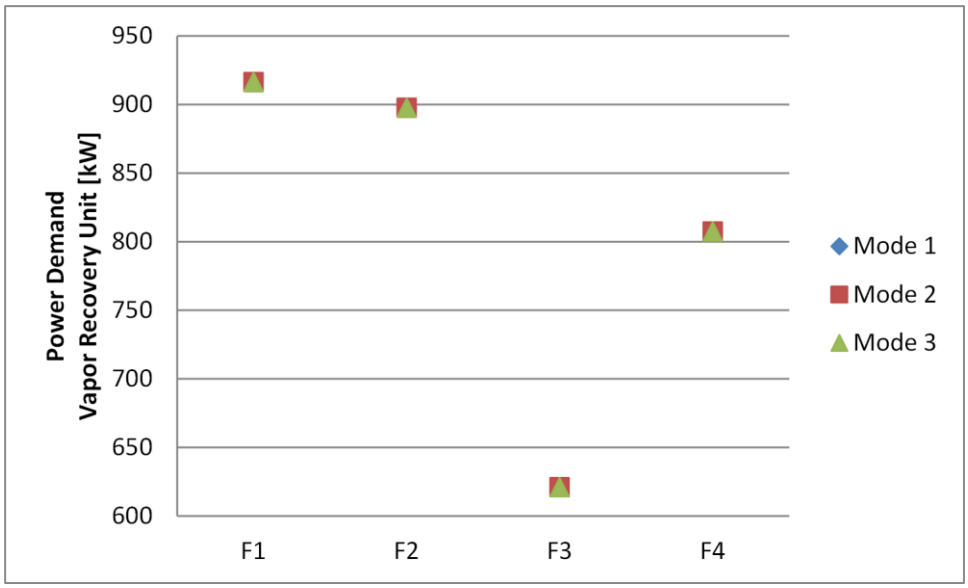

Figure 60. Power demand of Cooling Water System.

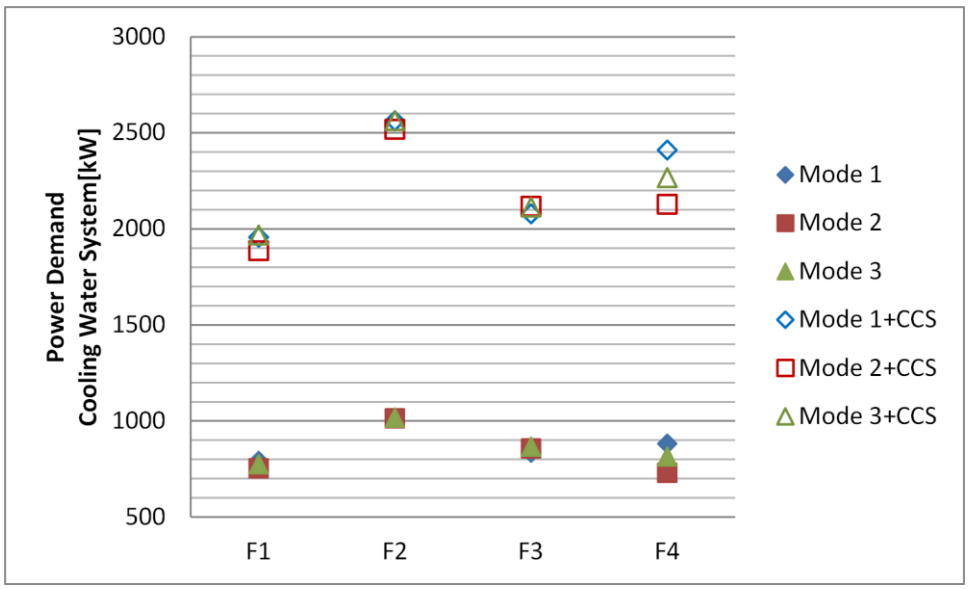

Power demand of cooling water systems is presented in Figure 60. As can be seen from this figure, results are higher in FPSO with CCS than in Reference FPSO owing mainly to the additional consumption of water used in the coolers of the CCS. On average, values of power demand for the cooling system of FPSO with CCS are 2.6 times greater than power consumption in Reference FPSO. Another interesting aspect is that Well-fluid F4 shows a noticeable dispersion in comparison with the other fluids. This may be explained for the lack of CO_2 membranes treatment and compression processes.

Figure 61 shows the power demand of the hot water system. There are negligible differences (0.25%) between power demand for Reference FPSO and FPSO with CCS. The expected pattern is mainly defined by the heat demand in the production heater F1>F3>F2>F4. Variations in the patterns showed in Figure 61 are due to heat requirements in fuel gas treatment and heat demand in the CO_2 removal unit.

Figure 61. Power demand of Hot Water System.

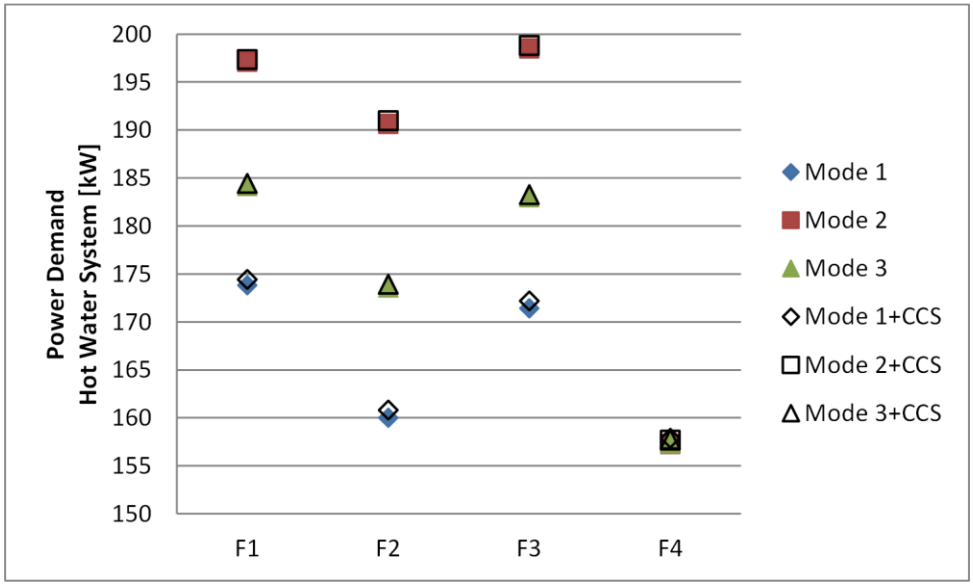

4.3 Exergy demand for heating processes

Exergy demand for heating processes refers to the quantity of exergy supplied by hot water to increase the temperature of some oil, water or gas streams. Figure 62 shows the results of the exergy demand to heat the oil stream leaving from the oil preheater in the first separation stage of the separation train.

Figure 62. Exergy demand of the production heater for Reference FPSO and FPSO with CCS.

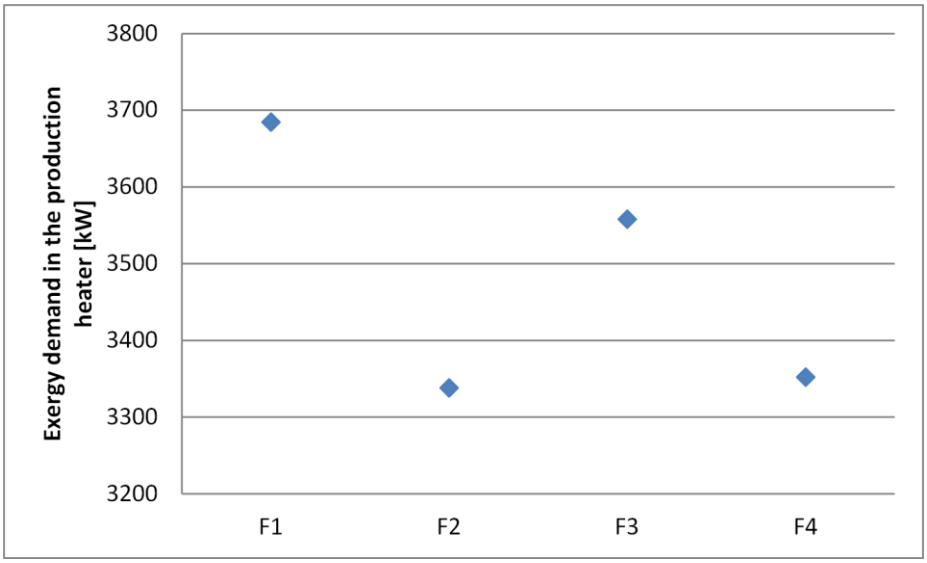

As mentioned previously, the separation process does not depend on the CCS, so the exergy demand is the same for Reference FPSO and FPSO with CCS. It is apparent from this figure that the pattern F1>F3>F4>F1 coincides with the heavy hydrocarbons C_5-C_{20+} composition pattern showed in Figure 34. Heavy hydrocarbons influence directly in the mass flow of the oil leaving from the FWKO to the oil pre-heater and production heater.

Figure 63. Exergy demand of the heater of the CO_2 removal unit for Reference FPSO and FPSO with CCS.

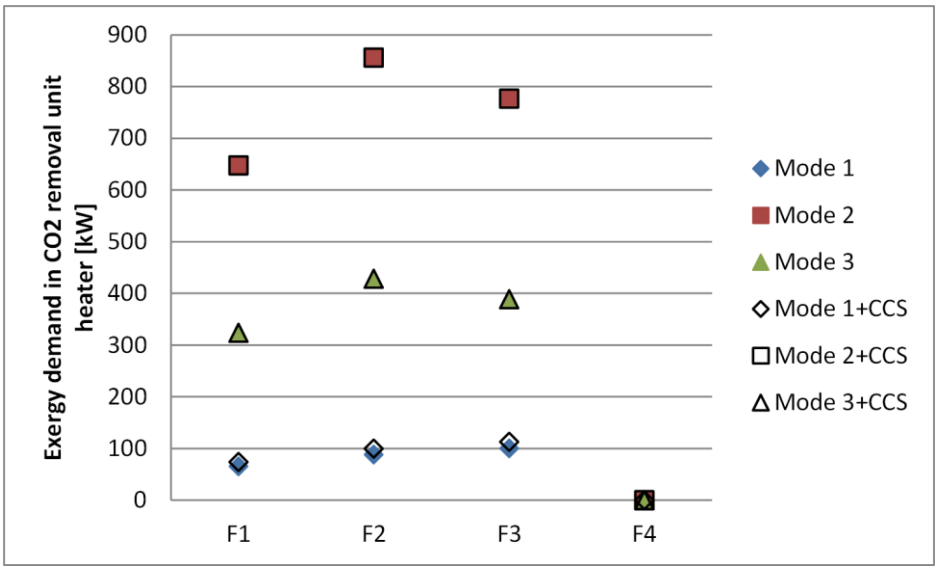

Results of the exergy demand of the heater of the CO_2 removal unit are shown in Figure 63. As can be seen in this figure, the exergy demand for well-fluid F4 is zero because gas does

not require to be treated in the CO_2 membrane unit. Mode 2 presents the highest exergy demand values and its pattern F2>F3>F1 is similar to the C_1-C_4+CO_2 pattern showed in Figure 34. An identical behavior can be also seen in Mode 3, but its exergy demand is 50% less than in Mode 2. There are not differences for Reference FPSO and FPSO with CCS in these operation modes. In the Mode 1, the exergy demand is directly proportional to the fuel gas consumption in the gas turbine. Exergy demand is 12.5% higher in the FPSO with CCS than in the Reference FPSO.

Figure 64. Exergy demand of the fuel gas heater - GT1 - for Reference FPSO and FPSO with CCS.

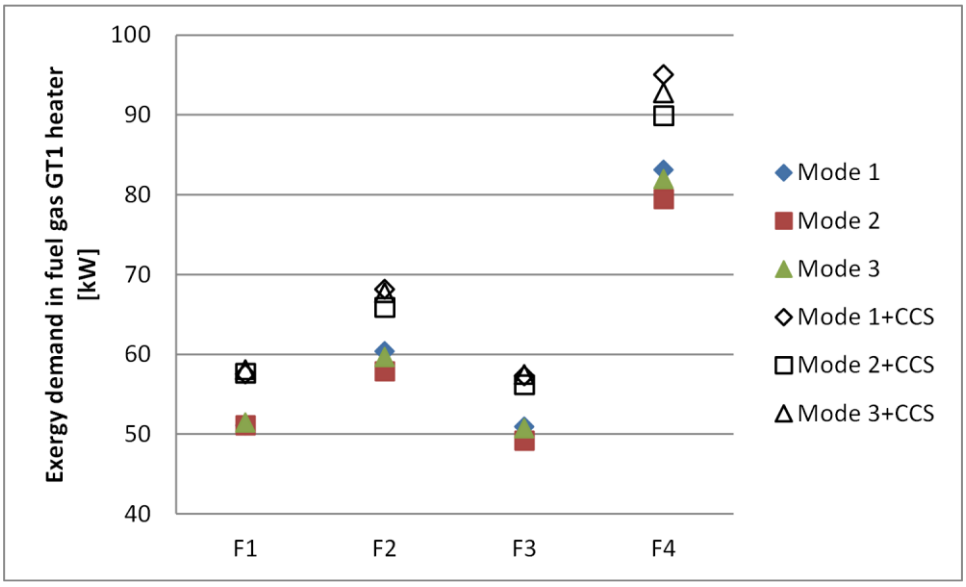

Exergy demand of the fuel gas heater for the GT1 is presented in Figure 64. As can be seen in this figure, exergy demand is much lower than in previous systems. The pattern is affected by the flow rate, temperature and mass heat capacity of the fuel gas. For well-fluid F4, temperature has a noticeable influence in the exergy demand. For example, F4 temperature is about 27 °C while temperature for other well-fluids is 37 °C. The low temperature of F4 implies a higher exergy demand in order to increase the temperature of the fuel gas in the heater. Additionally, it is important to note that a slightly higher value of mass heat capacity of well-fluid F4 (2.58 kJ/kg-C) in comparison with the other well-fluids (2.42 kJ/kg-C on average) may also explain the high exergy demand of well-fluid F4. A comparison of the previous figures reveals that production heater is the main exergy consumer in the heating processes of the FPSO, followed by CO_2 removal heater, and fuel gas heaters.

4.4 Exergy flow rates

The results of physical, chemical and total exergy flow rate obtained for different streams in Modes 1, 2, and 3, are presented in Table 14,

Table 15, and Table 16, respectively. On the one hand, it can be seen from these tables that chemical exergy flow rate of the Crude Oil stream is 99.9% of the total exergy flow rate for the four well-fluids simulated, while for the Oil, Gas (injection), Gas (exportation) and Fuel GT1 streams, the chemical exergy flow rate is 99.9%, 98.5%, 98.8% and 99.1% of the total exergy flow rate, respectively. The small variations are due to the differences in the pressure of these streams, which slightly changes the physical exergy component. According to the previous results, high chemical exergy flow rates of the hydrocarbons streams are expected due to the high value of specific chemical exergy in comparison with the physical exergy. On the other hand, when different streams are compared on the same well-fluid operation, it can be noted that the total exergy flow rate of the Water and CO_2 streams is considerably lower than in the other streams. Exergy losses in the Exhaust gas stream are, on average, 13.5% of the total exergy flow rate entering the FPSO. This exergy input consists of the exergy flow rate of the fuel GT1 and fuel GT2 streams (data for fuel GT2 is not shown).

Table 14. Exergy flow rate [kW] of useful input and output streams in Mode 1 for Reference FPSO.

		Crude Oil	Water	Oil	Gas (injection)	CO2 (injection)	Fuel GT1	Exhaust Gas
Fluid 1	Physical	11306	196	609	19787	143	1366	16760
	Chemical	8289393	469	6768862	1368097	272	152686	3150
	Total	8300699	665	6769471	1387884	415	154052	19909
Fluid 2	Physical	14079	181	514	24863	391	1603	23271
	Chemical	7675418	444	5910301	1583924	745	180084	3732
	Total	7689497	625	5910814	1608788	1136	181687	27003
Fluid 3	Physical	11976	221	604	19803	757	1398	17258
	Chemical	7545903	499	6340168	1050490	1441	152173	3213
	Total	7557879	720	6340772	1070293	2197	153570	20471
Fluid 4	Physical	13389	176	543	24315	0	1678	22055
	Chemical	7658687	432	5698222	1778416	0	182501	3751
	Total	7672075	608	5698766	1802731	0	184180	25806

Table 15. Exergy flow rate [kW] of useful input and output streams in Mode 2 for Reference FPSO.

		Crude Oil	Water	Oil	Gas (export)	CO2 (injection)	FUEL GT1	Exhaust Gas
Fluid 1	Physical	11306	196	609	16110	1421	1365	15945
	Chemical	8289393	469	6768862	1362509	2701	152595	3236
	Total	8300699	665	6769471	1378620	4122	153960	19182
Fluid 2	Physical	14079	181	514	18522	3856	1536	21899
	Chemical	7675418	444	5910301	1575735	7231	172558	3818
	Total	7689497	625	5910814	1594257	11087	174094	25717
Fluid 3	Physical	11976	221	604	12703	6037	1350	17798
	Chemical	7545903	499	6340168	1031401	11159	146910	3471
	Total	7557879	720	6340772	1044103	17196	148259	21270
Fluid 4	Physical	13389	176	543	21347	0	1604	20577
	Chemical	7658687	432	5698222	1786502	0	174416	3585
	Total	7672075	608	5698766	1807848	0	176020	24162

Table 16. Exergy flow rate [kW] of useful input and output streams in Mode 3 for Reference FPSO.

		Crude Oil	Water	Oil	Gas (export)	Gas (injection)	CO2 (injection)	FUEL GT1	Exhaust Gas
Fluid 1	Physical	11306	196	609	7140	11024	710	1375	16594
	Chemical	8289393	469	6768862	603847	760717	1351	153720	3210
	Total	8300699	665	6769471	610987	771741	2061	155095	19804
Fluid 2	Physical	14079	181	514	13906	8185	1906	1583	22864
	Chemical	7675418	444	5910301	882898	696329	3616	177890	3792
	Total	7689497	625	5910814	896804	704514	5522	179473	26656
Fluid 3	Physical	11976	221	604	5344	11408	2961	1392	17760
	Chemical	7545903	499	6340168	437794	603110	5579	151523	3353
	Total	7557879	720	6340772	443138	614518	8540	152915	21113
Fluid 4	Physical	13389	176	543	9565	13431	0	1655	21588
	Chemical	7658687	432	5698222	800521	980459	0	179938	3699
	Total	7672075	608	5698766	810086	993890	0	181593	25286

4.5 Exergy performance

In this section, the results of exergetic criteria of performance are presented and discussed. Destroyed exergy is calculated for the FPSO systems and the whole platform, while exergy efficiency is only calculated for FPSO overall plant.

Destroyed exergy is the first exergy criterion assessed. The results for destroyed exergy in the separation train are presented in Figure 65. These results are the same for all operation modes, and for Reference FPSO and FPSO with CCS. As indicated by the results, the separation train presents the highest exergy destruction when well-fluid F4 is processed. Processing with the well-fluid F2 shows the lowest value of destroyed exergy in the separation train. Its destroyed exergy is approximately 10% lower than it is with well-fluid F4. The pattern of the destroyed exergy is mainly influenced by the exergy variation between inlet and outlet streams. Power consumption has a minimum influence on the behavior of the destroyed exergy showed in Figure 65. There is not a direct relation between results in Figure 65 and the compositions presented in Figure 34.

Figure 65. Destroyed exergy in the Separation Train for Reference FPSO and FPSO with CCS.

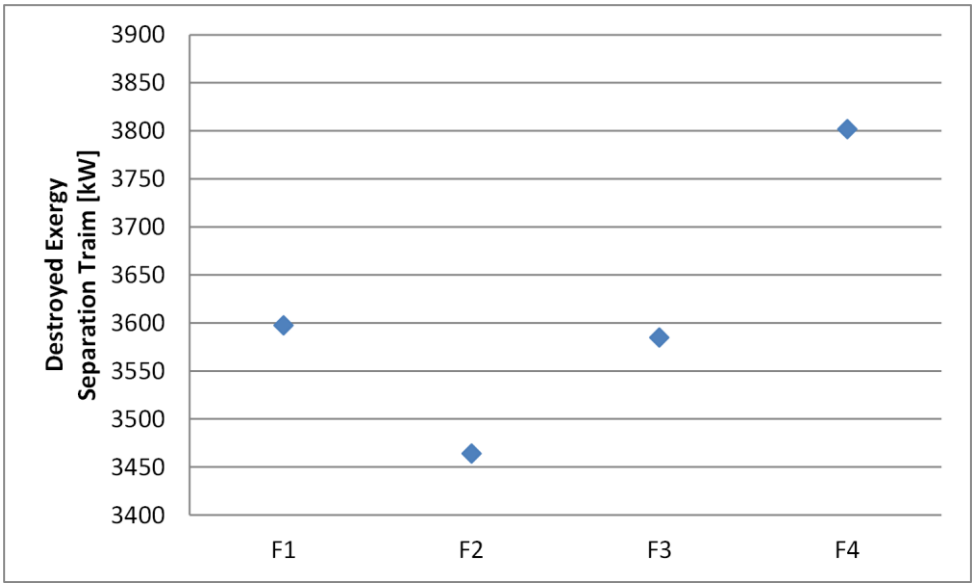

The results of the destroyed exergy in the Compression Train are shown in Figure 66. As indicated by this figure, for the well-fluids F1, F2, and F3, the destroyed exergy in Mode 2 is higher than in Mode 3 and Mode 1. However, for the well-fluid F4, the highest exergy destruction occurs in Mode 1 followed by Mode 3 and Mode 2. The variations for well-fluid

F4 are due to the influence of the treatment gas process in CO_2 capture unit which leads to noticeable variations in the power requirement for CO_2 compression and injection. Another aspect that can be observed in Figure 66 is that the dispersion of the destroyed exergy of the well-fluid F4 is greater than F2 and F1. This aspect may be explained by the behavior of the power demand of CO_2 compressor train *CO2-CT* shown in Figure 48.

Figure 66. Destroyed exergy in the Compressor Train for Reference FPSO and FPSO with CCS.

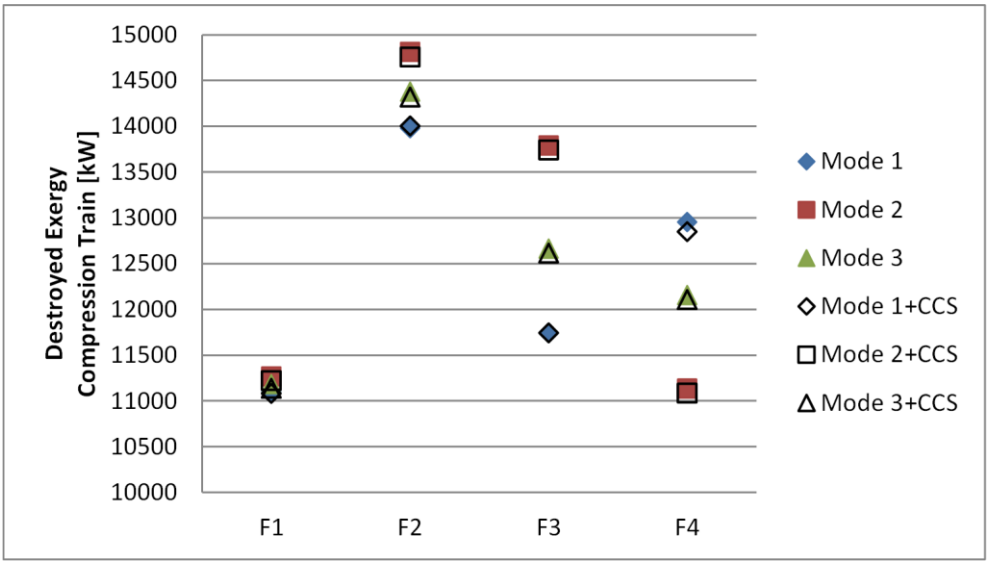

Figure 67. Destroyed exergy in the Hot Water System for Reference FPSO and FPSO with CCS.

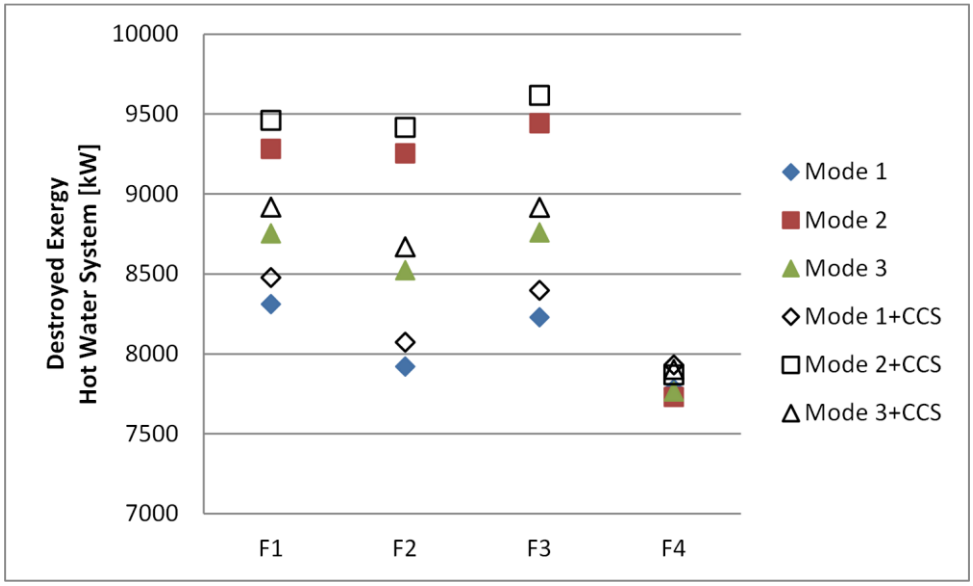

Figure 67 gives the results of the destroyed exergy in the Hot Water System. The highest value for the Mode 2 shown for well-fluids F1, F2, and F3, may be explained by the fact that, in comparison with Mode 3 and Mode 1, this operation mode requires greater exergy demand for heating the gas treated in the CO_2 membranes unit. When well-fluid F4 is analyzed, it is possible to note that there are no significantly differences between the destroyed exergy for the three operation modes. It is a consequence of the non-existence of the CO_2 treatment process. The differences between the results for Reference FPSO and FPSO with CCS are due to the higher fuel gas demand which implies higher exergy consumption for heating.

The destroyed exergy for Cooling Water System is presented in Figure 68 and Figure 69 for Reference FPSO and FPSO with CCS, respectively. Results for FPSO with CCS are higher than Reference FPSO due to the greater consumption of cooling water in the CCS system. For well-fluids F1, F2, and F3, the slight variations in the destroyed exergy pattern for the operation modes may be explained by the high influence of the cooling demand in the CO_2 compression train. As can be seen from these figures, when FPSO operates with the well-fluid F4, cooling water demand in the CO_2-CT is not required, then, the destroyed exergy is proportional to the cooling water demand of the gas compression train.

Figure 68. Destroyed exergy in the Cooling Water System for Reference FPSO.

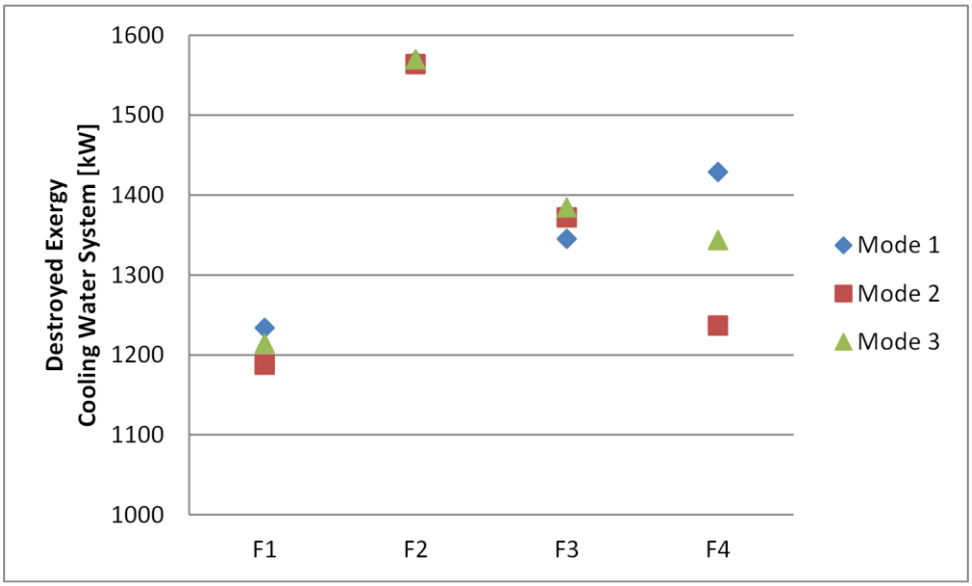

Figure 69. Destroyed exergy in the Cooling Water System for FPSO with CCS.

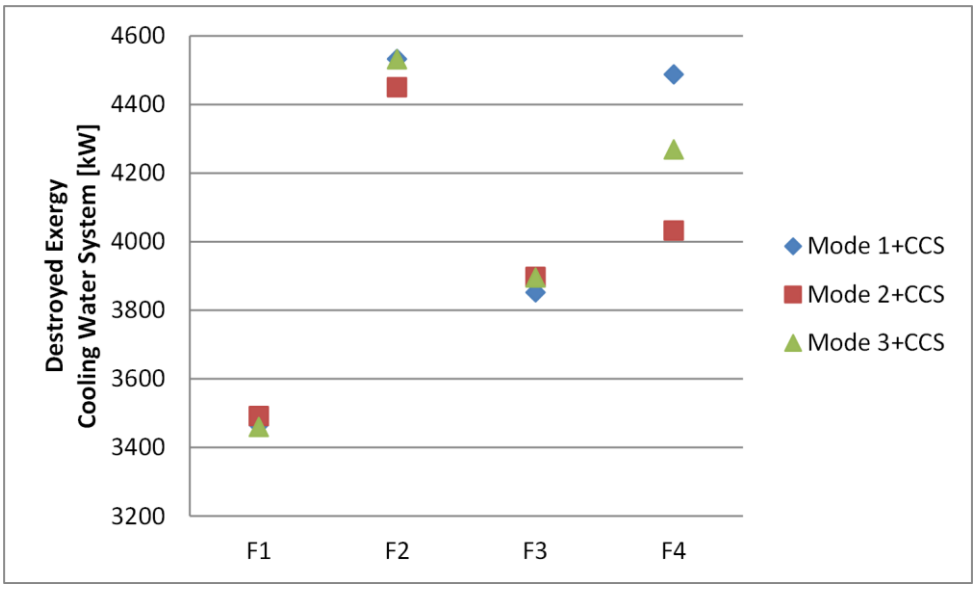

Figure 70. Destroyed exergy of the overall plant for Reference FPSO and FPSO with CCS.

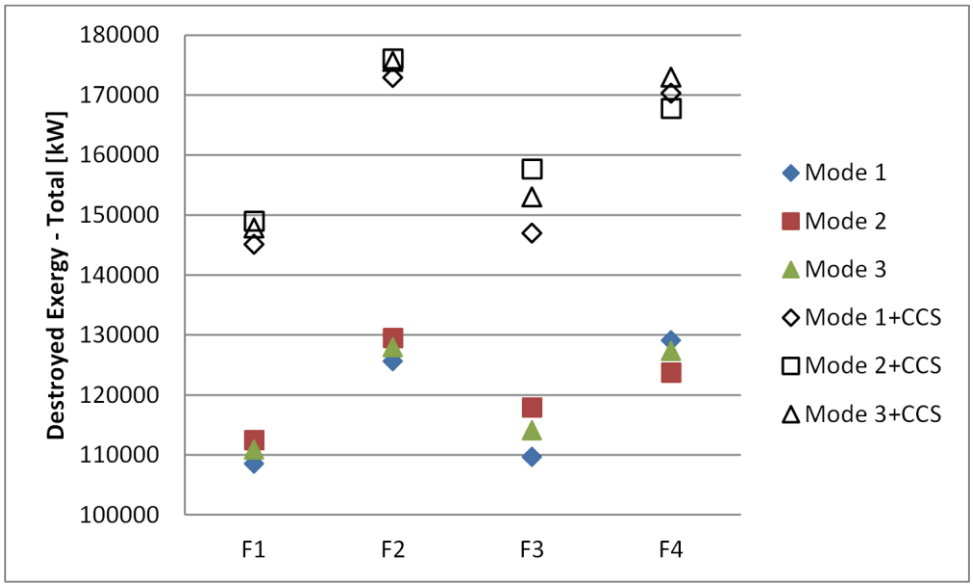

The destroyed exergy of the overall plant is presented in Figure 70. The destroyed exergy pattern is similar for Reference FPSO and FPSO with CCS. When the FPSO is operating with the well-fluid F2, the destroyed exergy reaches its maximum value in each operation mode. However, minimum values of destroyed exergy are obtained when FPSO operates with the well-fluid F1. For a fixed well-fluid, it is possible to note for F1, F2, and F3 that the FPSO has more exergy destruction when is operated in Mode 2 followed by Modes 3 and 1. There are two possible explanations for this result. The first explanation is related to the high requirement of exergy for gas heating in the CO_2 membrane unit in the Mode 2, in

comparison with Modes 1 and 3. The second explanation is associated with the power demand of the CO_2-CT and its cooling requirement. For well-fluid F4 the destroyed exergy is given by Mode 1 > Mode 3 > Mode 2 for the case of Reference FPSO, and Mode 3 > Mode 1 > Mode 2 for the FPSO with CCS. The reason for this difference is not clear but it may have something to do with the destroyed exergy of the CCS system.

Finally, from previous destroyed exergy findings it is possible to establish the classification of each the system for Reference FPSO and FPSO with CCS according to the indicator *relative exergy destruction* ϵ, see Table 17.

Table 17. *Relative exergy destruction* of the systems.

Reference FPSO		FPSO with CCS	
System	ϵ (% on average for all modes)	System	ϵ (% on average for all modes)
Gas turbine 1	72.9	Gas turbine 1	61.4
Compression train	10.5	Compression train	7.8
Hot water system	7.1	Hot water system	5.4
Separation train	3.0	Separation train	2.2
Water injection system	2.7	Water injection system	2.0
Gas turbine 2 (CO_2)	1.6	Gas turbine 2 (CO_2)	1.2
Cooling water system	1.1	Cooling water system	2.5
		CCS	16.8

Results of exergy efficiency are presented in Figure 71. These results indicate that FPSO presents, on average, the highest values of exergy efficiency operating with the well-fluid F1, followed by the values of well-fluids F3, F2, and F4. Average values of exergy efficiency for Reference FPSO are in the range of 15.63% to 16.68%. The exergy efficiency is on the order of 16.55% to 16.68% for well-fluid F1, 16.20% to 16.41% for well-fluid F2, 16.27% to 16.66% for well-fluid F3, and 15.63% to 15.71% for well-fluid F4.

For fixed well-fluids, it is possible to observe that the most efficient operation mode is the Mode 2 followed by the Mode 3 and Mode 1, although the variations in exergy efficiency are very small: 0.13%, 0.21%, 0.39%, and 0.13% for well-fluids F1, F2, F3, and F4, respectively. These results show that although small, the operation mode has a definite influence on the energy efficiency of the plant.

Exergy efficiencies for FPSO with CCS are, on average, 10.7% lower than exergy efficiencies in Reference FPSO, which is equal to a reduction of 1.73 points, on average. This reduction in exergy efficiency is compensated by the mitigation of the CO_2 emissions. The pattern of average exergy efficiencies for the FPSO with CCS scenarios is similar to the Reference FPSO: F1>F3>F2>F4. Exergy efficiencies of FPSO with CCS are in the range of 13.82%-14.95%. Exergy efficiencies for F1, F2, F3 and F4 well-fluids are in the 14.80%-14.95%, 14.47%-14.67%, 14.58%-14.91%, and 13.82%-14.06% ranges, respectively.

A comparison of the different well-fluids shows that, in the FPSO with CCS, operation Mode 2 is more efficient than Modes 3 and 1. This is the same pattern for Reference FPSO. Exergy efficiency for each well-fluid has variations of 0.15%, 0.19%, 0.33%, and 0.24% for F1, F2, F3, and F4, respectively. These variations have the same order of magnitude as those in the Reference FPSO.

Figure 71. Exergy efficiency for Reference FPSO and FPSO with CCS.

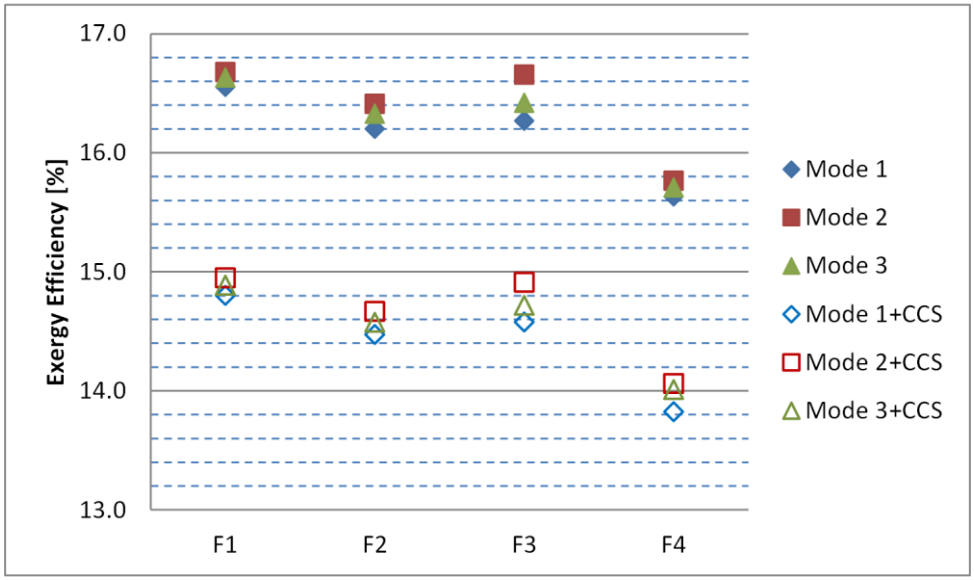

Specific Exergy Consumption SEC for Reference FPSO and FPSO with CCS is shown in Figure 72. Both the reference FPSO and the FPSO with CCS have the same pattern of SEC. As can be seen in this figure, the pattern of SEC in descending order is F2, F4, F3, and F1, for each operational mode. SEC is in the range of about 863-1206 MJ_b/Sm^3oe, 761-1006 MJ_b/Sm^3oe, and 819-1114 MJ_b/Sm^3oe, for operation Modes 1, 2, and 3 in Reference FPSO, respectively, while for FPSO with CCS, SEC is in the range of 863-1206 MJ_b/Sm^3oe, 761-1006 MJ_b/Sm^3oe, and 819-1114 MJ_b/Sm^3oe, for operation Modes 1, 2, and 3, respectively.

Figure 72. Specific Exergy Consumption for Reference FPSO and FPSO with CCS.

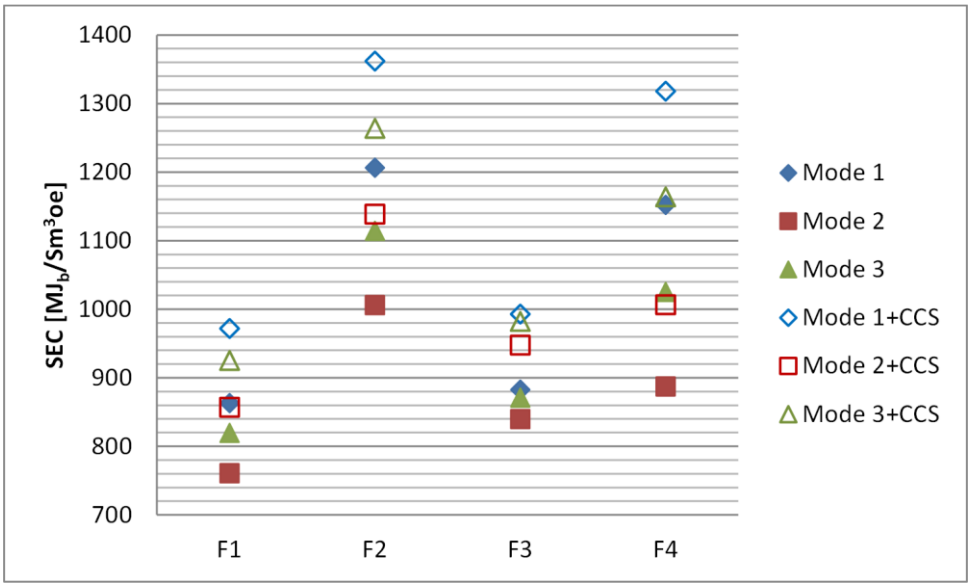

When each operation mode is compared for a fixed well-fluid, it can be seen in Figure 72 that FPSO with CCS has higher SEC values than Reference FPSO. For all scenarios analyzed, SEC values are, on average, 13.1% higher in FPSO with CCS. Further, the results indicate that operation Mode 1 has higher SEC values than Mode 3 and Mode 2.

Figure 73. Specific Exergy Destruction for Reference FPSO and FPSO with CCS.

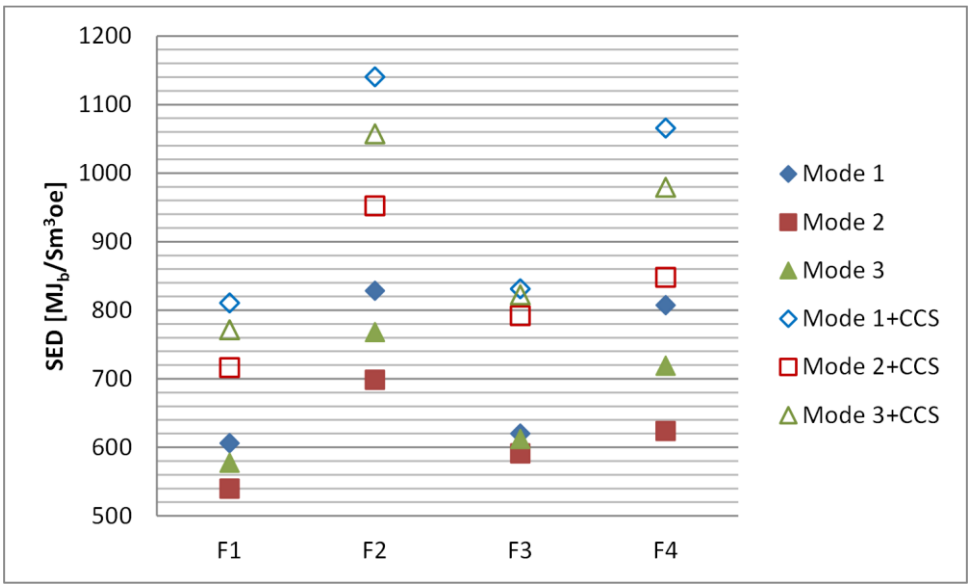

Figure 73 shows how Specific Exergy Destruction SED varies for the different scenarios analyzed. Similar to the previous results of SEC, the pattern of SED is Mode 1>Mode

3>Mode 2 for each well-fluid and FPSO plant. SED values for FPSO are between 540-810 MJ_b/Sm^3oe, 698-1140 MJ_b/Sm^3oe, 591-831 MJ_b/Sm^3oe, and 624-1065 MJ_b/Sm^3oe, for well-fluids F1, F2, F3, and F4, respectively. SED values in FPSO with CCS are, on average, 34.8% higher than the SED values in Reference FPSO. For a fixed operation mode, FPSO has the highest SED with well-fluid F2 followed by well-fluids F4, F3, and F1.

When comparing the results of this study with those obtained by Voldsund et all (VOLDSUND et al., 2013c) for a fixed offshore platform (SEC is in the range about 25 to 500 MJ_b/Sm^3oe and SED is in the range of 20-160 MJ_b/Sm^3oe), it is possible to note that SEC and SED indicators for this work have, on average higher ranges. These results can be explained in part by the differences in the well-fluid conditions and the configuration of the processes in the offshore platform. In spite of the differences that exist between this study and the research of Voldsund et all., the order of magnitude is in agreement with the previous research.

4.6 Environmental performance

Figure 74 and Figure 75 show the results of CO_2 emissions for the Reference FPSO and FPSO with CCS, respectively. The general behavior of the carbon emissions for the different operation modes in the two FPSO plants is similar: the highest emissions occur in F2 followed by F3, F4, and F1. CO_2 emissions in FPSO with CCS are, on average, 11.2% of the CO_2 emissions in Reference FPSO for all operation modes and well-fluids. This result indicates that the implementation of the CCS system reduces the CO_2 emissions in 88.8%. When CO_2 emissions are compared for the different well-fluids in a fixed operation mode, the findings suggest that power demand and CO_2 content in the well-fluid may have a marked influence in the pattern of CO_2 emissions.

A comparison of the carbon emissions of the operation modes, for a fixed well-fluid, shows that for well-fluids F1, F2, and F3, Mode 2 produces more CO_2 than Mode 3 and Mode 1. However, for well-fluid F4, the CO_2 emissions in Mode 1 are higher than in Mode 3 and Mode 2. As mentioned previously for other results, the CO_2 compression and injection process have a noticeable influence in different parameters, such as power demand and carbon emissions. For this reason, CO_2 emissions for well-fluid F4 are directly related to the power demand in the gas compression train, whereas CO_2 emissions for F1, F2, and F3 are more influenced by CO_2 compression power demand.

For fixed well-fluids, results of absolute CO_2 emissions in Figure 74 and Figure 75 showed the Mode 2 as the main pollution operation mode followed by Mode 3 and Mode 1, except for the well-fluid F4 for which the pattern is Mode 1>Mode 3>Mode 2. When normalized CO_2 emissions are plotted, see Figures 76 to 79, it is possible to note that the operation Mode 1 presents the highest CO_2 normalized and CO_2 normalized to exergy of the product streams, followed by Mode 3 and Mode 2.

Figure 74. CO_2 emissions for Reference FPSO.

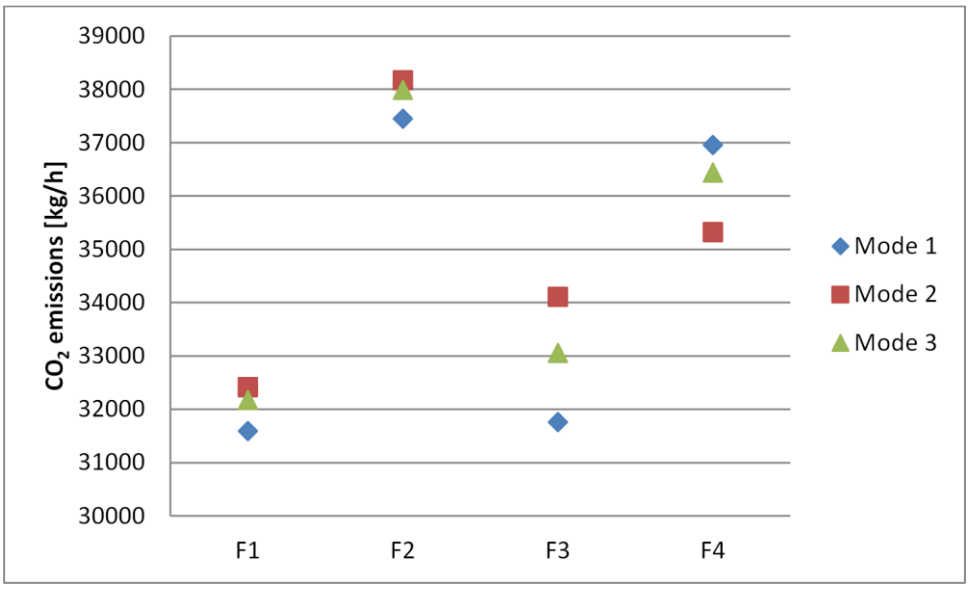

Figure 75. CO_2 emissions for FPSO with CCS.

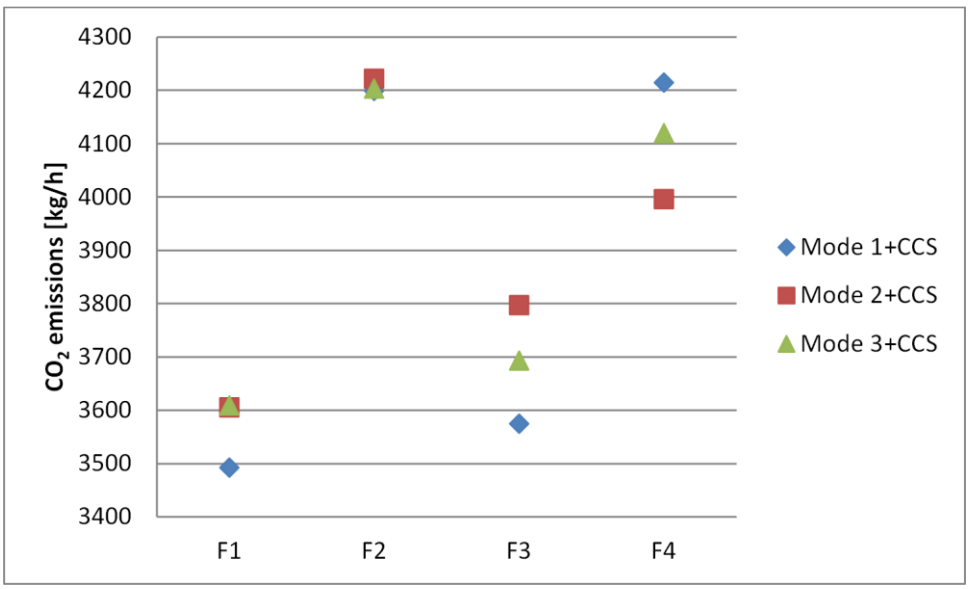

For a fixed operation mode, the results in Figure 76 and Figure 77 indicate that FPSO operation with well-fluid F2 has the highest index of CO_2 emissions per unit of production. The general pattern of $CO_{2,norm}$ emissions is, in descending order, F2>F4>F3>F1.

CO_2 emissions per unit of production $CO_{2,norm}$ for Reference FPSO are presented in Figure 76. When well-fluid F1 is processed, CO_2 emissions in Mode 1 and Mode 3 are 13.5% and 7.7% higher than in Mode 2, respectively, while for F2, F3, and F4 these values are 20.0% and 10.8%, 5.1% and 3.7%, and 29.9% and 15.6%, respectively.

Figure 76. CO_2 normalized for Reference FPSO.

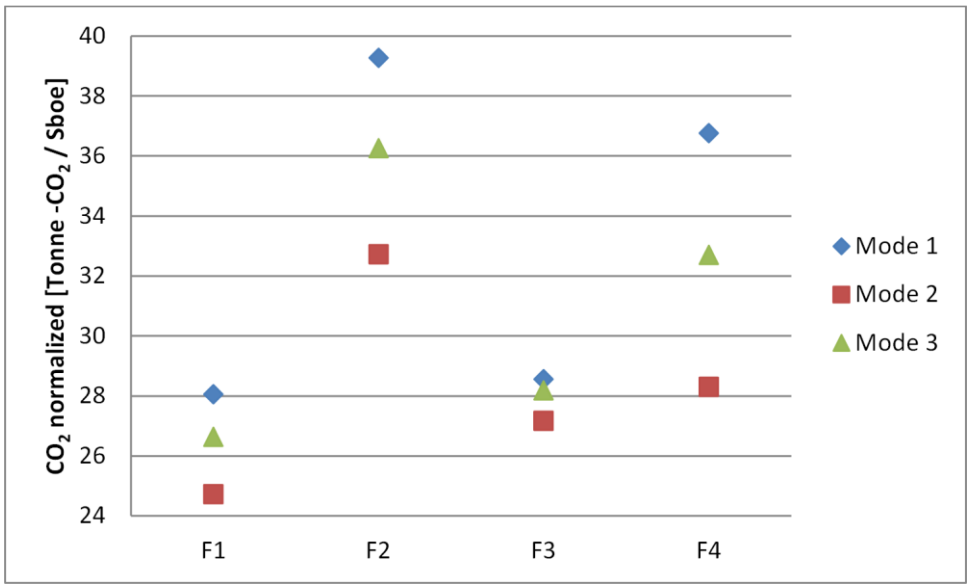

Figure 77 shows CO_2 emissions per unit of production for FPSO with CCS. When well-fluid F1 is processed, CO_2 emissions in Mode 1 and Mode 3 are 12.5% and 8.6% higher than in Mode 2, respectively, while for F2, F3, and F4 these values are 21.3% and 10.9%, 6.0% and 4.1.5%, and 30.6% and 15.5%, respectively. The pattern of CO_2 normalized is similar for the two FPSO plants.

Figure 77. CO_2 normalized for FPSO with CCS.

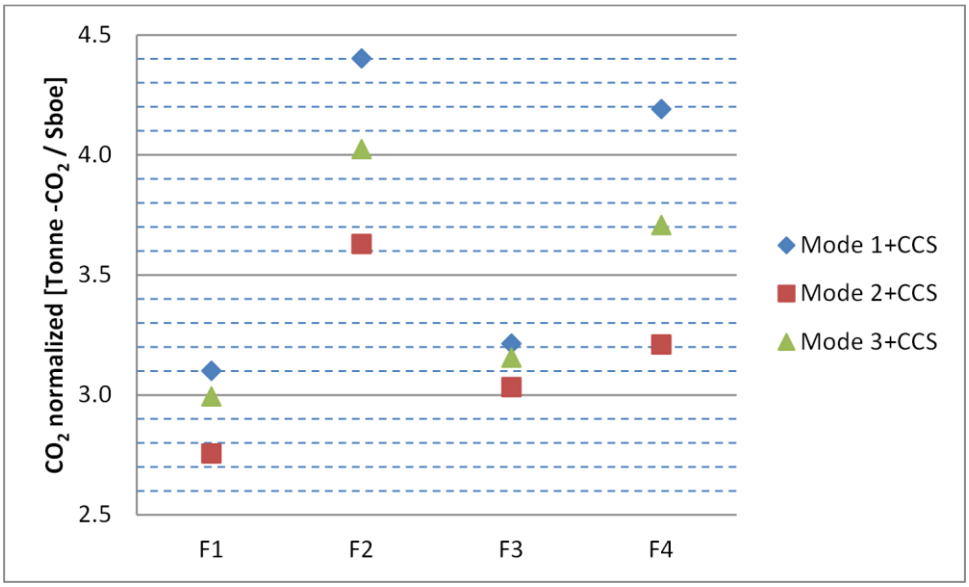

Results of the CO_2 normalized to exergy of the product streams $CO_{2,prod}$ for Reference FPSO and FPSO with CCS are shown in Figure 78 and Figure 79, respectively. The highest amount of CO_2 by unit of exergy of the product streams occurs when FPSO operates with well-fluid F4. On the contrary, the lowest amount occurs with well-fluid F1. For this environmental indicator, it is possible to note that there is a variation in relation to the $CO_{2,norm}$ pattern: F4>F2>F3>F4.

When well-fluid F1 is processed in Reference FPSO, $CO_{2,prod}$ emissions in Mode 1 and Mode 3 are 17.3% and 9.6% higher than in Mode 2, respectively, while for F2, F3, and F4 these values are 24.6% and 12.9%, 8.4% and 5.5%, and 37.8% and 19.0%, respectively. For FPSO with CCS, the ratio between $CO_{2,prod}$ emissions in Mode 1 and Mode 3 in relation to Mode 2 are 16.3% and 10.5%, 25.9% and 13.0%, 9.3% and 5.9%, and 38.5% and 19.0% for well-fluids F1, F2, F3, and F4, respectively.

Figure 78. CO_2 normalized to exergy of the product streams for Reference FPSO.

Figure 79. CO_2 normalized to exergy of the product streams for FPSO with CCS.

A comparison of the three results from Figure 74 to Figure 79 for Reference FPSO vs. FPSO with CCS reveals a reduction of 88.8% in the CO_2 emission indicators when CCS is implemented.

The present results about environmental performance are significant in at least major two respects. First, they make it possible to establish that the metric of the indicator has a decisive influence when evaluating the environmental performance of the plant. On the one hand,

absolute CO_2 emissions metric places the operation Mode 2 as the one with the highest level of pollution for well-fluids F1, F2, and F3, except for F4, where Mode 2 has the highest CO_2 emissions level. On the other hand, normalized CO_2 emissions metric identifies the operation Mode 1 as that which has the greatest specific emissions. Second, the well-fluid composition affects the emission indicators and, depending on the metric of the indicator, a fluid may have greater or lesser influence on the environmental performance of the plant.

5 CONCLUSIONS AND FURTHER WORK

Conclusions

In this work, a comparative exergy and environmental analysis of a FPSO unit operating with and without CCS have been developed, giving results by which the influence of well-fluid composition and operation mode on the FPSO performance can be understood.

The metric of the indicators plays a significant role when comparing the different scenarios of operation of the platform. Although absolute and specific indicators are used in the oil industry, specific or normalized indicators give a better comparison of FPSO scenarios performance.

The implementation of the CCS has shown to be an adequate alternative for the reduction of the environmental impact by carbon. A reduction of 88.8% in CO_2 emissions is penalized with a reduction in exergy efficiency of 1.7 points. An aspect that has an advantage in the implementation of the CCS, is the recovery of the exergy of the combustion gases of the gas turbine to satisfy the exergy requirement in the reboiler.

The calculation of performance indicators for a specific system may follow an explainable pattern based, for example, on composition. When the plant is analyzed in its entirety, the identification of patterns becomes difficult due to the confluence of the different systems, together with the influence of the operation modes and the well-fluids.

Exergy efficiency showed low sensitivity to variations in the operating mode. However, it has higher sensitivity to well-fluid composition, varying by approximately in 1 percentage point in both the Reference FPSO and FPSO with CCS.

Both SEC and SED indicators have a strong dependence on operation mode. For all scenarios in Reference FPSO and FPSO with CCS, the highest values of these indicators occur in Mode 1 followed by Mode 3 and Mode 2 (Mode 1>Mode 3>Mode 2).

The well-fluid composition and the operation mode have a marked influence on the environmental performance of the FPSO. The absolute CO_2 emissions are greater for

operation Mode 2 followed by Mode 3 and Mode 1 (Mode 2>Mode 3>Mode 1), but this only happens for fluids in which CO_2 treatment by membranes is required. However, normalized CO_2 emissions have a different behavior, and they are higher for operation Mode 1 followed by Mode 3 and Mode 2 (Mode 1>Mode 3>Mode 2) in all well-fluids.

Well-fluid F1 showed to have the lowest CO_2 emissions indicators followed by F3, F4, and F2. Unfortunately, it was not found a pattern in the well-fluid compositions that can be used to describe the environmental performance of the FPSO.

Further work

Prediction models or simulations tools could be implemented to understand the behavior of the reservoir. Recovery strategies based on fluid injection (water, gas, CO_2) affect the future performance of the reservoir, and its prediction is not a simple task, especially for new reservoirs (EZEKWE, 2011).

Liquid carryover effect in the separation train should be simulated and studied to evaluate the impact of this phenomenon in the processing plant.

The separation train scheme with continuous water recycle to the FWKO separator inlet must be modelled and simulated to compare the results with those obtained in this thesis. Because the information about this water recycle scheme is lacking, team effort with FPSO engineers is suggested to understand the process and to calibrate the models.

The inclusion of antisurge control in all compression trains is recommended to assess the influence of the compressor control system in the FPSO performance. Previous works performed by (ORTIZ; GALLO, 2015; VOLDSUND et al., 2012) are very useful in order to deal this topic.

Different fractions of gas bypass for the injection process could be simulated to investigate more scenarios between Mode 1 (all gas is injected) and Mode 2 (all gas is exported).

Future work needs to be done in order to develop more automatized routines for the following calculations or simulation steps: a) chemical and total exergy; b) performance parameters; c)

adjust of injection pressures and recalculation of the total power demand; and d) FPSO and CCS simulations integration and final convergence. The Aspen HYSYS®-Excel® integration tool should be utilized for this purpose.

6 REFERENCES

ABDOLLAHI-DEMNEH, F. et al. Calculating exergy in flowsheeting simulators: A HYSYS implementation. **Energy**, v. 36, n. 8, p. 5320–5327, 2011.

AMROLLAHI, Z.; ERTESVÅG, I.; BOLLAND, O. Thermodynamic analysis on post-combustion CO_2 capture of natural-gas-fired power plant. **Journal of greenhouse gas control**, v. 3, p. 422–426, 2011.

ARNOLD, K.; STEWART, M. **Surface production operations: design of oil-handling systems and facilities**. USA: Butterworth-Heinemann, 1998.

ASPEN TECHNOLOGY INC. **HYSYS® 2004.2 simulation basis**. Cambridge – USA.

BARRERA, J. E.; BAZZO, E.; KAMI, E. Exergy analysis and energy improvement of a Brazilian floating oil platform using Organic Rankine Cycles. **Energy**, v. 88, p. 67–79, 2015.

BARRERA, J. E.; SAHLIT, A. A.; BAZZO, E. **Exergy analysis and strategies for the waste heat recovery in offshore platforms**. Proceeding of 22nd International congress of mechanical engineering - COBEM 2013. Riberão Preto, Brazil: 2013.

BG BRASIL. Energy efficiency program - FPSO Introduction. 2013.

BG GROUP. Programa de eficiência energética - Chamada de propostas. 2012.

BROOKS, F. J. **GE gas turbine performance characteristics GE power systems**. Available on: <http://www.up.farsscript.ir/uploads/13316846411.pdf>. Accessed on 17/02/2017.

CARRANZA SANCHEZ, Y. A. et al. **Energy and exergy performance of three FPSO operational modes**. Proceeding of the 23rd ABCM International congress of mechanical engineering. Rio de Janeiro - Brazil: 2015.

CARRANZA SÁNCHEZ, Y. A.; OLIVEIRA JR, S. DE. **Exergy analysis of petroleum offshore platform process plant with CO_2 capture.** Proceeding of the 27st International conference on efficiency, cost, optimization, simulation and environmental impact of energy systems - ECOS 2014. Turku, Finland: 2014a.

CARRANZA SÁNCHEZ, Y. A.; OLIVEIRA JR, S. DE. **Evaluación de la exergía destruida en los componentes de una plataforma de petróleo y gas offshore con captura de CO_2**. VIII Conferencia científica internacional de ingeniería mecánica. Villa Clara, Cuba: 2014b.

CARRANZA SÁNCHEZ, Y. A.; OLIVEIRA JR, S. DE. Exergy analysis of offshore primary petroleum processing plant with CO_2 capture. **Energy**, v. 88, p. 46–56, 2015a.

CARRANZA SÁNCHEZ, Y. A.; OLIVEIRA JR, S. DE. **Assessment of the exergy performance of a floating, production, storage and offloading (FPSO) unit: influence of**

three operational modes. Proceeding of the 28th International conference on efficiency, cost, optimization, simulation and environmental impact of energy systems - ECOS 2015. Pau - France: 2015b.

DEVOLD, H. Oil and gas production handbook. **An Introduction to oil and gas production**, p.82, 2006.

DINCER, I.; ROSEN, M. A. **Exergy-energy, environment and sustainable development**. Amsterdam: Elsevier Ltd., 2007.

EZEKWE, N. **Petroleum reservoir engineering practice**. Boston - USA: Prentice Hall, 2011.

FALK-PEDERSEN, O.; DANNSTRÖM, H. Separation of carbon dioxide from offshore gas turbine exhaust. **Energy conversion and management**, v. 38, p. S81–S86, 1997.

FORECAST INTERNATIONAL. **The market for gas turbine electrical power generation**. Available on: <https://www.forecastinternational.com/fistore/prod.cfm?PD_RECNO=16021&title=The-Market-for-Gas-Turbine-Electrical-Power-Generation>. Accessed on 17/02/2017.

FORMIGLI, J. **Pre-salt reservoirs offshore Brazil: perspectives and challenges**. Energy Conference. Miami: 2007.

GE ENERGY. **GateCycle**, 2013.

GONG, M.; WALL, G. On exergy and sustainable development - Part 2: Indicators and methods . **Exergy, an international journal**, v. 1, n. 4, p. 217–233, 2001.

HETLAND, J. et al. Integrating a full carbon capture scheme onto a 450 MWe NGCC electric power generation hub for offshore operations: Presenting the Sevan GTW concept. **Applied energy**, v. 86, n. 11, p. 2298–2307, 2009.

INTERNATIONAL ASSOCIATION OF OIL&GAS PRODUCERS. **Environmental performance indicators–2014 data**. 2015. Available on: <http://www.iogp.org/pubs/2014e.pdf>. Accessed on 17/02/2017.

INTERNATIONAL ASSOCIATION OF OIL AND GAS PRODUCERS; THE GLOBAL OIL AND GAS INDUSTRY ASSOCIATION FOR ENVIRONMENTAL AND SOCIAL ISSUES. **Guides for implementing ISO 50001 energy management systems in the oil and gas industry**. 2013. Available on: <http://www.ogp.org.uk/pubs/482.pdf>. Accessed on 17/02/2017.

JONES, V. T.; MATTHEWS, M. D.; RICHERS, D. M. Light hydrocarbons for petroleum and gas prospecting. **Handbook of exploration geochemistry**, v. 7, n. C, p. 133–212, 2000.

KOTAS, T. J. **The exergy method of thermal plant analysis**. Florida: Krieger Publishing Company, 1995.

KVAMSDAL, H. M. et al. Maintaining a neutral water balance in a 450 MWe NGCC-CCS power system with post-combustion carbon dioxide capture aimed at offshore operation. **International journal of greenhouse gas control**, v. 4, n. 4, p. 613–622, 2010.

MANNING, F. S.; THOMPSON, R. E. **Oilfield processing - Volume two: crude oil**. Oklahoma: 1995.

MATHER, A. **Offshore engineering - An introduction**. London: Witherby & Company Limited, 2000.

MCCARRICK, M.T.; MACKENZIE, K. **LM2500 to LM2500 + DLE gas turbine combined cycle plant repowering**. 2012. Available on: <https://powergen.gepower.com/content/dam/gepower-pgdp/global/en_US/documents/product/lm2500-combined-cycle-plant-repowering-whitepaper.pdf>. Accessed on 17/02/2017.

MUELLER, W.; ROOBAERT, N. Standardization adds value to FPSO topsides. **Offshore**, 2008.

NATIONAL COMMISSION ON THE BP DEEPWATER HORIZON OIL SPILL AND OFFSHORE DRILLING. **A brief history of offshore oil drilling**. Staff working paper n. 1, p. 1–18, 2010. Available on: <https://library.villanova.edu/Find/Record/1262717/Details>. Accessed on 17/02/2017.

NGUYEN, T.-V. et al. On the definition of exergy efficiencies for petroleum systems: Application to offshore oil and gas processing. **Energy**, v. 73, p. 264–281, 2014a.

NGUYEN, T.-V. **Modelling, analysis and optmisation of energy systems on offshore platforms**. Technical University of Denmark, 2014.

NGUYEN, T. VAN et al. Exergetic assessment of energy systems on North Sea oil and gas platforms. **Energy**, v. 62, p. 23–36, 2013.

NGUYEN, T. VAN et al. Life performance of oil and gas platforms: site integration and thermodynamic evaluation. **Energy**, v. 73, p. 282–301, 2014b.

OFFSHORE CENTER DENMARK. **Overview of the Brazilian oil and gas industry**. 2009. Available on: http://www.offshorecenter.dk/filer/files/Project/Internationalisering/OCDreportBrazil.pdf>. Accessed on 21/06/2016.

OFFSHORE ENERGY TODAY. **Offshore drilling: history and overview**. Available on: <http://www.offshoreenergytoday.com/offshore-drilling-history-and-overview/>. Accessed on 21/06/2016.

OLIVEIRA JR, S. DE. **Exergy: production, cost and renewability**. London: Springer, 2013.

OLIVEIRA JR, S. DE; VAN HOMBEECK, M. Exergy analysis of petroleum separation processes in offshore platforms. **Energy conversion and management**, v. 38, p. 1577–1584, 1997.

OPEC. **Annual statistical bulletin**. 2016. Available on: <http://www.opec.org/opec_web/static_files_project/media/downloads/publications/ASB2016.pdf>. Accessed on 21/06/2016.

ORGANISATION FOR ECONOMIC CO-OPERATION AND DEVELOPMENT. **OECD core set of indicators for environmental performance reviews**. 1993. Available on: <http://teclim.ufba.br/jsf/indicadores/OECD CORE INDIC.PDF>. Accessed on 17/02/2017.

ORTIZ, H. Y.; GALLO, W. L. R. **First and Second Law analysis of CO_2 offshore compression system**. Proceeding of the 23rd ABCM International congress of mechanical engineering. Rio de Janeiro - Brazil: 2015.

PETRAKOPOULOU, F. et al. **Post-Combustion CO_2 capture with monoethanolamine in a combined-cycle power plant: exergetic, economic and environmental assessment, greenhouse gases - Emission, measurement and management**. In: DR GUOXIANG LIU (Ed.). InTech, 2012.

PLANETE ENERGIES. **Offshore oil and gas production**. Available on: <http://www.planete-energies.com/en/medias/close/offshore-oil-and-gas-production>. Accessed on 22/06/2016.

PULKRABEK; WILLARD. **Engineering fundamentals of the internal combustion engine**. New Jersey: Pearson Prentice-Hall, 2004.

RAYMOND, M.; LEFFLER, W. **Oil and gas production in nontechnical language**. Oklahoma - USA: PennWell Corporation, 2006.

RIAZI, M. **Characterization and properties of petroleum fractions**. Baltimore: ASTM International Stardards Worldwide, 2005.

RIGZONE. **Oil and gas conversion calculator**. Available on: <http://www.rigzone.com/calculator/default.asp#calc>.

RIVERO, R. et al. The exergy of crude oil mixtures and petroleum fractions : calculation and application. **International journal of applied thermodynamics**, v. 2, n. 3, p. 115–123, 1999.

RIVERO, R. **Application of the exergy concept in the petrochemical industry**. Efficiency, costs, optimization, simulation and environmental aspects of energy systems. Tokyo: 1999

ROSA, A. J.; CARVALHO, R. DE S.; XAVIER, J. A. D. **Engenharia de reservatórios de petróleo**. Rio de Janeiro-Brazil: Editora Interciência, 2006.

SADDIQ, H. A. et al. Modelling of gas turbine and gas turbine exhaust and its utilization as combined cycle in utility system. **International journal of scientific & engineering research**, v. 6, n. 4, p. 925–933, 2015.

SCHACH, M. O. et al. Exergoeconomic analysis of post-combustion CO_2 capture processes. **Computer aided chemical engineering**, v. 28, p. 997–1002, 2010.

SEINFELD, J. **Atmospheric chemistry and physics of air pollution**. New York: John Wiley & Sons, 1986.

SHELL. **Comprehensive guide to offshore oil and gas development**. 2011. Available on: <http://s05.static-shell.com/content/dam/shell/static/usa/downloads/alaska/os101-ch3.pdf>. Accessed on 20/07/2016.

SILVA, J. A. M. et al. On the exergy determination for petroleum fractions and separation processes efficiency. **Heat transfer engineering**, v. 363, p. 974–983, 2014.

SZARGUT, J. **Exergy analysis of thermal, chemical, and metallurgical processes**. New York: Hemisphere Publishing Corporation, 1988.

TURNS, S. R. **An introduction to combustion: concepts and applications**. Singapore: McGraw-Hill, 2000.

U.S. ENERGY INFORMATION ADMINISTRATION. **International energy statistics**. Available on: <https://www.eia.gov/cfapps/ipdbproject/IEDIndex3.cfm?tid=5&pid=57&aid=6>. Accessed on 21/06/2016.

U.S. ENERGY INFORMATION ADMINISTRATION (EIA). **Brazil - International energy data and analysis.** 2015. Available on: <http://www.eia.gov/countries/cab.cfm?fips=br>. Accessed on 21/06/2016.

VOLDSUND, M. et al. **Exergy analysis of the oil and gas separation processes on a North Sea oil platform**. Proceedings of 23rd International conference on efficiency, cost, optimization, simulation and environmental impact of energy systems - ECOS 2010. Lausanne, Switzerland: 2010.

VOLDSUND, M. et al. **Evaluation of the oil and gas processing at a real production day on a North Sea oil platform using exergy analysis**. Proceedings of 25th International conference on efficiency, cost, optimization, simulation and environmental impact of energy systems - ECOS 2012. Perugia, Italy: 2012.

VOLDSUND, M. et al. Exergy analysis of the oil and gas processing on a North Sea oil platform a real production day. **Energy**, v. 55, p. 716–727, 2013a.

VOLDSUND, M. et al. **Comparative study of the sources of exergy destruction on four North Sea oil and gas platforms**. Proceedings of 26th International conference on efficiency, cost, optimization, simulation and environmental impact of energy systems, ECOS 2013. 2013b.

VOLDSUND, M. et al. **Performance indicators for evaluation of North Sea oil and gas platforms**. Proceedings of 26th International conference on efficiency, cost, optimization, simulation and environmental impact of energy systems, ECOS 2013. 2013c.

VOLDSUND, M. et al. Exergy destruction and losses on four North Sea offshore platforms: a comparative study of the oil and gas processing plants. **Energy**, v. 74, p. 45–58, 2014.

WALL, M.; LEE, R.; FROST, S. **Offshore gas turbines (and major driven equipment) integrity and inspection guidance notes**. 2006. International business. Available on: <http://www.hse.gov.uk/research/rrpdf/rr430.pdf>. Accessed on 21/06/2016.

WORLD BANK GROUP; ECOFYS. **Carbon pricing watch 201**5. 2015. Available on: <http://documents.worldbank.org/curated/en/387741468188935412/pdf/96602-REVISED-WP-P153405-PUBLIC-Box393190B.pdf>. Accessed on 21/06/2016.

YANG, Y.; ZHAI, R. MEA-based CO_2 capture technology and its application in power plants. **Paths to sustainable energy**, p. 499–510, 2010.

YOUNG, J. B.; WILCOCK, R. C. Modeling the air-cooled gas turbine: Part 1-General Thermodynamics. **Journal of turbomachinery - ASME**, v. 124, p. 207213, 2002.

APPENDIX A. Gas injection pressure.

Table 18. Required injection pressure as function of CO_2 composition and gas flow.

CO_2 % (v/v)		5	10	15	20	25	30	35	40	45	50	55	60	65	70	75	80	85	90	95
MW (g/mol)		23	24	25	26	27	28	30	31	32	33	34	35	36	37	38	40	41	42	43
Gas injection flow ($10^6 Nm^3/d$)	***0.2***	497	482	468	454	439	424	408	392	377	360	344	327	310	293	276	258	240	222	204
	0.4	498	484	470	455	441	426	410	395	379	363	347	330	314	297	280	262	245	227	208
	0.6	500	486	472	458	443	428	413	398	382	367	351	334	318	301	284	267	250	232	214
	0.8	503	489	475	461	446	432	417	402	386	371	355	339	323	306	289	272	255	238	220
	1.0	506	492	478	464	450	436	421	406	391	376	360	344	328	312	295	279	262	245	227
	1.2	509	496	482	469	455	440	426	411	396	381	366	350	335	319	302	286	269	252	235
	1.4	513	500	487	473	460	446	432	417	403	388	373	357	342	326	310	293	277	260	243
	1.6	518	505	492	479	465	452	438	424	409	395	380	365	349	334	318	302	286	269	252
	1.8	523	510	498	485	472	458	445	431	417	403	388	373	358	343	327	311	295	279	262
	2.0	528	516	504	492	479	466	453	439	425	411	397	382	367	352	337	321	305	289	273
	2.2	534	523	511	499	486	474	461	448	434	420	406	392	377	363	347	332	316	300	284
	2.4	509	496	482	469	455	440	426	411	396	381	366	350	335	319	302	286	269	252	235
	2.6	511	498	485	471	457	443	429	414	399	384	369	354	338	322	306	289	273	256	239
	2.8	513	500	487	473	460	446	432	417	403	388	373	357	342	326	310	293	277	260	243
	3.0	515	502	489	476	463	449	435	420	406	391	376	361	345	330	314	298	281	265	248
	3.2	518	505	492	479	465	452	438	424	409	395	380	365	349	334	318	302	286	269	252
	3.4	520	508	495	482	469	455	441	427	413	399	384	369	354	338	322	306	290	274	257
	3.6	523	510	498	485	472	458	445	431	417	403	388	373	358	343	327	311	295	279	262
	3.8	525	513	501	488	475	462	449	435	421	407	392	378	363	347	332	316	300	284	267
	4.0	528	516	504	492	479	466	453	439	425	411	397	382	367	352	337	321	305	289	273
	4.2	531	519	507	495	482	470	457	443	430	416	401	387	372	357	342	326	311	295	278
	4.4	534	523	511	499	486	474	461	448	434	420	406	392	377	363	347	332	316	300	284
	4.6	537	526	514	503	490	478	465	452	439	425	411	397	383	368	353	338	322	306	290
	4.8	541	530	518	507	495	482	470	457	444	430	417	403	388	374	359	343	328	312	296
	5.0	544	533	522	511	499	487	475	462	449	436	422	408	394	379	365	349	334	318	302
	5.2	548	537	526	515	503	492	479	467	454	441	428	414	400	385	371	356	340	325	309
	5.4	550	541	530	519	508	496	485	472	460	447	433	420	406	392	377	362	347	331	315
	5.6	550	545	535	524	513	502	490	478	465	452	439	426	412	398	383	369	353	338	322
	5.8	550	549	539	529	518	507	495	483	471	458	446	432	419	404	390	375	360	345	329
	6.0	550	550	544	534	523	512	501	489	477	465	452	439	425	411	397	382	367	352	336

Source: Author´s elaboration. Data of typical FPSO operation. Maximum gas injection pressure depends on the injection gas flow, the gas composition (mainly the CO_2 content), and the quantity and dimensions of injection wells.

APPENDIX B. Composition of some streams from simulation results.

Table 19. Mole fractions of processed Oil stream

	F1	F2	F3	F4
Methane	0.05	0.04	0.05	0.06
H2O	0.50	0.49	0.52	0.49
C20+*	28.70	23.13	33.53	27.86
n-C11	4.75	5.67	4.89	4.83
n-Decane	5.84	6.41	5.57	5.98
n-Nonane	6.37	6.85	6.37	6.53
n-Octane	7.91	8.21	7.50	8.00
n-Heptane	6.16	6.19	5.51	5.50
n-Hexane	4.17	5.16	4.50	5.27
n-Pentane	2.61	3.23	3.40	3.28
i-Pentane	1.58	1.63	0.95	1.85
n-Butane	2.32	2.69	1.61	2.80
i-Butane	0.84	0.81	0.47	0.93
Propane	1.38	1.30	0.87	1.40
Ethane	0.24	0.21	0.17	0.23
Oxygen	0.00	0.00	0.00	0.00
Nitrogen	0.00	0.00	0.00	0.00
n-C19	2.37	2.40	2.02	2.07
n-C18	2.60	2.54	2.19	2.39
n-C17	2.56	2.84	2.40	2.35
n-C16	2.83	3.13	2.66	2.57
n-C15	3.62	3.52	2.99	3.36
n-C14	3.69	3.96	3.37	3.59
n-C13	4.48	4.45	3.80	4.23
n-C12	4.33	4.99	4.30	4.41
CO2	0.10	0.16	0.35	0.01

Source: Author´s elaboration. Data from Aspen HYSYS® simulations.

Table 20. Mole fractions of Gas export and Fuel gas streams

	F1	F2	F3	F4
Methane	76.08	75.55	79.00	79.82
H2O	0.00	0.00	0.00	0.00
C20+*	0.00	0.00	0.00	0.00
n-C11	0.00	0.00	0.00	0.00
n-Decane	0.00	0.00	0.00	0.00
n-Nonane	0.00	0.00	0.00	0.00
n-Octane	0.00	0.00	0.00	0.00
n-Heptane	0.01	0.01	0.02	0.01
n-Hexane	0.04	0.05	0.14	0.04
n-Pentane	0.25	0.30	0.68	0.24
i-Pentane	0.25	0.26	0.28	0.23
n-Butane	1.74	1.97	1.59	1.69
i-Butane	1.01	0.97	0.71	0.93
Propane	6.68	6.66	5.05	6.05
Ethane	10.40	10.49	8.89	9.41
Oxygen	0.00	0.00	0.00	0.00
Nitrogen	0.55	0.75	0.63	0.50
n-C19	0.00	0.00	0.00	0.00
n-C18	0.00	0.00	0.00	0.00
n-C17	0.00	0.00	0.00	0.00
n-C16	0.00	0.00	0.00	0.00
n-C15	0.00	0.00	0.00	0.00
n-C14	0.00	0.00	0.00	0.00
n-C13	0.00	0.00	0.00	0.00
n-C12	0.00	0.00	0.00	0.00
CO2	3.00	3.00	3.00	1.10

Source: Author´s elaboration. Data from Aspen HYSYS® simulations.

Table 21. Mole fractions of Gas (injection) stream

	F1	F2	F3	F4
Methane	69.68	62.27	53.74	79.82
H2O	0.00	0.00	0.00	0.00
C20+*	0.00	0.00	0.00	0.00
n-C11	0.00	0.00	0.00	0.00
n-Decane	0.00	0.00	0.00	0.00
n-Nonane	0.00	0.00	0.00	0.00
n-Octane	0.00	0.00	0.00	0.00
n-Heptane	0.01	0.01	0.02	0.01
n-Hexane	0.03	0.04	0.10	0.04
n-Pentane	0.23	0.25	0.46	0.24
i-Pentane	0.23	0.21	0.19	0.23
n-Butane	1.60	1.62	1.08	1.69
i-Butane	0.92	0.80	0.48	0.93
Propane	6.12	5.49	3.43	6.05
Ethane	9.52	8.65	6.05	9.41
Oxygen	0.00	0.00	0.00	0.00
Nitrogen	0.50	0.62	0.43	0.50
n-C19	0.00	0.00	0.00	0.00
n-C18	0.00	0.00	0.00	0.00
n-C17	0.00	0.00	0.00	0.00
n-C16	0.00	0.00	0.00	0.00
n-C15	0.00	0.00	0.00	0.00
n-C14	0.00	0.00	0.00	0.00
n-C13	0.00	0.00	0.00	0.00
n-C12	0.00	0.00	0.00	0.00
CO2	11.16	20.04	34.01	1.10

Source: Author´s elaboration. Data from Aspen HYSYS® simulations.

APPENDIX C. Code for physical exergy calculations in HYSYS.

The following Visual Basic code for physical exergy flow rate calculations of different streams of the FPSO was taken from Abdollahi-Demneh et al. (ABDOLLAHI-DEMNEH et al., 2011).

```
Sub PostExecute()
    On Error GoTo ErrorHandler
    Dim Stream As Fluid
    Set Stream=ActiveObject.DuplicateFluid
    Dim Exergy As RealVariable
    Set Exergy=ActiveVariableWrapper.Variable
    Dim T0,P0,H,S,H0,S0 As Double
    Dim X As InternalVariableWrapper
    Set X=ActiveObject.GetUserVariable("AmbTemp")
    T0=X.Variable.GetValue()
    Set X=ActiveObject.GetUserVariable("AmbPres")
    P0=X.Variable.GetValue()
    If (Stream.VapourFraction.IsKnown And Stream.Pressure.IsKnown And
Stream.MolarFlow.IsKnown And T0<>-32767 And
Stream.MolarFractions.IsKnown(0)) Then
        H=Stream.MolarEnthalpy.GetValue("kJ/kgmole")
        S=Stream.MolarEntropy.GetValue("kJ/kgmole-C")
        Stream.Temperature.SetValue(T0,"C")
        Stream.Pressure.SetValue(P0,"kPa")
        Stream.TPFlash()
        H0=Stream.MolarEnthalpy.GetValue("kJ/kgmole")
        S0=Stream.MolarEntropy.GetValue("kJ/kgmole-C")
        Exergy.SetValue((H-H0-(T0+273.15)*(S-
S0))*Stream.MolarFlow.GetValue("kgmole/h"),"kJ/h")
    Else
        Exergy.Erase()
    End If
    ErrorHandler:
End Sub
```

APPENDIX D. Excel Worksheet for chemical exergy calculation.

Table 22. Excel Worksheet for chemical exergy calculation

Component	From Szargut		From HYSYS				Chemical Exergy [kJ/mol]		
	Chem Ex (g/v) Bq [kJ/mol]	Chem Ex (l) Bq [kJ/mol]	***Vapour mole frac***	***Liquid mole frac***	***Aquous mole frac***	*Activity coefficient*	gas/vapor	liquid	aquous
Methane	831.7	831.7	**0.730**	**0.049**	**0.000**	1	606.4	40.1	0.0
H_2O	9.5	0.9	**0.000**	**0.000**	**0.000**	1	0.0	0.0	0.0
C20+	23285.1	23285.1	**0.000**	**0.239**	**0.000**	1	0.0	5571.4	0.0
n-C11	7376.9	7376.9	**0.000**	**0.040**	**0.000**	1	0.0	291.5	0.0
n-Decane	6716.8	6716.8	**0.000**	**0.049**	**0.000**	1	0.1	326.4	0.0
n-Nonane	6064.9	6064.9	**0.000**	**0.053**	**0.000**	1	0.2	321.0	0.0
n-Octane	5413.1	5413.1	**0.000**	**0.066**	**0.000**	1	0.8	354.8	0.0
n-Heptane	4761.7	4761.7	**0.000**	**0.051**	**0.000**	1	1.7	241.2	0.0
n-Hexane	4118.5	4114.5	**0.001**	**0.034**	**0.000**	1	3.2	139.0	0.0
n-Pentane	3463.3	3461.8	**0.002**	**0.023**	**0.000**	1	5.9	80.5	0.0
i-Pentane	3463.3	3461.8	**0.002**	**0.015**	**0.000**	1	5.2	52.9	0.0
n-Butane	2805.8	2805.8	**0.009**	**0.037**	**0.000**	1	25.4	102.9	0.0
i-Butane	2805.8	2805.8	**0.006**	**0.016**	**0.000**	1	15.5	45.7	0.0
Propane	2154.0	2154.0	**0.046**	**0.054**	**0.000**	1	99.4	115.5	0.0
Ethane	1495.8	1495.8	**0.090**	**0.030**	**0.000**	1	133.5	45.0	0.0
Oxygen	4.0	4.0	**0.000**	**0.000**	**0.000**	1	0.0	0.0	0.0
Nitrogen	0.7	0.7	**0.005**	**0.000**	**0.000**	1	-0.1	0.0	0.0
n-C19	12612.0	12612.0	**0.000**	**0.020**	**0.000**	1	0.0	249.3	0.0
N-C18	11957.9	11957.9	**0.000**	**0.022**	**0.000**	1	0.0	258.9	0.0
n-C17	11303.9	11303.9	**0.000**	**0.021**	**0.000**	1	0.0	241.2	0.0
n-C16	10649.5	10649.5	**0.000**	**0.024**	**0.000**	1	0.0	250.6	0.0
n-C15	9995.8	9995.8	**0.000**	**0.030**	**0.000**	1	0.0	301.1	0.0
n-C14	9341.8	9341.8	**0.000**	**0.031**	**0.000**	1	0.0	287.2	0.0
n-C13	8687.8	8687.8	**0.000**	**0.037**	**0.000**	1	0.0	324.4	0.0
n-C12	8034.1	8034.1	**0.000**	**0.036**	**0.000**	1	0.0	289.8	0.0
CO_2	19.9	19.9	**0.110**	**0.024**	**0.000**	1	1.6	0.3	0.0
						Σ	898.8	9930.8	0.0
R [kJ/mol-K]	0.00831447		**From HYSYS**		**Phase molar fraction**		**0.7**	**0.3**	**1.0**
T0 [K]	298.15			Phase Chemical Exergy [kJ/mol]			612.6	3162.2	0.0
MW [kg/kmol]	**85.96**			***Chemical Exergy***		***3774.8***	***[kJ/mol]***	***43913.2***	***[kJ/kg]***

Source: Author´s elaboration.

APPENDIX E. Useful conversions and data

Conversions (RIGZONE, 2016):

1 m^3 = 6.2898 Barrel

1 Barrel = 42 gallons

1 Barrel of oil equivalent (boe) = 169.9 m^3

1 Tonne of oil equivalent (toe) = 7.33 Barrel of oil equivalent (boe)

1 m^3 of oil equivalent = 1069.6 Sm^3 of gas natural

Stock tank conditions:	15.5°C and 1 atm (RIAZI, 2005)
Standard conditions:	15.5°C and 1 atm (ASPEN TECHNOLOGY INC., 2005)
Normal conditions:	20°C and 1 atm (from FPSO operator)